CONTRACT NO. A932-126
FINAL REPORT
APRIL 1996

Atmospheric Pollutant Emission Factors From Open Burning of Agricultural and Forest Biomass by Wind Tunnel Simulations:

Volume 1

CALIFORNIA ENVIRONMENTAL PROTECTION AGENCY

AIR RESOURCES BOARD
Research Division

Final Report

Atmospheric pollutant emission factors from open burning of agricultural and forest biomass by wind tunnel simulations

Prepared for the California Air Resources Board
Sacramento, California

CARB Project No. A932-126
Determination of Emissions from Open Burning of Agricultural and Forestry Wastes:
Phase II

Volume 1

April 1996

B. M. Jenkins, Principal Investigator
Department of Biological and Agricultural Engineering, University of California, Davis

S. Q. Turn, R. B. Williams, M. Goronea, H. Abd-el-Fattah, J. Mehlschau, N. Raubach
Department of Biological and Agricultural Engineering, University of California, Davis

D.P.Y. Chang, M. Kang
Department of Civil and Environmental Engineering, University of California, Davis

S.V. Teague, O.G. Raabe
Institute for Toxicology and Environmental Health, University of California, Davis

D.E. Campbell, T.A. Cahill
Air Quality Group, Crocker Nuclear Laboratory, University of California, Davis

L. Pritchett, J. Chow
Desert Research Institute, University of Nevada System, Reno

A. Daniel Jones
Facility for Advanced Instrumentation, University of California, Davis

The statements and conclusions in this report are those of the University and not necessarily those of the State Air Resources Board. The mention of commercial products, their source or their use in connection with material reported herein is not to be construed as actual or implied endorsement of such products.

Abstract

Atmospheric pollutant emission factors were determined by wind tunnel simulations of spreading and pile fires for eight different types of fuel including barley, rice and wheat straw, corn stover, almond and walnut tree prunings, and Douglas fir and Ponderosa pine slash. Cereal straws and stover were burned in fires spreading against an impressed wind induced by the wind tunnel blower. Pile burns in wood fuels were naturally ventilated through the side doors of the wind tunnel without assistance from the blower. Concentrations of gaseous and condensed phase species were monitored by sampling the constrained fire plume in the wind tunnel stack, 10 m above the tunnel floor. A conveyor system making up the floor of the wind tunnel was used with spreading fires to provide extended sampling times. Fires were allowed to spread naturally into a fuel bed moving continuously downstream on the conveyors. The flame position was held stationary in the tunnel by advancing the conveyor at a speed equal to the fire spreading rate. Loading rates were matched to published yields of crop residue. Wood fuels were burned in stationary piles of 35 to 45 kg each.

Measured were emissions of CO, NO, NO_x, SO_2, total hydrocarbons, CH_4, non-methane hydrocarbons, total sulfur, CO_2, particulate matter, volatile organic compounds (VOC), and polycyclic aromatic hydrocarbons (PAH). Filter and sorbent from one test with rice straw were submitted for analysis of chlorinated dioxins and furans. Size distributions of particulate matter were obtained via cascade impactor. Elemental compositions of particulate matter in the total, 2.5 μm, and 10 μm size classes were analyzed to construct source profiles. Distributions of elements in particulate matter by size fraction were also evaluated using an eight-stage impactor. Bulk aerosol absorption coefficients were determined from light transmission measurements through filter samples.

Results from spreading fires are presented for two configurations of the wind tunnel earlier determined to have greatest impact on particulate matter emission rates from rice straw. A configuration designated CEWF utilized an adjustable ceiling extended to the leading edge of the fire with an auxiliary floor inserted immediately below the fuel bed. The alternate configuration designated CRNF made use of neither.

Compared across the various fuel types, the emission factors by compound were often quite similar. Barley and wheat straw fuels produced higher levels of products of incomplete combustion, and spread more slowly as a result of reduced fuel loading rate compared to rice straw and corn stover. Enhanced levels of smoldering were associated with higher levels of CO and hydrocarbon emissions. In general, burning rates below 5 g s^{-1} were associated with higher emissions of CO, total hydrocarbons, and particulate matter, and lower emissions of NO_x and SO_2. Although only small piles of wood fuels were burned, comparisons with full scale field data (where possible) suggest that wind tunnel results can be scaled appropriately by proper allocation of the mass of fuel burned in the flaming and smoldering stages. Particulate matter emissions are an exception. Wind tunnel results from smoldering with wood fuels were always less than published field values, but the number of wind tunnel experiments was limited and the comparatively small amount of material burned may have reduced the relative mass involved in smoldering compared to the field. Flaming stage results were quite similar to field results for fine particulate matter, but low for total particulate matter, most likely due to the lower total intensity and lower wind induced entrainment of the small scale burns.

NO_x emissions were heavily influenced by fuel nitrogen concentrations. Sulfur analyses showed a substantial amount of variation in the partitioning of sulfur among ash, SO_2 in

the gas phase and particulate matter. Barley straw was unique among cereal crop residues in producing large amounts of sulfur in particulate matter, principally as sulfate. Total sulfur analyses of stack gas were inconclusive as to the presence of other gaseous sulfur species due to instrument interference from CO_2. Carbon, potassium, and chlorine dominated particulate matter compositions. Carbon was present principally in organic forms, potassium and chlorine in ionic forms. VOC emissions from Douglas fir and Ponderosa pine slash were high in comparison to the other fuels. PAH emission factors were higher for wheat straw and barley straw than for other fuels. Bulk aerosol absorption coefficients from filter samples varied from about 1 to 5 $m^2\ g^{-1}$, with an average of 2.7 $m^2\ g^{-1}$. Dioxin and furan analyses detected small levels of 1,2,3,4,6,7,8-HpCDD, 1,2,3,4,6,7,8,9-OCDD, and 1,2,3,4,6,7,8,9-OCDF, but no TCDD was found above the detection limit.

Factors significantly affecting the spreading rates and to some extent the emission factors for cereal fuels were inlet air temperature, loading rate, and wind speed (as inlet air mass flow rate). Burning rate variations correlated well with air temperature and loading rate. Relative humidity was less significant in influencing fire spread. Inlet air temperature was observed to increase spreading rate in rice straw by 0.05 m $min^{-1}\ K^{-1}$. Increased wind speed was observed to slow fire spread in the CEWF configuration. Emission factors for CO, hydrocarbons, and particulate matter were higher and NO_x and SO_2 lower in virtually every CEWF experiment when compared to the CRNF configuration with the same fuel. For particulate matter, this result was contrary to observations from earlier studies with rice straw, and is believed to be due to differences in the physical characteristics of the fuel, but requires further investigation. Averages of the two configurations were computed as a means of applying the results to the determination of emission offset allowances for biomass utilization facilities. More controlled experiments are recommended for understanding the influences of fuel and ambient conditions on fire behavior and pollutant formation.

Table of Contents

Volume 1:

Table of Contents (continued)

Nomenclature

		Units
A_f	area of exposed filter	m^2
A_s	area of stack	m^2
b_{ap}	aerosol absorption coefficient	km^{-1}
B_{ap}	bulk aerosol absorption coefficient	$m^2\ g^{-1}$
C_{aC}	ash carbon concentration	--
$C_{aC,f}$	fuel carbon concentration, end of smoldering	--
$C_{aC,o}$	fuel carbon concentration, start of smoldering	--
C_{aH}	ash hydrogen concentration	--
C_{aN}	ash nitrogen concentration	--
C_{aS}	ash sulfur concentration	--
CEWF	ceiling extended, with auxiliary floor	
C_{fC}	dry fuel carbon concentration	--
C_{fH}	dry fuel hydrogen concentration	--
C_{fN}	dry fuel nitrogen concentration	--
C_{fS}	dry fuel sulfur concentration	--
C_i	concentration of gas species *i* in stack gas	ppmv
$\overline{C_i}$	traverse average concentration for gas species *i*	ppmv
C_{pC}	concentration of carbon in particulate matter	--
$C_{pNH_4^+}$	concentration of NH_4^+ in particulate matter	--
$C_{pNO_3^-}$	concentration of NO_3^- in particulate matter	--
C_{PM}	measured concentration of particulate matter	$mg\ m^{-3}$
$C_{PMo,}$	actual concentration of particulate matter	$mg\ m^{-3}$
C_{PMC}	stack carbon concentration due to particulate	ppm
C_{pS}	concentration of sulfur in particulate matter	--
CRNF	ceiling retracted, no auxiliary floor	
D	conveyor travel during traverse	m
D_p	probe nozzle diameter	m
$\dot{E}$	energy release rate	kW
f_i	emission factor for species i	% of fuel dry mass
$\bar{f}_i$	average emission factor for species *i*	% of dry fuel mass
f_{PM}	emission factor for particulate matter	% of dry fuel mass
I	fireline intensity	$kW\ m^{-1}$
I_e	intensity of transmitted light, exposed filter	arbitrary
I_o	intensity of transmitted light, unexposed filter	arbitrary
k	unit conversion coefficient = 10^{-1}	
k'	unit conversion coefficient = 10^3	
k''	unit conversion coefficient = 10^2	
L	width of wind tunnel	m
M	fuel moisture content wet basis	--
m'_a	mass of ash	g
m_a	total residual ash generation	g
$\dot{m}_{aC}$	ash carbon mass flow rate	$g\ s^{-1}$
$\dot{m}_{air}$	inlet air mass flow rate	$g\ s^{-1}$

Nomenclature (continued)

		Units
$\dot{m}_{aN}$	ash nitrogen mass flow rate	g s^{-1}
$\dot{m}_{aS}$	mass flow rate of sulfur in ash	g s^{-1}
m_d	mass of dry fuel gasified	g
m_f	fuel mass, end of smoldering	g
$\dot{m}_{fC}$	fuel carbon mass flow rate	g s^{-1}
m_{fd}	total dry fuel consumption	g
$\dot{m}_{fd}$	dry fuel consumption rate	g s^{-1}
$\dot{m}_{fN}$	fuel nitrogen mass flow rate	g s^{-1}
$\dot{m}_{fS}$	mass flow rate of sulfur in fuel	g s^{-1}
m_{fv}	total mass of fuel volatilized	g
$\dot{m}_{fv}$	fuel volatilization rate	g s^{-1}
m_{fw}	total moist fuel consumption	g
$\dot{m}_{fw}$	moist fuel consumption rate	g s^{-1}
$\dot{m}_g$	average stack gas mass flow rate	kg s^{-1}
MMAD	mass median aerodynamic particle diameter	µm
$\dot{m}_{N,PM}$	mass flow rate of nitrogen in PM	g s^{-1}
m_o	fuel mass, start of smoldering	g
$\dot{m}_{sC}$	carbon released to stack (stack carbon transfer)	g s^{-1}
$\dot{m}_{S,PM}$	mass flow rate of sulfur in PM	g s^{-1}
$\dot{m}_{S,SO_2}$	mass flow rate of sulfur in SO2	g s^{-1}
m_t	total fuel mass	g
m_v	mass of dry fuel organic matter	g
m_w	mass of fuel moisture	g
$\dot{m}_{w,c}$	water released by combustion of fuel	g s^{-1}
$\dot{m}_{w,e}$	moisture released by evaporation	g s^{-1}
$\dot{m}_{w,f}$	water vapor from fuel combustion	g s^{-1}
$\dot{m}_{w,s}$	stack water vapor mass flow rate	g s^{-1}
NMHC	non-methane hydrocarbons	
NO_x	oxides of nitrogen as NO_2	
PAH	polycyclic aromatic hydrocarbons	
PM	total particulate matter	
PM10	particulate matter ≤ 10 µm aerodynamic diameter	
PM2.5	particulate matter ≤ 2.5 µm aerodynamic diameter	
p_s	saturation water vapor pressure in inlet air	Pa
$p_{s,s}$	saturation water vapor pressure in stack gas	Pa
p_t	total pressure	Pa
p_v	water vapor pressure in inlet air	Pa
$p_{w,s}$	water vapor pressure in stack gas	Pa
Q_a	heating value of ash	MJ kg^{-1}
Q_f	heating value of fuel	MJ kg^{-1}
$\dot{q}_i$	energy in products of incomplete combustion	kW

Nomenclature (continued)

		Units
Q_i	heating value of species *i*	MJ kg^{-1}
$\dot{Q}_s$	heat release rate	kW
r_d	dry fuel loading rate	g m^{-2}
r_w	moist fuel loading rate	g m^{-2}
Stk	Stokes number = $\tau u/D_p$	--
t	duration of traverse	s
T_{dp}	dew point temperature	°C
t_f	end time for traverse	s
THC	total hydrocarbons	
T_i	impinger outlet temperature	K or °C
t_o	start time for traverse	s
T_s	stack gas temperature	K or °C
u	instantaneous stack gas velocity	m s^{-1}
$\bar{u}$	average stack gas velocity	m s^{-1}
$\hat{u}$	estimated instantaneous stack gas velocity	m s^{-1}
$\hat{\bar{u}}$	estimated average stack gas velocity	m s^{-1}
u_p	gas velocity in probe nozzle	m s^{-1}
V_g	average stack gas flow rate	m^3 s^{-1}
V_s	sample volume of stack gas	m^3
VOC	volatile organic compounds	
W_i	molecular weight of species *i*	kg kg-mol^{-1}
W_s	molecular weight of stack gas	kg kg-mol^{-1}
x_w	volume fraction water vapor in inlet air	--
$x_{w,s}$	water vapor volume fraction in stack gas	--
y'_a	dry fuel ash mass fraction	--
y_a	mass fraction of residual ash in moist fuel	--
y_w	mass fraction water vapor in inlet air	--
$y_{w,s}$	water vapor mass fraction in stack gas	--
γ_C	approach to closure, carbon balance	%
Δm	weight change in 1 min	g
Δm_w	impinger and desiccant weight gain	g
ϕ	inlet air relative humidity	--
ϕ_s	stack gas relative humidity	--
$\bar{\rho}_g$	average stack gas density	kg m^{-3}
ρ_g	stack gas density	kg m^{-3}
ρ_s	density of sample gas	g m^{-3}
σ	geometric standard deviation	--
τ	particle relaxation time	s

1. Introduction

Biomass burning has long been known as a source of atmospheric pollutants, and more recently, the large scale impacts on global atmospheric chemistry have become more widely recognized. Agriculture, including forestry, often makes use of open burning for the rapid or agronomically effective disposal of crop residues or as a land clearing technique, but as population grows, previously rural areas urbanize, and more is discovered about the health impacts of environmental pollutants, the practice becomes increasingly controversial. Whereas once protected under state law, agricultural burning in California is undergoing a systematic curtailment, with mandated reductions already imposed for one crop (rice). Such restrictions follow a worldwide trend towards legislated reduction in emissions from agricultural burning.

Quantifying the impacts of agricultural burning requires knowledge of the pollutant loads introduced by the practice. Regional scale assessments of pollutant loads are normally done indirectly, using emission factors, or emission indices as they are sometimes called, relating pollutant mass emitted to the original fuel mass consumed. Estimates of total fuel consumption then provide estimates of total emission load. The magnitudes of the emission factors for any pollutant and fuel type in general depend on the burning conditions.

Estimates of emissions factors for various pollutant species and agricultural fuels have previously been determined in both field and laboratory studies. The laboratory or "burning tower" experiments conducted by Darley and co-workers at UC Riverside during the 1960's and 1970's produced information on a comprehensive set of agricultural fuels important to California (Darley, et al., 1973; Darley, 1977; Darley, 1979). Results of these and other experiments have been compiled in the reference documents produced by the US Environmental Protection Agency (US EPA, 1985). Field data have been obtained in a number of studies, including the important work of Goss and Miller (1973) for rice straw and that of Ward, et al., (1989) for logging debris. The major criticisms applied to the results of these efforts appear to center around the small fuel masses used in the laboratory experiments, and the uncertainty introduced into the determination of emission factors by the need to accurately measure CO_2 concentrations in field studies. In the latter case, pollutant plume concentrations are typically related to the fuel mass burned by completing a carbon balance with CO_2 serving as a tracer for the fire. Because the majority of fuel carbon is converted to CO_2 in the fire, uncertainty in the determination of CO_2 concentration leads to uncertainty in the computed emission factor. Often, plume concentrations of CO_2 at the point of measurement are only slightly elevated above ambient levels, and small measurement errors lead to larger errors in emission factor due to background subtraction. Although laboratory studies in general avoid this problem by permitting direct measures of fuel conversion, the extent to which the laboratory burning conditions adequately simulate the field burning conditions leads to further uncertainty in the emission factors derived in this manner.

Additional motivation for accurate emission factors arises from state policy allowing emission offset credits to new facilities using biomass fuels. The assignment of credits requires knowledge of the pollutant emission levels in the field as well as from the facility. The procedure adopted by the California Air Resources Board (CARB), the authorizing agency, utilizes emission factors along with other factors pertaining to burning practice. This latter motivation served as the original stimulus for the program described here in seeking to corroborate existing emission factor data and in increasing the number of compounds analyzed.

This report gives results of laboratory test burns conducted in a combustion wind tunnel with eight different fuel types: barley straw, corn stover, rice straw, wheat straw, almond prunings, walnut prunings, Ponderosa pine slash, and Douglas fir slash. These are important fuel types burned in California. Previous surveys (Jenkins, et al., 1992) of agricultural burning have shown the four fuels rice straw, wheat straw, almond prunings, and walnut prunings comprise 95% of the agricultural biomass burned in the state (exclusive of prescribed forest burns and wildfires). Ponderosa pine and Douglas fir are two of the more important commercial timber species in California, and contribute substantially to the amount of slash burned. Barley straw and corn stover are burned to a lesser extent than the other crop residues, but nonetheless have been allowed as offset fuels.

A wind tunnel approach was adopted to address some of the uncertainties associated with smaller scale laboratory apparatus and full scale field tests. The wind tunnel design in general permitted the use of larger fuel samples than earlier burning tower studies, while at the same time allowing direct determinations of fuel consumption. The burns could also be conducted with good control over fuel conditions. The question of similarity between wind tunnel and field remains as a disadvantage of wind tunnel tests. Full simulation was not attempted, instead, the major characteristics of wind speed, inlet flow velocity profile, turbulence intensities, fuel moisture, and fuel loading were matched as closely as possible. The influence of some of these parameters on the emission rates for particulate matter were assessed in some detail during an earlier study (Jenkins, et al., 1993a; 1993b).

Two kinds of fires were conducted: spreading fires and pile fires. All field crop residues including barley, wheat, and rice straw and corn stover, were burned as spreading fires, in which the fire was allowed to propagate along a quasi-linear front into the upstream unburned fuel bed. Only fires spreading against the wind (backing fires) were conducted. Wind-aided fires, those spreading in the same direction as the wind (heading fires), were not conducted. No specific accommodations were made in the wind tunnel design for wind-aided fires because such conditions are outside prescribed burning procedures for crop residues in California. The unique feature of the wind tunnel was a set of conveyors for moving the fuel bed into the combustion zone at a rate equal to the fire spreading rate. In this way, the tests could be conducted for indefinite periods, giving extended sampling times. The details of the wind tunnel design for spreading fires were reported earlier (Jenkins, et al., 1990; 1991)

All wood fuels (almond and walnut prunings and Ponderosa pine and Douglas fir slash) were burned in stationary pile fires. The sizes of the piles burned (30 - 50 kg each) were smaller than what would normally be encountered in the field. The principal purpose of conducting these burns was to provide detailed emissions data not yet available from field studies. The extent to which these data can be applied to the larger scales is examined by comparison against existing field data.

The fires described here were intended to give representative data for field conditions. In the case of spreading fires, earlier investigations had shown particulate matter emissions to depend to some extent on the various operating configurations of the wind tunnel. For this reason, spreading fires with each fuel type were conducted using the two configurations giving the extremes in particulate matter emission factor in the earlier work (Jenkins, et al., 1993a; 1993b). Fires in all fuel types under each configuration were repeated at least once to give some measure of repeatability. Not all possible field conditions were tested, and application of the data should take this into consideration.

The second part of the report describes the general methodology and apparatus used in conducting the experiments. The wind tunnel is described, along with the instrumentation and analytical procedures. The chronology of the tests is also given. Specific test procedures and results are given in section 3 of the report, organized by fuel type. Comparisons of results among fuel types appear in section 4 preceding the summary and conclusions. The report is organized into three volumes, with the second and third volumes containing results for individual tests in cereal fuels and wood fuels, respectively.

2. Materials and Methods

2.1. Wind tunnel

The wind tunnel used in the experiments was an open-circuit, forced-draft type comprised of three main sections: an inlet section, a combustion test section, and a stack sampling section, arranged as shown in Figure 2.1.1. Details of the original tunnel design were given by Jenkins, et al. (1990). Several modifications were subsequently made to the tunnel, and are discussed below. The wind tunnel was located outside. Ambient air was used without conditioning for all tests.

2.1.1. Conveyor system, spreading fires

As mentioned earlier, the wind tunnel incorporated a system of conveyors for moving the fuel bed downstream when operating with spreading fires. The inlet section housed the primary fuel conveyor. This flexible belt conveyor was exposed at the upstream end so that fuel could be loaded continuously while the fuel bed was transported into the combustion test section. At the junction of the inlet section with the combustion test section, the fuel moved off the flexible conveyor and onto a secondary steel conveyor on which it was burned. The primary conveyor returned underneath the inlet duct to the fuel loading section. The steel conveyor consisted of stainless steel rods carried between two mild steel link chains at each side of the tunnel. The unlubricated link chains were driven at the upstream end and supported on mild steel angles welded to the tunnel walls. The transverse stainless steel rods were situated along the chains at intervals of approximately 100 mm. The chains and rods, like all surfaces of the wind tunnel, were washed with ethanol and rinsed with water to remove oils remaining from manufacturing or applied for storage. The steel conveyor exited the downstream end of the combustion test section at the top of an ash bin, and returned underneath the tunnel. The return path of the conveyor was originally open, but was later enclosed, as in Figure 2.1.2. During the return transit, the conveyor cooled to near ambient temperature. The conveyors were operated only with spreading fires. A fine mesh stainless steel screen interwoven through the stainless steel support rods was added to retain fine fuel particles on the conveyor. In previous tests without the support screen, small burning particles falling through the conveyor onto the tunnel floor caused the incoming fuel to ignite ahead of the main fire front anytime conveyor speed exceeded the fire spread rate. This generated a wide ignition front uncharacteristic of field fires.

A single variable-speed DC motor was used to operate both conveyors at the same linear velocity. The motor speed was controlled manually, either at the motor or from inside an instrument cabin located next to the wind tunnel. The speed was adjusted to maintain the fire at a fixed location in the tunnel.

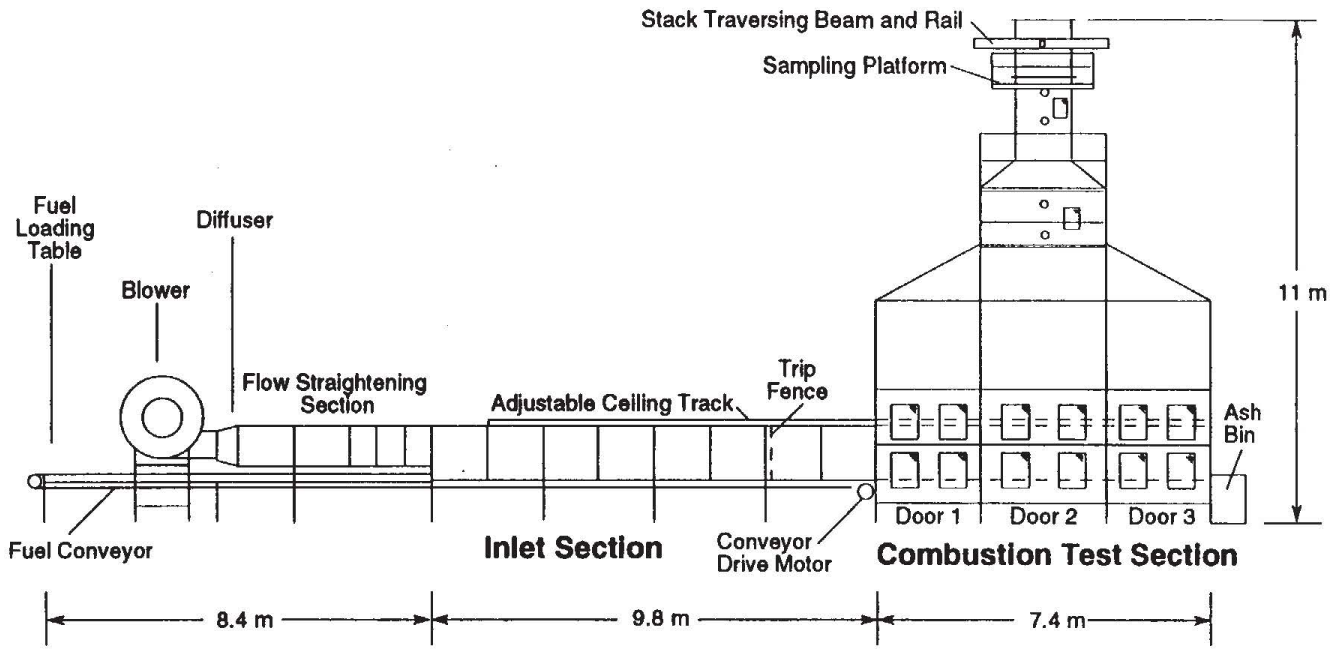

Figure 2.1.1. Exterior schematic, combustion wind tunnel.

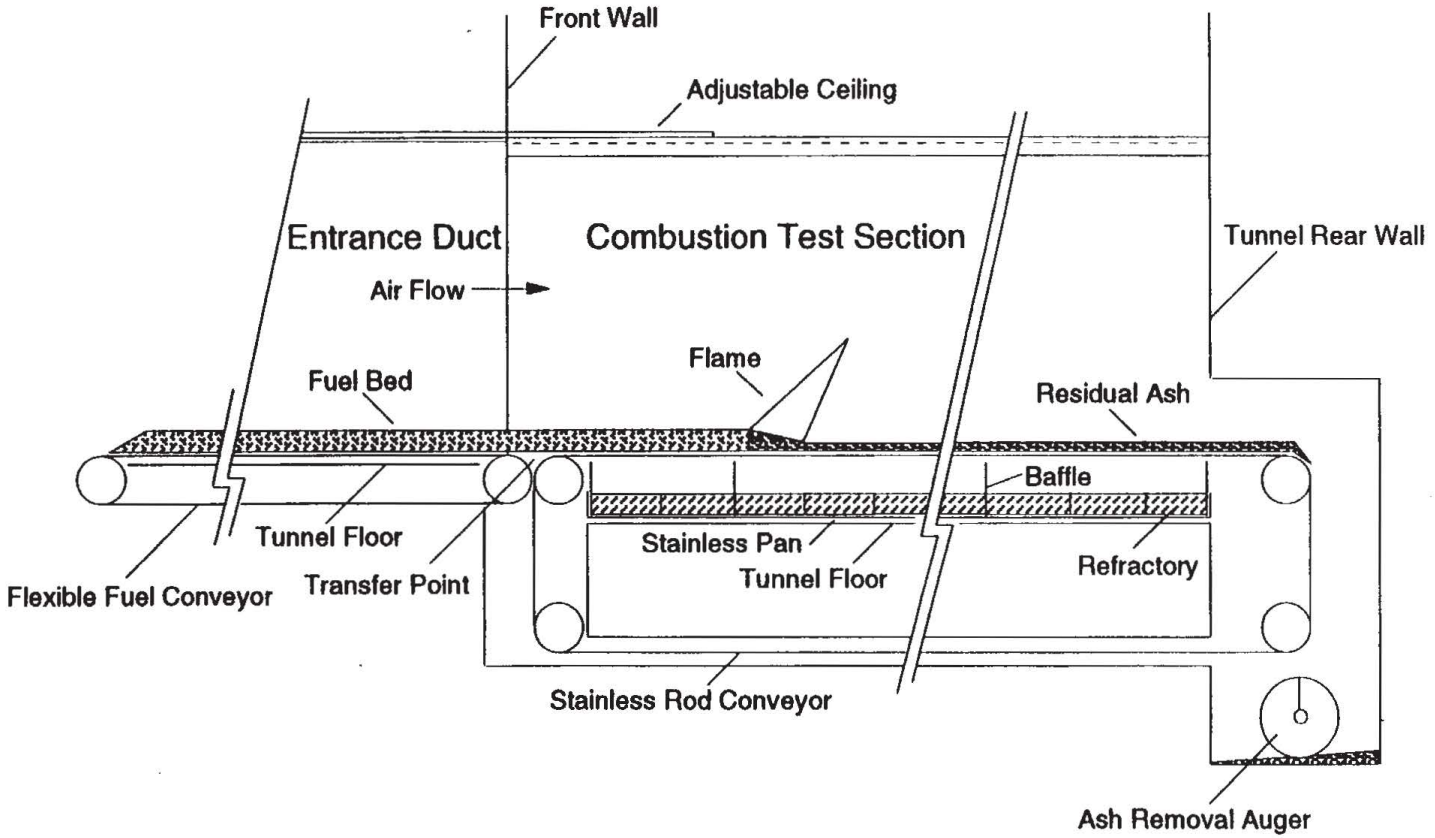

Figure 2.1.2. Schematic arrangement of conveyors used with spreading fires.

2.1.2. Inlet section

The inlet section included the primary belt conveyor, blower, flow straightening section, and flow development section. Located on top of the flow development section was a track supporting an adjustable ceiling which could be moved into the combustion test section. The entire inlet section was 18.2 m long. The primary belt conveyor was exposed over the first 2 m for fuel loading, then moved under the blower and flow straightening section with approximately 150 mm vertical clearance. The belt conveyor carrying the fuel bed joined the air flow about 5 m downstream of the blower, and was fully enclosed in the 9.8 m long flow development section until reaching the combustion test section. The fuel surface served as roughness on the floor of the flow development section to aid in the development of the boundary layer profile. The development section duct was 1.2 m square, with a length equal to 8 hydraulic diameters. A trip fence consisting of a 25 mm square wire mesh screen was situated across the duct above the fuel 2.4 m upstream of the combustion test section.

The air flow for the spreading fires was generated by a centrifugal blower driven by a 45 kW electric motor located at the upstream end of the inlet section. The maximum air speed (duct flow rate divided by duct area) produced by the blower was about 10 m s^{-1}, but speeds under 4 m s^{-1} were used for the spreading fires to better match prevailing field conditions. Such velocities were found in field measurements to be typical of the average wind velocity in the first 1 m above the straw layer during open burning (Jenkins, et al., 1990). The tunnel flow was straightened through two 40 and three 60 mesh wire screens located downstream of the blower. The air flow rate and velocity were adjusted by varying the open area of the dampers at the inlet of the blower. The outlet dampers were left fully open.

2.1.3. Combustion test section

The combustion test section extended 7.4 m downstream from the inlet section. An ash bin located at the end of the combustion test section received residual fuel material (ash and partially burned fuel) from the steel rod conveyor. The combustion test section extended upwards approximately 4 m above the rod conveyor before beginning to taper into the sampling stack. The 1.2 m width of this section was the same as the inlet section. The walls were made from welded 16 gage mild steel sheet, unpainted on the interior. The combustion section and the stack were supported on an exterior welded steel scaffold.

Access to the combustion test section was through three large doors located on each side of the tunnel. Each door was approximately 1.2 m high and 1.5 m long, and contained two glass windows for observing the fire when the doors were closed. The doors were hinged at the top, and opened outwards as shown in Figure 2.1.4. The windows were manufactured of a glass having low coefficient of thermal expansion, and no breakage was encountered with the flame held directly on the glass. The windows were sealed against the doors with silicon sponge gaskets in spring loaded frames. An additional row of six windows was situated above the doors on each side, and another window was located in the end wall above the ash bin.

The bottom floor of the combustion test section was made of refractory bricks, the upper surface lying 150 mm beneath the rod conveyor. Sheet steel baffles were positioned across the tunnel at intervals of 1 m along the floor below the conveyor (Figure 2.1.2). The purpose of the baffles was to restrict air motion beneath the fuel bed in certain configurations, in a manner similar to the stubble layer in a field burn. The baffles were

also intended to restrict any air flows arising from leakage in the ash bin or at the junction of the primary and secondary conveyors near the entrance to the combustion test section.

An auxiliary floor made from sheet steel panels could be positioned immediately below the rod conveyor extending from the entrance of the combustion test section past the fire. This floor was supported on the same steel angles that supported the conveyor chains. When installed, the chains ran directly on the floor panels. The auxiliary floor was used to test the effect of blocking ventilation from below, as in the case of a fire spreading through a fuel bed resting on the ground. The influences due to the presence of the floor were detailed in an earlier study (Jenkins, et al., 1993a; 1993b). The auxiliary floor was observed in the earlier tests to reduce the particulate matter emission rate, probably by restricting air flow through the smoldering zone behind the main fire front.

Residual material, referred to in the following as ash, was discharged from the ash bin by a 200 mm diameter motor driven auger. All ash was recovered in bags attached to the outlet of the discharge auger. Access to the ash bin was through a sliding door in the end wall. The ash bin was cleaned after each test, and any material not removed by the auger was recovered by hand.

An adjustable ceiling could be extended into the combustion tests section from the front (upstream) wall. The ceiling was made from mild sheet steel panels, supported on unlubricated rollers, and moved along steel angles welded to the tunnel wall on each side at a height of 1.2 m above the rod conveyor (the height of the inlet duct). The purpose of the ceiling was to sustain the inlet velocity profile up to the fire, following the analysis of Fleeter, et al. (1984). When used, the ceiling was extended only to the front edge of the fire, and not past it. The ceiling was moved manually. Once positioned, the location of the fire with respect to the ceiling was controlled by adjusting the conveyor speed. The ceiling was used only with spreading fires. The position of the ceiling was found to have an effect on the flame characteristics. When extended to the usual fire position, 2 m downstream of the entrance to the combustion test section (at the second window downstream), and with the wind speed in the inlet duct set for the normal range of 2 to 4 m s^{-1}, the flame was bent over by the flow. When retracted to the front wall, with the same inlet duct wind speeds and the fire held at the same position, the flame became erect and increased in length. With the ceiling retracted, the flow decelerated rather rapidly due to the sudden expansion at the combustion test section entrance. The velocity profiles at low wind speed indicated an extremely adverse pressure gradient with flow separation under these conditions. The influences of the two ceiling positions on flow characteristics, flame behavior, and particulate matter emissions were investigated in detail and reported by Jenkins, et al. (1993a, 1993b).

The adjustable ceiling and auxiliary floor allowed different operating configurations of the wind tunnel. Four configurations were tested in the earlier study mentioned above (Jenkins, et al., 1993a, 1993b). The configurations were described by the position of the ceiling and whether the auxiliary floor were used or not. The designations were as follows:

1) with the ceiling extended downstream to the front or leading edge of the fire, and without the auxiliary floor, the wind tunnel configuration was designated CENF (ceiling extended, no floor).

2) with the ceiling retracted to the front wall of the combustion test section and without the auxiliary floor, the configuration was designated CRNF (ceiling retracted, no floor).

3) with the ceiling extended and with the auxiliary floor installed, the configuration was designated CEWF (ceiling extended, with floor).

4) with the ceiling retracted to the front wall and with the auxiliary floor installed, the configuration was designated CRWF (ceiling retracted, with floor).

Each of the configurations was tested using fires in rice straw at a low wind speed of about 2 m s^{-1}, and a higher wind speed of 3 to 3.5 m s^{-1}. The lowest particulate matter emission factor was generated using the CEWF high wind speed configuration, while the highest was found for the CRNF low wind speed configuration. In the spreading fire experiments described here, separate tests were made using these two extreme cases--the CEWF high wind speed configuration and the CRNF low wind speed configuration.

2.1.4. Stack sampling section

A large hood fixed to the top of the combustion test section ducted the combustion products past the emissions sampling equipment. Beginning at the top of the combustion test section, the hood tapered longitudinally in two steps to the final longitudinal stack width of 1.2 m. The hood and stack retained the constant transverse tunnel width of 1.2 m, making the stack 1.2 m square. Catwalks were placed at three heights along the hood and stack. The catwalks were accessed by ladders. A manually operated hoist was attached to the tunnel at the middle catwalk for lifting equipment.

A stack traversing system was located near the top of the stack, just above the uppermost catwalk (Figure 2.1.1). The traversing system consisted of a 75 x 100 mm rectangular steel tube carried on a sliding steel curtain wall on the stack duct, as illustrated in Figure 2.1.3. The beam was used to support the thermocouple, anemometer, and some of the probes used during sampling. The beam was carried on rollers inside a steel saddle on the exterior of the duct. The saddle was fixed to the curtain wall, which moved along the stack on another set of rollers. A slot cut in the stack wall provided access to the stack flow. The sheet steel curtain kept the slot closed for all positions of the beam. The beam was moved in and out of the stack on the carrier saddle and the curtain wall moved back and forth along the stack to position the sampling equipment at each of the traverse points. The positioning was done manually. Each traverse point was identified by marks made on the tunnel wall and the support beam (coordinates 1-6 in Figure 2.1.3 were labeled on the beam, A-D on the stack wall above the steel curtain). When extended to the innermost traverse point, the beam and probes occupied somewhat less than 5% of the stack area. The beam was located 2 hydraulic diameters (2.4 m) downstream of the final hood contraction, and 0.5 hydraulic diameter (0.6 m) upstream of the stack exit. A 24 point traverse was used. The individual sampling locations are shown by the cross-marks in Figure 2.1.3. Although CARB method 1 specified a 25 point traverse for such a square stack, the traverse beam carrier mechanism interfered with the stack wall at each end. To provide adequate clearance and support, CARB approved a 24 point traverse. Due to the turbulent conditions in the stack, a 24 point traverse was not thought to be substantially less effective than a 25 point traverse.

2.1.5. Burning platform, pile fires

Pile fires, with the exception of the first tests with walnut prunings, were conducted on a platform suspended on load cells giving continuous records of weight. The platform was added after the first pile burns to improve determinations of fuel consumption rate. The addition of a continuous CO_2 analyzer at the same time provided a means to check the

stack velocity measured with a hot film anemometer in these more intense pile fires. Analyses following the first pile burns suggested the anemometer was more seriously affected by the more intense flame radiation than was the case with the spreading fires.

The platform was mounted across the wind tunnel through the center doors directly beneath the stack (Figure 2.1.4). An expanded steel mesh deck sat atop two inverted-U shaped steel supports kept upright by cross bracing. The supports straddled the wind tunnel, and stood on the ridges of steel angles running along each side. The angles were hung from load cells at each end. The load cells were in turn suspended from two rectangular bars resting on the wind tunnel frame. The center doors could not be fully closed with the platform installed, but all doors were left partially open during the pile burns to provide a free flow of air to the fires. A fine mesh stainless steel screen was placed over the expanded mesh prior to fuel loading to retain fuel ash generated by the fire.

2.2. Instrumentation and sampling equipment

The sampling system was designed to obtain emission rates for particulate matter, gases, volatile organic compounds (VOC) and polycyclic aromatic hydrocarbons (PAH). Four different sampling probes were used for particulate matter characterization. A combination of continuous analyzers and gas chromatography was used for gas analysis. A separate probe was used for VOC sampling, whereas the PAH sampling made use of the same probe employed for total particulate matter sampling. The sampling scheme is depicted in Figure 2.2.1. A list of instrumentation appears in Table 2.2.1.

2.2.1. Particulate Matter

Particulate matter was sampled using four probes, two carried on the traversing beam described in section 2.1.4, and two with fixed inlets positioned just overhead of the traversing plane. These latter two probes entered through the top of the stack and the inlets were positioned out of line with any of the traverse positions so as to avoid being directly behind the traverse beam. The probes carried on the beam were used for total particulate matter and particle size determinations. The other two probes were used almost exclusively to obtain samples for chemical characterization and source profiling. These probes are here identified by the name of the laboratory performing the chemical analysis (DRI or CNL, see below). The total filter was also used in analyzing PAH.

2.2.1.1. Total particulate matter

The probe used to obtain total particulate matter (PM) concentrations in the stack flow was carried on the traverse beam. The procedure was based on CARB method 17 (CARB, 1987) for in-stack sampling. The probe nozzle was a stainless steel buttonhook made from seamless tubing, 9.5 mm inside diameter (i.d.), with a sharp tapered leading edge. The nozzle diameter was selected to give isokinetic conditions in the neighborhood of 10 L min^{-1} sample flow rate.

The sample was collected on 47 mm diameter teflon coated glass fiber filters (Pallflex type TX40HI20, Pallflex Products Corp., Putnam, Conn.) loaded in a stainless steel holder with stainless steel support screens. The inlet was attached to the filter holder with stainless steel tube connectors. The filter holder was attached in the same manner to a 12.7 mm outside diameter (o.d.) stainless steel tube running through the traverse beam. A 9.5 mm o.d. teflon tube was pushed through the stainless steel tube into

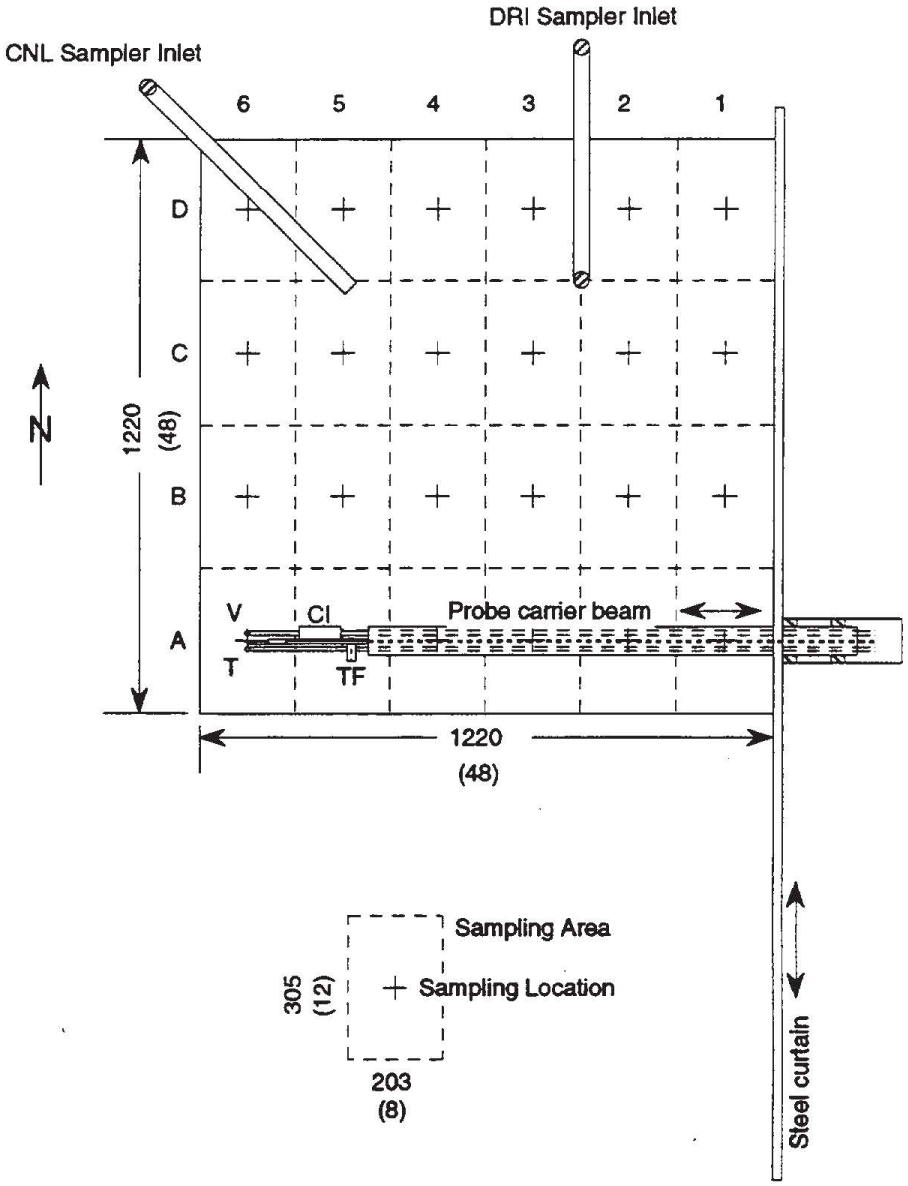

Figure 2.1.3. Stack traverse grid showing probe carrier beam and fixed inlets. CI = cascade impactor, TF = total filter. Dimensions in mm (inches).

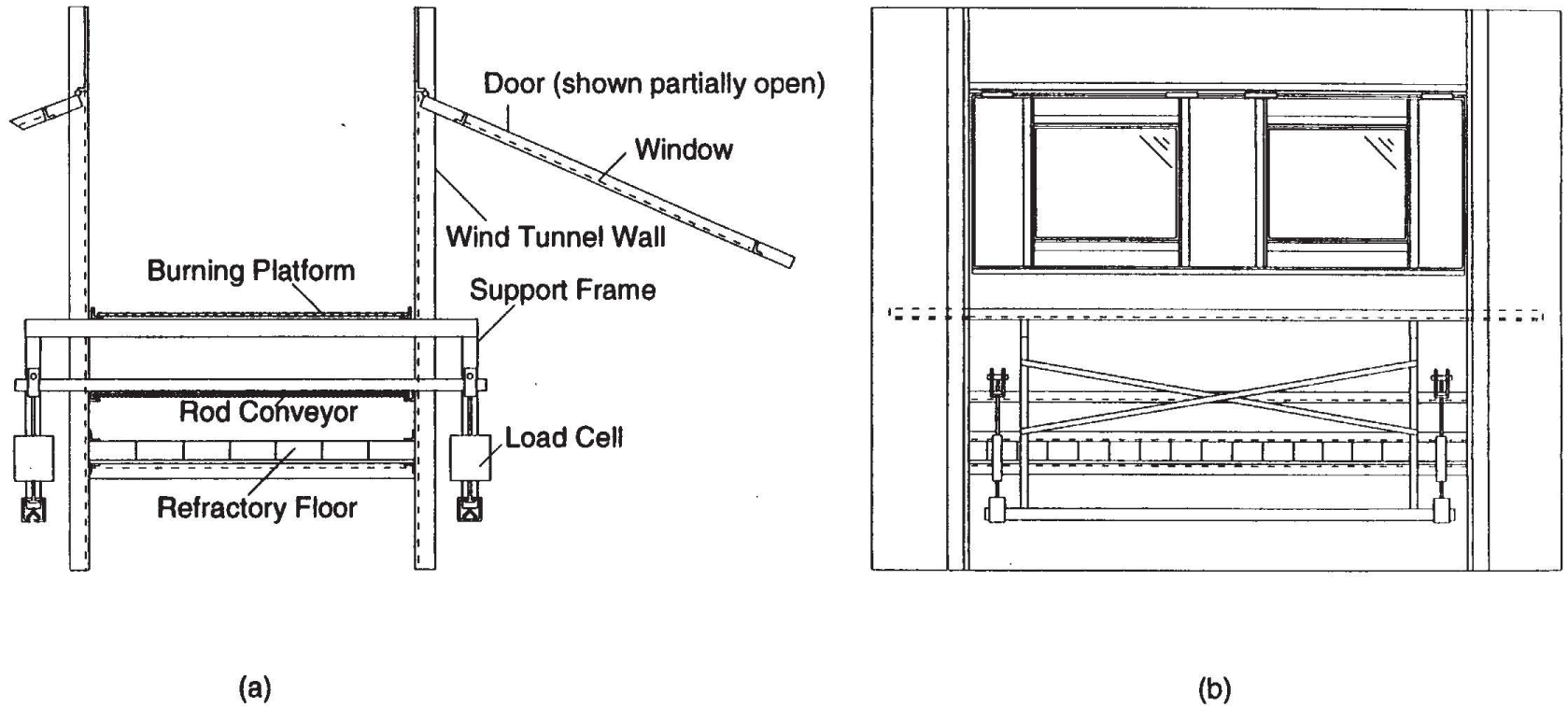

Figure 2.1.4. Sketch of wind tunnel showing weighing platform used with pile fires.
(a) tranverse view. (b) longitudinal view.

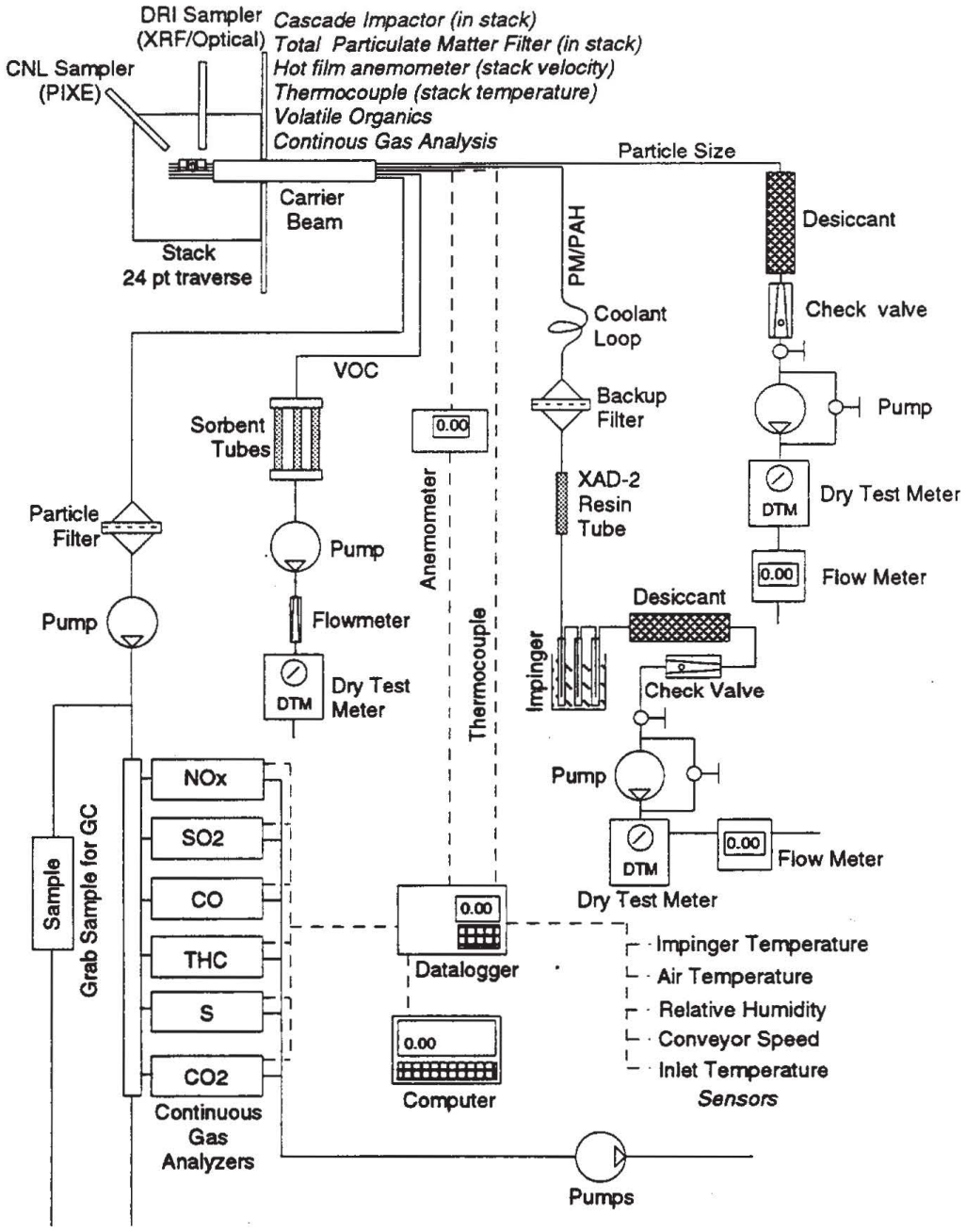

Figure 2.2.1. Schematic of stack sampling and monitoring systems.

Table 2.2.1. Sampling instrumentation and equipment.

Measurement	Device	Method
Total particulate matter	Total filter with back-up filter	Pallflex model TX40HI20-WW 47 mm teflon coated glass fiber filters Isokinetic stack traverse Total filter in-stack Mass concentration: gravimetric
Particle size distribution	Sierra Instruments model 228 cascade impactor	Pallflex model TX40HI20-WW 47 mm teflon coated glass fiber filters Isokinetic stack traverse Impactor in-stack Mass distribution: gravimetric
Particulate matter composition	DRI 4-stage impactor	Teflon and Quartz filters following 2.5 and 10 µm single-stage impactors Isokinetic fixed inlet Mass concentration: gravimetric Elemental: XRF Organic, Elemental Carbon: Thermal/optical reflectance Cl^-, NO_3^-, $SO_4^=$: Ion chromatography K^+, Na^+: AAS NH_4^+: Automated colorimetry
Particulate matter composition and bulk aerosol absorption coefficient	CNL teflon membrane total filter	Anisokinetic fixed inlet 10 m inlet for sample cooling/aging Mass concentration: gravimetric Elemental: PIXE Hydrogen: PESA Bap: LIPM
CO*	continuous analyzer	(1) Anarad model 500, NDIR (2) Anarad model AR-60, NDIR dual channel with CO_2
NO, NO_x	continuous analyzer	Monitor Labs model 8840, Chemiluminescence
SO_2	continuous analyzer	Monitor Labs model 8850, UV Fluorescence
Total S	continuous analyzer	Meloy model SA 285, Flame photometric
THC*	(3) grab/GC (4) continuous analyzer	(3) Hewlett-Packard model 5730A GC, Porapak N column with FID (4) Beckman model 400, FID
CO_2*	(1) grab/GC (2) continuous analyzer	(1) Hewlett-Packard model 5730A GC, Porapak Q column with TCD (2) Anarad model AR-60, NDIR dual channel with CO
CH_4	grab/GC	Hewlett-Packard model 5730A GC, Porapak N column with FID
C_2, C_3 hydrocarbons	grab/GC	Hewlett-Packard model 5730A GC, Porapak N column with FID
Stack gas velocity	hot film anemometer	Kurz model 455
Stack gas temperature	thermocouple	Omega type K, ungrounded 1.6 mm inconel sheath, stack traverse
Impinger outlet temperature	thermocouple	Omega type K, ungrounded 1.6 mm inconel sheath, stack traverse
Inlet air temperature	thermocouple	Omega type T, ungrounded 1.6 mm inconel sheath

Table 2.2.1. Sampling instrumentation and equipment (continued)

Measurement	Device	Method
Ambient air temperature	thermistor	Campbell Scientific model 201 probe
Ambient air relative humidity	sulfonated polystyrene probe	Phys-Chem model PCRC-11 in Campbell Scientific model 201 probe
Conveyor speed and travel	cam activated switch on gear drive shaft	count of switch closures in 1 min
Fuel weight, pile fires	platform suspended on 4 load cells	(2) Interface model SM250 load cells
sample gas volume	dry test meters	
sample gas flow rate	hot film orifice meter	
data recording	electronic	Campbell Scientific CR21X dataloggers with serial output to laptop computers

*Periods of use shown by numbers in parentheses: (1) prior to April 1993, (2) April, 1993, (3) prior to August 1992, (4) August 1992 and later.

the back of the filter holder, and sealed against the stainless tube at the outside end with another tube connector.

Outside the stack, the teflon line continued through a coolant loop in a ambient temperature water bath to a back-up filter in another 47 mm stainless steel holder for collecting any particles formed in the line past the in-stack filter. The back-up filters were also of the teflon coated glass fiber type. Downstream from the back-up filter were a glass trap filled with XAD-2 resin beads for PAH collection, three glass impingers in an ice-bath, desiccant, check valve, air-tight sample pump (Gast model DAA-V132-GB, Gast Manufacturing Corp., Benton Harbor, MI) with inlet and by-pass valves for adjusting flow rate, dry test meter (Singer model DTM-115, American Meter Division, Philadelphia, PA) for total sample gas volume, and a hot-film type flow meter for instantaneous flow rate, all connected with teflon tubing. Isokinetic conditions were maintained by setting pump flow to give inlet velocity equal to stack velocity measured with a hot-film anemometer carried on the traverse beam adjacent to the sample probes.

Three identical probes (consisting of the inlet buttonhook and in-stack filter holder) were used, one for each of two replications and a third serving as a field blank, although occasionally this third probe was also used to collect sample. Filters were weighed and loaded at the Facility for Advanced Instrumentation (FAI) at UC Davis, usually the evening prior to the test. Because the filters were used for PAH analysis, rather than desiccating them, they were equilibrated in the balance case to constant weight. Equilibration under the same conditions at final weighing was done to reduce loss of organic compounds. The probes were capped after loading. The back cap was removed just prior to mounting the probe on the traversing beam. Leak checking was done with the probe capped at the inlet. The front cap was removed just prior to starting the sampling traverse. Following the tests, the probes were capped and returned to the FAI laboratory for filter weighing and extraction for PAH analysis. Immediately after removal from the probes, filters were placed on the weighing pan in the balance case and allowed to come to constant weight, which usually occurred within 10 min. The filter blanks and back-up filter were handled in the same manner, and used to check for any irregularities in the equilibration or weighing procedures. For computing total concentration, the sample weight from the back-up filter was allocated to each total filter collected on the same date according to the proportion of time each traverse occupied out of the total sample time. This generally meant adding 0.1 to 0.2 mg to the total filter

weight, and represented less than 5% of the original total filter mass in all cases except the test of 21 October 92. The back-up filter sample weight obtained on this run was 0.9 mg and amounted to 9% of the total filter weight. Concentrations obtained from the three other samplers used to collect particulate matter (cascade impactor, DRI, and CNL samplers), which included equilibration under desiccant as well as in ambient laboratory air, were compared against the results of the total filter as an additional check on the procedures. As discussed later, the observed particulate matter concentrations from the total filter were consistent with anticipated trends, and showed no apparent difficulties with moisture equilibration. As used here, total particulate matter refers to the total filter fraction, and does not include the condensable fraction of the impingers, as this fraction was analyzed separately for VOC and PAH. The method, which deviates from the standard CARB method 17, utilized the second back-up filter downstream from the primary in-stack filter to collect condensing material.

2.2.1.2. Particle size distribution

Particulate matter size distribution was determined by cascade impactor (Sierra Instruments model 228, Carmel Valley, California). The impactor was mounted in-stack alongside the total filter on the traverse beam. Seven aerodynamic stages were used ahead of the final filter representing approximate size fractions of 15, 8, 5, 3, 1, 0.7, 0.4, and < 0.4 μm. The actual aerodynamic diameters were determined for each test from the flow rates used. The impactor used a 12.7 mm i.d. stainless steel buttonhook inlet with sharp edged nozzle. The lengths of the impactor and total particulate matter inlets were designed to position the nozzle openings in the same longitudinal and horizontal planes, separated by 40 mm. The inlet used on the impactor was shorter than that used for the total filter because of the longer length of the cascade impactor. The clearance between the two probe inlets permitted a thermocouple and hot film anemometer to be placed between them while retaining the standard clearance of 19 mm to avoid probe interference as per CARB methods 2 and 17 (CARB, 1987).

Desiccated, weighed 47 mm diameter teflon coated glass fiber filters were used for all stages of the impactor. Filters for the aerodynamic stages were hand punched. A single impactor was used for all experiments. The impactor was reloaded on site after each test. The filters were unloaded and placed in labeled plastic filter cassettes. The impactor stages were washed in isopropanol and air dried using zero air prior to reassembly. Exposed filters were desiccated prior to final weighing.

The impactor was mounted onto a 12.7 mm diameter stainless steel tube running the length of the traversing beam in the same manner as the total filter probe. The outlet of the stainless steel tube was connected via a polyethylene tube to a desiccant canister, check valve, air-tight sample pump with bypass valve, dry test meter for total volume, and flow meter for instantaneous flow rate (Figure 2.2.1). The probe inlet opening was sized to give isokinetic conditions in the neighborhood of 20 L min^{-1}, previously determined to be an effective flow rate for the impactor.

2.2.1.3. Source profiling, DRI sampler

Chemical analyses of particulate matter were carried out by staff of the Desert Research Institute (DRI), University of Nevada, Reno. The results of these analyses serve as source profiles for emissions from the individual fuels. The sampler used to collect the samples for these analyses was constructed by DRI and consisted of a single isokinetic inlet ahead of four single stage impactors and filters. Two size fractions were collected on each of two different filter media. Particles in the two size classes 10 μm aerodynamic

diameter or less (PM10) and 2.5 μm or less (PM2.5) were collected on both teflon membrane filters and pre-fired quartz fiber filters. The flow rate through each impactor and filter was held constant at 10 L min^{-1}. The inlet flow was kept isokinetic by over-sampling the stack gas flow, with the excess gas simply exhausted to atmosphere. All lines connecting filters to the flow metering system were labeled according to filter type and size fraction. The impactors were also labeled by filter type and size fraction and matched accordingly to the sample lines to retain calibration. Details of the construction are provided by Pritchett, et al. (1992).

The inlet for the DRI sampler was fixed in the stack approximately as shown in Figures 2.2.1 and 2.1.3. Access was through the top of the stack with the nozzle pointing into the upward stack flow. The nozzle was located overhead of the traverse beam between two lines of traverse. Flow rates through each of the filters were determined by pressure drop across calibrated orifices. Differential pressure was observed manually throughout each sampling period. Deviations from set-point were corrected by manually adjusting a regulating valve in each line. Make-up flow rate was set on the basis of the stack velocity measured with the hot-film anemometer mounted on the traverse beam. Before starting the DRI sampler, the stack velocity was measured in the vicinity of the inlet nozzle, and the make-up orifice set-point pressure drop read from a calibration chart.

All filters were loaded into and unloaded from the filter holders at DRI. Loaded filters were capped front and back, labeled, bagged in plastic, frozen, and shipped overnight to UCDavis in insulated containers on blue ice. Filters were kept frozen until shortly before the time of use. Filters were labeled in pairs. Each pair contained one teflon filter and one quartz filter labeled T and Q respectively. When loaded into the impactors, the back filter cap was removed first, then the front cap, and the filter holder outlet connected to the flow metering system by the appropriate sample line. Two O-rings were used to seal the filter holders against the impactor outlet tubes. The sampler inlet nozzle was kept capped until initiating sampling. Sampling times were set to yield 1 to 4 mg total sample mass on each filter. Because particulate matter concentrations were not known *a-priori*, sampling times were estimated based on observations of stack opacity and fire characteristics. Typical sampling time was 20 to 40 minutes. Sampling times were adequate to collect desired sample mass, except in the case of one traverse during smoldering with Douglas fir. Field blanks were obtained on each test date by loading a pair of filters (one each teflon and quartz) into the sampler, but not pulling any flow. The blanks were left in the sampler for the same length of time as the exposed filters, and otherwise handled in the same manner. Laboratory blanks were retained by and analyzed at DRI.

After sampling, filters in the filter holders were unloaded from the impactors, capped, bagged, and placed in an insulated container on blue ice. The container with filters was shipped overnight to DRI on the day of sampling or held in a freezer until shipment. The sampler inlet system and impactors were disassembled and cleaned with methanol, triple rinsed with distilled water, and air dried in a clean room prior to any subsequent test. All openings were sealed with clean plastic film until reassembly on the wind tunnel.

Teflon membrane filters were equilibrated in air at 20±5°C and 30±5% relative humidity for 24 h prior to weighing. PM10 and PM2.5 mass concentrations were determined from the teflon filters, and were compared with the total filter determinations, as discussed later. Teflon filters were analyzed by X-ray fluorescence (XRF) for 38 elements Al through U. Punches from the quartz fiber filters were analyzed for elemental and organic carbon using a thermal/optical reflectance (TOR) method. Extracts from the quartz filters were analyzed for Cl^-, NO_3^-, and $SO_4^=$ by ion chromatography, K^+ and Na^+ by atomic

absorption spectrophotometry, and NH_4^+ by automated colorimetry. The procedures used in the analyses were described in detail by Chow (1987). Analysis flags describing certain attributes of the filters and the analysis were assigned by the DRI analyst at disassembly and during analysis. These flags are defined in Table 2.2.1.3.1. Analysis flags for specific elements were also assigned where errors were known or suspected, and appear in the results.

Table 2.2.1.3.1. Analysis flags assigned to filter samples by DRI.

Flag	Description
H	filter holder assembly proble
F5, f3	teflon membrane substrate separated from support ring
i1	inhomogeneous sample deposit
i4	foreign particles on filter
S, s	sample validity suspect
V, v	sample invalid
w6	mass estimated based on PM2.5/PM10 ratio

2.2.1.4. Source profiling and absorption coefficient, CNL sampler

Another fixed sampling inlet was located in the wind tunnel stack for chemical characterization of particulate matter by the Air Quality Group of Crocker Nuclear Laboratory (CNL), UC Davis. The location of the inlet is shown in Figures 2.1.3 and 2.2.1. This inlet consisted of 38 mm diameter aluminum tubing with the opening placed just overhead of the stack and the entrance aligned 90° to the flow direction. The inlet descended vertically some 10 m to ground level. Details of the inlet design and sampling procedures were given by Campbell (1992). The long inlet was intended to provide additional smoke aging and cooling for polar nephelometer measurements undertaken as part of Campbell's study. The results of those analyses are reported elsewhere (Campbell, 1992). A series of tests were conducted to evaluate particle diffusion to the walls of the inlet tube. A comparison of filter samples collected at the top of the stack and at ground level found good agreement in total mass concentrations, with only 1% indicated loss. Fairly good agreement was found as well for scattering coefficients determined from the filter samples.

All sampling was done at ground level. Two-stage oil free pumps with flow restricting ball valves were used to pull the sample at approximately 50 L min^{-1}, yielding an inlet velocity of approximately 0.7 m s^{-1}. No attempt was made to adjust the flow to maintain isokinetic conditions at the inlet. For the size class below 8 μm, a Stokes number analysis indicated little particle size bias based on the expected anisokinetic conditions (Campbell, 1992). Cascade impactor results showed most of the particulate mass to be in the size class below 8 μm, and little loss was expected overall. Comparisons of chemical analyses of particulate matter collected using this inlet with those collected through the DRI inlet, which was maintained isokinetic, showed few discrepancies. As discussed later, comparisons with other particle samplers show the total concentrations from the CNL samples to be lower in general, suggesting influences due to the anisokinetic conditions, particle loss to the walls of the long inlet, or errors in sample flow rate determination.

The sample flow rate was monitored by pressure drop on a calibrated orifice. Samples were collected on pre-weighed 47 mm teflon membrane filters mounted in polycarbonate filter holders. Filters were loaded, labeled, and leak-checked under clean laboratory air. Prior to loading, the opacity of each filter was measured using a laser integrating plate method (LIPM). The result of this analysis was used with LIPM measurements of the exposed filter to determine absorption coefficient. After loading, the filters were capped and boxed. Sampling was done through a tee with flanged aluminum adapters at the base of the inlet. A filter holder containing a clean filter was held against a face gasket on one side of the tee, while a dummy holder and filter were installed on the opposite side of the tee. The dummy filter was connected to the sample pump with air-tight snap-in tube connectors. The pump was started, and the sample flow rate set, and the inlet line purged. The dummy filter was then disconnected, and the clean filter connected to the pump. Usually only very small adjustments to the flow rate were needed following the filter change. Sampling times were typically on the order of 3 to 20 min per filter, depending on the type of fire. After sampling, the pump was shut off, and the filter holder removed with the filter and capped.

The filters were submitted to gravimetric analysis for mass concentration, LIPM for optical analysis, and particle induced x-ray emission (PIXE) analysis for characterization of elements heavier than aluminum. Hydrogen was concurrently analyzed by proton elastic scattering analysis (PESA). PIXE and PESA analyses were carried out using the cyclotron at CNL. Procedures for the analyses conducted at CNL were described by Campbell (1992) and the procedures for PIXE and LIPM by Cahill, et al. (1984). LIPM yields a bulk determination of the absorption coefficient for the particle deposit based on the fraction of laser light transmitted through the deposit. An estimate of the aerosol absorption coefficient due to particles was obtained by dividing the bulk absorption coefficient by an imaginary path length given as the ratio of the sample gas volume to the exposed filter area.

2.2.1.5. DRUM samples

Size fractionated samples for PIXE/PESA analyses were collected during the full runs from 10 July through 23 October 92. The samples were collected from the same inlet as the CNL total filters using an eight stage Davis rotating universal-size monitor (DRUM) impactor (Cahill, et al., 1987). This device collects samples on continuous teflon strips wrapped around individual drums. Size selective inlets segregate the particles into size fractions of 10 - 15, 5 - 10, 2.5 - 5, 1.15 - 2.5, 0.56 - 1.15, 0.34 - 0.56, 0.24 - 0.34, and 0.07 - 0.24 μm. The DRUM sampler is designed for continuous monitoring, but in this case was used without the motor drive. For each test, a sample was collected at a single location on each strip. The drums were rotated to displace each subsequent sample 2 mm along the strips. The sampler was not available for use after 23 October 92.

The strips were analyzed in the same manner as the CNL total filters. When loaded into the accelerator, the detectors were aligned on the first sample spot on the strips. Following analysis on each spot, the strips were advanced 2 mm automatically to the next sample spot. Because the samples were not precisely located at 2 mm intervals, the analysis was not always performed with the same deposit density, and are strictly qualitative. The results are therefore used only to show relative element concentrations and relative abundance within samples.

2.2.2. Gas analysis

Gas analysis was performed using continuous on-line analyzers and by taking grab samples for later analysis by gas chromatography (GC). The sampling system is schematically illustrated in Figure 2.2.1, with additional detail in Figure 2.2.2.

2.2.2.1. Continuous gas analysis

Continuous analyzers were available initially for CO, NO, NO_x, SO_2, and total sulfur. A total hydrocarbon (THC) analyzer was added after the first few tests. CO_2 analysis on all spreading fires was accomplished by GC, but after the first pile burn, continuous CO_2 analysis was added. The original CO analyzer was replaced with a new CO analyzer concurrently with the addition of the CO_2 analyzer. The final analyzer arrangement is shown in Figure 2.2.2. All analyzers included scaled voltage outputs which were monitored continuously via electronic datalogger and computer, with screen display and final storage on disk (see section 2.2.5 below).

The CO analyzer used initially was an Anarad model AR-500 (Anarad Inc., Santa Barbara, California) unit employing infrared absorption. This analyzer was more prone to zero drift than any of the other instruments, and was plumbed with a separate zero-air source for frequent zero check. The subsequent CO/CO_2 analyzer was an Anarad model AR-60 using infrared absorption over a longer path length with much less zero drift. The NO_x analyzer was a Monitor Labs model 8840 chemiluminescent type (Monitor Labs, San Diego, California). The SO_2 analyzer was a Monitor Labs model 8850 fluorescent type. Both these analyzers were found in practice to be quite stable. The total hydrocarbon analyzer was a Beckman model 400 (Beckman Instruments, Fullerton, California) using a flame ionization detector (FID). This analyzer was also quite stable. The total sulfur analyzer was a Meloy model A285 flame photometric type (Meloy Laboratories, Springfield, Virginia). This analyzer was highly sensitive to the level of CO_2 in the sample gas, and was used principally to give qualitative comparisons with the SO_2 analyzer. Response of all instruments was found to be linear with the exception of the total sulfur analyzer with increasing concentrations of CO_2. The response of the total sulfur analyzer to blends of SO_2 calibration gas in zero air, and in zero-air with CO_2 is shown in Figure 2.2.3. The instrument was first calibrated at 1.9 ppmv SO_2 in zero air. When further diluting with zero air, the analyzer overestimated at intermediate concentrations. In blends using CO_2, the analyzer response at 0.4 ppmv SO_2 and 4,100 ppmv CO_2 was about half the expected value.

All analyzers were stabilized prior to each test and calibrated before, after, and between experiments on each date. Calibration gases were obtained in concentrations close to those expected in the stack. A total of five calibration gas cylinders were used, with concentrations given in Table 2.2.2.1. The first cylinder was used routinely to calibrate the CO, NO_x, and SO_2 analyzers, but because it did not contain any oxygen, could not be used to calibrate the total sulfur analyzer. A separate cylinder (cylinder 3 in Table 2.2.2.1) was used to calibrate this instrument (cylinder 3 was obtained at a later date and with a lower SO_2 concentration to better match actual values). The second cylinder was used to calibrate the CO_2 and THC analyzers. This cylinder was originally specified to contain 5 ppmv of ethane as well, but this was inadvertently left out, and a separate cylinder (cylinder 4) was obtained. The ethane cylinder was used only for GC calibrations and not for the THC analyzer calibrations. A fifth cylinder containing 10 ppmv hydrogen was used for GC calibrations. The hydrocarbon analyzer was calibrated using a single composite value computed according to the manufacturer's published relative detector response for each of the hydrocarbon compounds in cylinder 2.

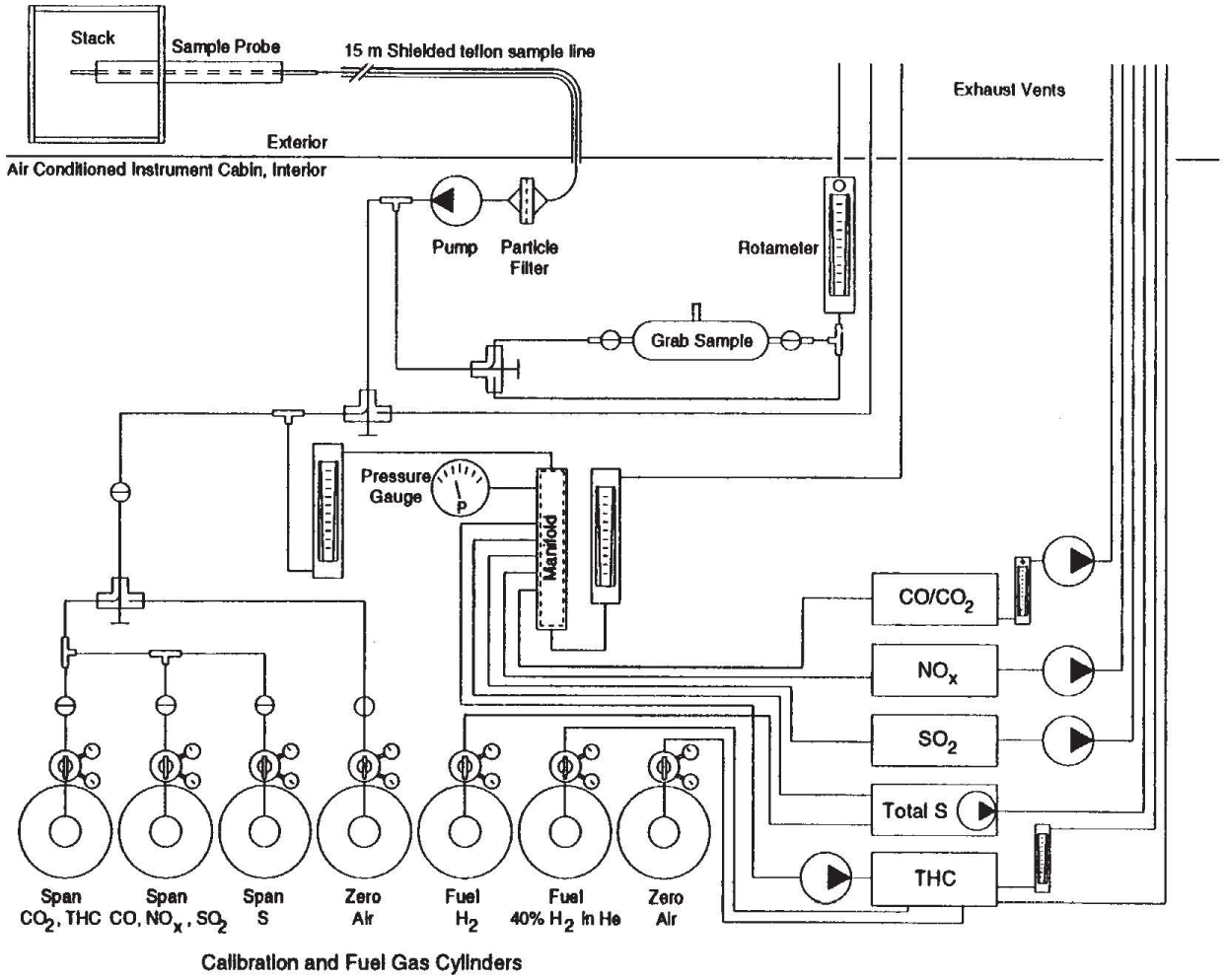

Figure 2.2.2. Plumbing schematic for continuous analyzers and grab sample system.

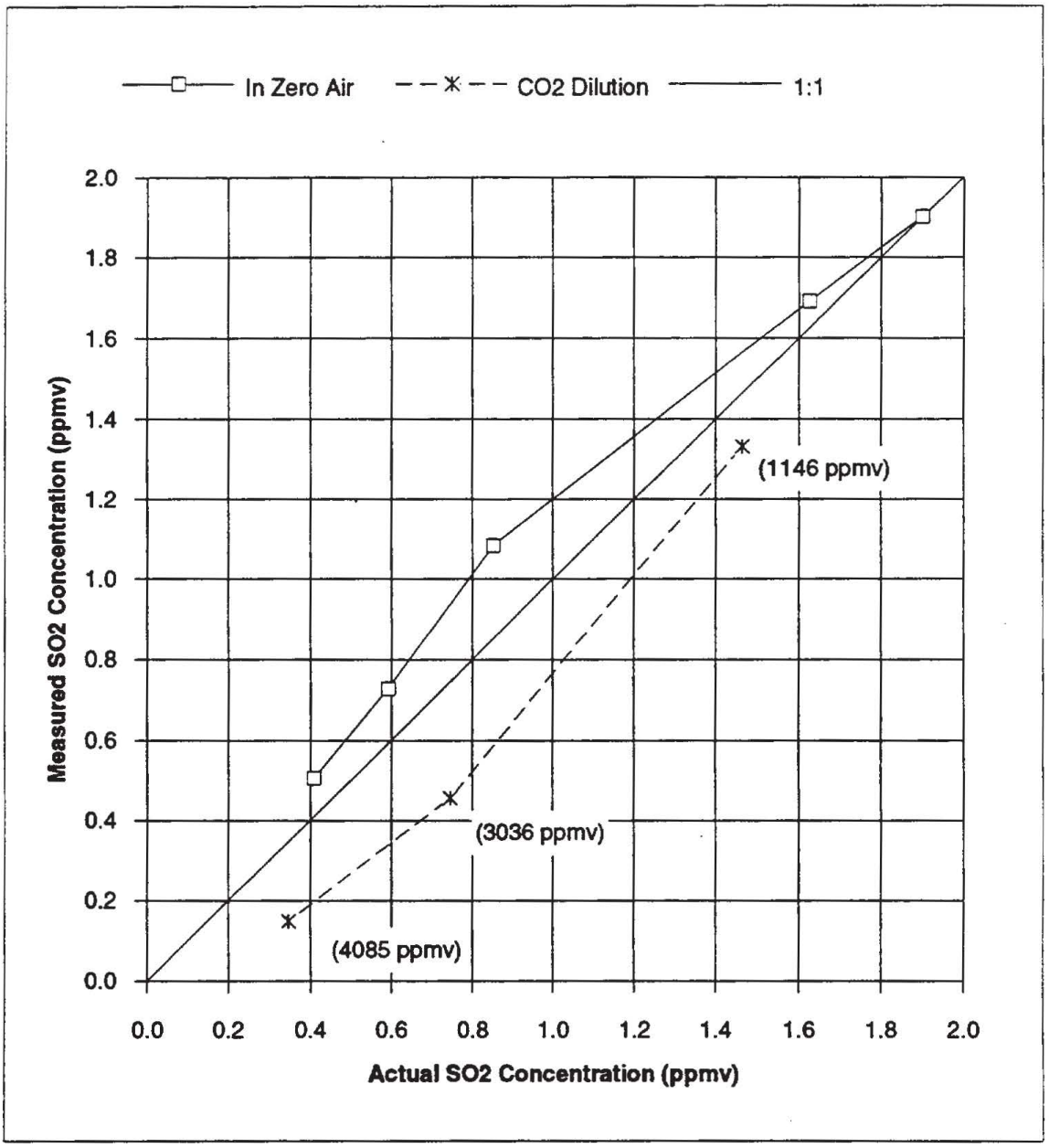

Figure 2.2.3. SO2 concentration from total sulfur analyzer for blends of SO2 in zero air and with varying concentrations of CO2. Instrument calibrated at 1.9 ppmv SO2. CO2 concentrations shown in parentheses.

The gas sample was collected as shown in Figure 2.2.2. The sample was drawn through a 6 mm (0.25 inch) o.d. stainless steel inlet tube extending through the traverse beam to the position of the total filter and cascade impactor inlets. The outer end of the tube was connected to a 15 m long, 6 mm (0.25 inch) o.d. teflon tube running from the sampling platform to the air conditioned instrument cabin housing the analyzers. The teflon sampling tube ran inside a 25 mm i.d. opaque black polyethylene tube from the top of the stack to the instrument cabin. The outlet of the teflon tube was connected to a filter holder.

Table 2.2.2.1. Calibration gas concentrations (ppmv).

	Cylinder 1	Cylinder 2	Cylinder 3	Cylinder 4	Cylinder 5
SO_2	4.93		1.90		
NO	8.00				
NO_x	8.18				
CO	207	99.6			
CO_2		4994.8			
CH_4		25.0			
C_2H_2		5.0			
C_2H_4		5.0			
C_2H_6				5.0	
C_3H_8		5.0			
H_2					10.0
N_2	Balance				
Air		Balance	Balance	Balance	Balance

Particles were separated from the flow on 25 mm diameter teflon coated glass fiber filters. The outlet of the filter holder was connected to an air-tight teflon-lined sample pump. From the pump, the flow was split to provide sample for the continuous analyzers as well as the grab sampling system. All valves and tubing were either stainless steel or teflon, with the exception of the rotameters which had polycarbonate cases.

The analyzer flow was directed through a three-way valve to the sampling manifold through a rotameter to monitor flow rate. When calibrating, the sample flow was simply directed to exhaust by rotating the three-way valve. Separate pumps on each analyzer drew sample from the stainless steel manifold at the required flow rates. A pressure gage was used to monitor manifold pressure, which was normally between 50 to 75 mm of water positive pressure. The outlet of the manifold was connected to the exhaust through a rotameter. The purpose of this outlet rotameter was to insure the flow to the manifold was in excess of that drawn by the analyzers. Plugging of the inlet particle filter became obvious as the manifold outlet rotameter indicated reduced flow. The filter was changed at such times. Calibration was done with the manifold outlet rotameter indicating the same flow as when sampling.

For calibration, the sample flow was diverted to exhaust, and the required zero or span gas fed to the manifold through the valving arrangement shown in Figure 2.2.2. Calibration gas flow was adjusted with the regulators on each cylinder. Loss of flow to the analyzers was prevented by opening the cylinder prior to diverting the sample flow to exhaust. With sufficient flow established from the calibration cylinder, the sample flow was removed by rotating the three-way valve, and the calibration gas flow adjusted to set the manifold outlet flow equal to the outlet sample flow. The manifold was allowed to fully purge with calibration gas and all analyzers allowed to reach a steady reading before any adjustments were made to the analyzers. Following calibration and prior to each test, background readings of ambient air were obtained from the stack. These were then used to provide background correction for the concentrations obtained during the fires.

Not shown in Figure 2.2.2 is a modification made in the sampling system when using the original CO analyzer. A separate line was run from the zero-air cylinder to the inlet of the CO analyzer through one port of a three-way valve, the other inlet port opening to the sample flow. In this way, the sample flow could be rapidly diverted from the CO analyzer only, and zero-air supplied to the analyzer to check for zero drift. The zero-air flow was set prior to each test to insure that the pressure in the analyzer gas column was the same as when sampling. Zero-drift was not a problem with the replacement analyzer, and this system was eliminated when the new analyzer was installed.

Also shown in Figure 2.2.2 is the plumbing arrangement for the fuels used with the THC and total S analyzers. The THC analyzer used a 40% hydrogen in helium fuel, with zero-air supplied as the oxidant for the FID. The total S analyzer utilized pure hydrogen fuel, with zero-air oxidant supplied by drawing cabin air through a charcoal filter. Separate teflon particulate filters were supplied by the manufacturer in the inlet lines of the NO_x and SO_2 analyzers. In practice, these were never observed to load, indicating good particle removal by the inlet filter ahead of the sampling pump. The sampling system was leak checked by plugging the stainless steel sampling inlet in the stack, closing off the grab sample line, and observing the sample flow at the manifold inlet. Beyond the pump, the sample was above ambient pressure. The inlet stainless steel and teflon lines were cleaned prior to the tests on each date.

2.2.2.2. Grab samples

Grab samples were collected in 500 mL glass flasks as illustrated in Figure 2.2.2. These flasks had either glass or teflon stopcocks and a sample extraction stem sealed with a silicone rubber septum. The stopcocks were sealed with silicone grease. The contents were analyzed by GC for H_2, CO, CO_2, CH_4, C_2H_2, C_2H_4, C_2H_6, C_3H_8, O_2, and N_2. The sample was collected by purging the flask with sample at 2 to 3 L min^{-1} for approximately 3 min, closing both stopcocks, and diverting the sample flow to exhaust by rotating the inlet three-way valve. The sample was under slight positive pressure. The flow through the grab sampling system was controlled via the valve on the outlet rotameter. The septum on the sampling vessel was replaced prior to each test.

The samples were analyzed within 48 hours on a Hewlett-Packard 5730A gas chromatograph. A 100 mL sample was withdrawn through the septum by syringe for injection into the GC. CO, O_2, and N_2 were analyzed by thermal conductivity detector (TCD) following separation on a 1.8 m x 3 mm molecular sieve 5A column with injector temperature at 150°C, detector temperature at 200°C, and oven temperature at 80°C. Helium was used as the carrier gas. CO_2 was analyzed on the TCD following separation on a 1.8 m x 3 mm Porapak Q column at an oven temperature of 45°C using helium carrier gas. H_2 was analyzed on the TCD after separation on the mol sieve column but

using a nitrogen carrier gas. Hydrocarbons were analyzed by flame ionization detector (FID) following separation on a 1.8 m x 3 mm Porapak N column with nitrogen carrier gas and 50°C oven temperature. The GC was calibrated prior to each run of 10 to 12 samples using the same gases listed in Table 2.2.2.1. The calibration was done by purging and filling a glass sample vessel with calibration gas at approximately the same pressure as the samples, and extracting the calibration sample and injecting it into the GC in the same manner as a test sample.

2.2.3. VOC sampling

The sampling protocol for volatile organic compounds (VOCs) was based on the sampling principles for a dual sorbent bed mini-VOST as described by James et al. (1986). A similar dual sorbent methodology was utilized by Chang (1988) for pilot-scale hazardous waste incinerator studies at the USEPA laboratory in Cincinnati. The volatile and semi-volatile compounds other than the PAHs were collected on dual bed sorbent tubes (Carbotrap 200/Carbon Molecular Sieve III - Supelco, Inc. Bellafonte, PA). The samples were drawn through a single 6 mm (1/8") o.d. teflon tube at approximately 90 mL min^{-1} and distributed through each of three sorbent tubes mounted in parallel as shown in Figure 2.2.1. The teflon tube was pushed through a 6 mm (0.25 inch) stainless steel support tube extending through the traversing beam. The tube inlet was positioned next to the total filter and cascade impactor inlets, and traversed the cross section of the stack with the other inlets. The sample tubes were shielded from direct sun light by covering them with aluminum foil. The sample pump (SKC Model 224-PCXR7, Fullerton, CA) was set to sample for pre-determined sampling periods. The total gas volume sampled through the three tubes was recorded with a dry gas meter (Singer model DTM-115, American Meter Division, Philadelphia, PA).

Prior to sampling, the flow rate to each sample tube was measured using a soap bubble flow meter. The flow rates were generally set in the range of 20 to 30 mL min^{-1} using an adjustable flow restriction in the sampling manifold.

Sorbent tubes were thermally desorbed in order to remove contaminants prior to use. Nitrogen gas was flushed through the tubes at the rate of about 50 mL min^{-1} while heating the tubes at 300 to 350°C for two hours in a tube conditioner unit (Envirochem Model TC-01, Kemblesville, PA).

In order to compute or estimate compound concentrations, standards were loaded onto previously cleaned sorbent tubes. The standard gas contained benzene, toluene, and styrene. Naphthalene was delivered to sorbent tubes from a liquid solution by syringe to the glass frit of the sorbent tube and evaporating the standard into a stream of nitrogen. Standards were analyzed at the same time as the samples. Samples were analyzed within 24 hours of the experiment and typically within about six hours.

The samples were analyzed by gas chromatography (Hewlett Packard 5890A) on an system equipped with a mass selective detector (Hewlett-Packard 5970 Series MSD) and data acquisition and analysis system (Hewlett-Packard Chem Station 59970). Samples were introduced onto a 30 m long DB-624 (J&W Scientific, Folsom, CA) capillary column using a capillary column inletting system (Environchem Unacon Series 810A, Kemblesville, PA). The GC was operated at a nominal helium flow rate of 1 mL min^{-1}, with a temperature program of 4 min hold at 40°C followed by a 10°C min^{-1} increase to 250°C with a total analysis time of 27 min. The MSD was operated in full scan mode collecting ions from 40 to 350 mass/charge ratio, with a 1 Hz scan rate.

The Hewlett Packard Chem Station software was used with the Wiley.L mass spectral library program to assist in the identification of compounds. Tentative identifications were checked with the boiling point of the tentative compound and its retention time on the DB-624 column. Because of co-elution and in some cases a high background level, the mass spectral library search did not always produce reasonable matches or misidentified compounds. By manually subtracting the adjacent background signal to reduce the presence of co-eluted mass fragments, and by using selective ion integrations, a more positive identification of a compound was possible. Compound boiling points were then checked to determine if the retention time on the column was close to that expected for the peak identified by the library search.

Concentrations of compounds, for which standards were available, were determined from the average of the tube samples corrected for the sample volume drawn through each tube. For those compounds which did not have standards, but for which positive identifications could by made, an approximate concentration was determined by comparison of the area of the toluene sample peak with the unknown sample peak. The method produces only an order of magnitude concentration (probably within a factor of three) because the ionization efficiency and number of ion fragments produced are not necessarily equal for toluene and the unknown compound.

In the case of naphthalene, there were problems with the standard delivery method in several of the initial sample runs so that the concentration of naphthalene reported was again based on the ratio of the toluene to naphthalene peak areas for standards and the sample in question.

The compounds identified over all fuel tests are listed in Table 2.2.3.1. The identification of dimethyloxirane is a possible mismatch. A number of significant peaks were not matched against specific species, and these are listed by retention time (min) in the table.

2.2.4. PAH sampling

The sampling system for polycyclic aromatic hydrocarbons (PAH) is shown schematically in Figure 2.2.1. Sampling was done through the total filter inlet described above. A continuous 9.5 mm (3/8" inch) o.d. teflon tube ran from the outlet of the total filter holder, through the 12.5 mm (0.5 inch) stainless steel support tube in the traverse beam, through an ambient temperature water bath, to the inlet of the stainless steel back-up filter holder. The teflon tube wall was sealed against the outlet end of the 12.5 mm stainless steel support tube in the traverse beam to prevent ambient air from moving up into the tube inlet in the total filter holder. The back-up filter was a 47 mm diameter teflon coated glass fiber filter of the same type used for the total filter. The back-up filter holder was connected via a teflon tube to a foil wrapped XAD-2 resin bead filled glass trap. A sintered glass frit retained the resin beads on the trap outlet side, and a glass wool plug was used in the inlet following filling. The traps were kept capped until installation in the sample line. They were always shielded with an aluminum foil wrapping. From the trap, sample flow passed via teflon tubing to a three stage glass impinger train in an ice bath. A thermocouple placed in the outlet of the impinger trap was used to continuously monitor outlet temperature. The impinger tips were all of the straight design ending 13 to 19 mm above the bottom of the impinger flasks. The outlet of the final impinger was connected to a desiccant canister. From there, the sample flowed through a check valve to the inlet of the air-tight sample pump, through a dry test meter for total volume, and finally through a hot film type flow meter to exhaust. The bypass and inlet valves of the pump were used to keep the inlet flow isokinetic as described for the total filter. Flow rate was set on the basis of the stack velocity monitored on the hot film anemometer carried on the traverse beam adjacent to the probe inlets in the stack.

Table 2.2.3.1. VOC compounds identified in wind tunnel samples.
(arranged by carbon number and molecular weight).

	C	H	O	N	Cl	Approximate Molecular Weight
Acetic acid	2	4	2			60
Propanone (acetone)	3	6	1			58
Methyl ester acetic acid (methylacetate)	3	6	2			74
Butane	4	10				58
Dimethyloxirane*	4	8	1			72
Pentene	5	10				70
Methylbutanone (isopropylmethyl ketone)	5	10	1			86
Furancarboxaldehyde (furfural)	5	4	2			96
Benzene	6	6				78
Dimethylbutane	6	14				86
Hexane	6	14				86
Phenol	6	6	1			94
Dimethylfuran	6	8	1			96
2-methyl 2-cyclopenten-1-one	6	8	1			96
2-chloro phenol	6	5	1		1	129
Toluene	7	8				92
Benzonitrile	7	5		1		103
Benzaldehyde	7	6	1			106
Methylphenol (hydroxy toluene)	7	8	1			108
Styrene	8	8				104
Xylene	8	10				106
Trimethylpentane	8	18				114
Benzofuran	8	6	1			118
Methoxymethylphenol (creosol)	8	10	2			138
Naphthalene	10	8				128
Unknown†	10	12				132
Alpha-pinene	10	16				136
Camphene	10	16				136
Δ3-Carene	10	16				136
Limonene	10	16				136
No match r.t. (6.7)						
No match r.t. (8.51)						
No match r.t. (8.71)						
No match r.t. (8.73)						
No match r.t.(6.4)						
No match r.t.(8.5)						

*possible alternatives include butanal, iso-butanal, 2-butene-1-ol, methallyl alcohol, butanone, tetrahydrofuran

†Possible compounds: alpha-dicyclopentadiene, 1-methyl indan, 2-methyl indan, tetralin (1, 2, 3, 4 tetrahydronapthalene)

Prior to the first test on each date, the cleaned and capped impingers and the desiccant canister were weighed. The first and third of the three glass impingers were loaded empty into the ice bath. The second impinger was loaded with 100 g of distilled water (determined by weighing the impinger while adding water) in the manner of CARB method 428 (CARB, 1987). The impinger arrangement of method 428 satisfies the requirements of method 429 as well, and was used throughout.

The total filter, inlet probe, and resin trap were changed prior to each test on each date. The impingers, desiccant, back-up filter, and teflon tubing were not changed between tests, but were instead used for all tests on each date. Impinger, tubing and back-up filter contents therefore represented integrated samples collected for a single fuel burned in a single configuration. Results from the total filter and resin trap give indications of repeatability among replicates. Due to the high levels of PAH observed, background samples were not collected for each test. Ambient levels were estimated to contribute not more than a few percent of total PAH for these analyses.

Following the completion of each test, the inlet probe including the filter holder and filter was capped front and back. The XAD-2 resin trap was removed, capped, and wrapped completely in another layer of aluminum foil. A new probe and resin trap were installed for the next test. At the completion of all tests for each date, the entire system was disassembled to the check valve. In addition to the probes and traps, the inlet teflon tube was capped on both ends. The impingers were capped and weighed. The desiccant trap was also weighed.

Filters and XAD-2 sorbents were Soxhlet extracted for 16 hours using dichloromethane after addition of perdeuterated PAH internal standards. Impingers were analyzed using liquid-liquid extraction (again using dichloromethane). Extracts were cleaned up using sequential column chromatographic steps with silica gel and alumina as column packing. PAH concentrations were determined using GC/MS and stable isotope dilution.

Although CARB Method 429 specifically indicates the method is not suitable for determining the partitioning of PAH among the different parts of the sampling train, individual components were analyzed separately to provide at least qualitative evaluations of the filter and sorbent fractions. Primary and back-up filters were analyzed separately. Impinger analyses were also used to check for breakthrough. In later samples, line rinses were combined with impinger extracts. Surrogate standards were added only to the XAD-2 sorbent modules.

Selected ion monitoring of molecular ions for all target analytes and standards was performed instead of full scanning analysis. Two groups of ions were monitored, with the first group consisting of anthracene and all targets eluting earlier, and the second group consisting of all analytes eluting after anthracene. Low resolution MS analysis was performed on a VG Trio-2 quadrupole GC/MS system. Limits of detection were judged to range from 2 - 50 ng depending on sample.

Target species included the 16 EPA priority PAH compounds plus 2-methylnaphthalene, benzo[e]pyrene and perylene. Deuterated standards were not available for 2-methylnaphthalene at the time of method development, naphthalene-d_8 was used as internal standard for this analyte.

2.2.5. Data acquisition and monitoring

Ambient and wind tunnel conditions were continuously monitored throughout each test using electronic dataloggers (Campbell Scientific model CR21X, Logan, Utah) incorporating analog-to-digital signal conversion and computers for partial data reduction, screen display, and recording on disk. The monitoring system is illustrated in Figure 2.2.1. This system recorded stack gas temperature, stack gas velocity, impinger outlet temperature, combustion test section inlet air temperature, ambient air temperature and relative humidity, conveyor speed (spreading fires only), and outputs from each gas analyzer. Responses from each sensor were recorded at one minute intervals, with the exception of the stack anemometer and conveyor speed transducer as noted below.

The stack gas temperature and impinger outlet temperatures were read using 1.6 mm o.d. inconel sheathed ungrounded type-K (chromel-alumel) thermocouples. Combustion test section inlet air temperature was monitored using a type-T (copper-constantan) thermocouple of similar construction.

Ambient air temperature was monitored by a thermistor located in the same mount as the ambient air relative humidity sensor. Relative humidity was obtained from a sulfonated polystyrene grid transducer (Phys-Chem Scientific model PCRC-11, New York, New York). Both sensors were situated in a gill radiation shield located adjacent to the wind tunnel. These sensors were eliminated when the continuous CO_2 analyzer was added due to the need to provide an additional input channel on the datalogger. After this, the ambient conditions were instead obtained from a weather station located approximately 1.5 km away from the wind tunnel test site and operated as part of the California Irrigation Management Information System (CIMIS). Average hourly data were available via modem from the central CIMIS storage computer in Sacramento, California. Previous comparisons of data from this weather station with data collected at the wind tunnel site showed very little difference.

The stack gas velocity was monitored with a single-axis hot-film anemometer (Kurz Instruments model 455, Carmel Valley, California) carried on the traverse beam between the total filter and cascade impactor probes (Figure 2.1.3). The anemometer output was sampled at 1 s intervals and averaged over 1 min for final storage. This anemometer was reported to be tolerant of particle-laden gas flows. The hot-film anemometer was adopted after tests with a standard S-type pitot-tube revealed the dynamic head too low to be read accurately (Jenkins, et al., 1993a). The anemometer employed two films, one to sense gas temperature and the other held at a temperature 100 K hotter and sensing gas velocity. The anemometer was calibrated in a wind tunnel at the Mechanical, Aeronautical, and Materials Engineering Department, UC Davis, and checked in the stack against another hot-film anemometer calibrated in a precision bench top wind tunnel (TSI Instruments model 8390, St. Paul, MN). The observed stack gas velocity was later compared with an estimated stack gas velocity computed via carbon balance (see Results). Under conditions of low flame radiation, such as occurred with spreading fires, the observed and computed velocities were similar. For pile fires, discrepancies between the measured gas velocities and those derived from carbon balances were found during the intense stages of flaming combustion. Under the more intense flame radiation from the pile fires during the flaming stages, radiation heat gain by the transducer offset convective heat loss. The higher radiation load would have reduced the necessary sensor heating, and caused a low output signal from the anemometer as the controller sought to maintain constant film temperature. This is believed to have produced errors in the direct measurement of stack gas velocity during the flaming stages of the pile fires.

Conveyor speed and total distance moved (conveyor travel) were monitored using an eight-lobed cam wheel mounted on the gear box output drive shaft. A follower riding on the cam wheel closed a switch with the passing of each cam lobe. The switch was connected to a pulse counter on the datalogger. Total pulses in 1 min were converted to conveyor travel, equal to the conveyor speed for that minute, by the displacement measured for each activation of the cam switch. Total conveyor travel was computed by summing the travel in each minute. Speed and total travel for each minute were stored on disk.

Voltage outputs from the gas analyzers were read in differential mode on the datalogger. Raw voltages were stored on disk, and later converted to concentration by the calibration factors for each instrument.

A separate datalogger and computer were used to monitor weight changes on the burning platform used for pile fires. Output voltages from the four load cells were read in differential mode on the datalogger, transmitted to the computer, and scaled by the calibration coefficients determined for each load cell for immediate display of weight. Weight measurements were made at 5 s intervals, averaged over 30 s, and recorded on disk. Static calibration was checked by placing known weights on the platform and observing load cell response.

2.3. Fuels

The fuels tested were almond tree prunings, barley straw, corn stover, Douglas fir slash, rice straw, Ponderosa pine slash, walnut tree prunings, and wheat straw. Fuel types, test dates, and wind tunnel configurations are listed in Table 2.3.1.

The tests were conducted over a one year period from 30 April 1992 to 30 April 1993. The first tests were conducted with rice straw collected during the fall of 1991. Straw from a M202 (medium grain) variety was swathed near ground level (50 to 75 mm above the soil surface), baled, and placed inside under cover for storage. These burns were intended principally to check the operating protocols. The test of 8 July 92 (test 3, Table 2.3.1) was aborted when the total filters were discovered to have been installed improperly. It is listed here only because filter samples were collected on the DRI sampler and results from these filters are reported later. The total filters were also installed improperly for the test of 9 June 92, although this was not known until the discovery on 8 July 92. Although results from these filters are included later, they are flagged as invalid. The total filters used on 30 April 92 were loaded on-site and were installed properly. The filter assembly problem was corrected prior to all tests after 8 July 92. These first tests in rice straw also showed the GC analysis to be inadequate for determination of total hydrocarbon concentration, and the THC analyzer was added prior to the tests in wheat straw on 11 August 92. The first pile burn on 12 Nov 92 in walnut prunings showed that CO_2 determinations and carbon balances would be improved with the addition of a continuous analyzer and weighing platform. All subsequent tests were therefore delayed until these two items were installed.

The tests with the 1991 crop year rice straw showed consistent differences in spreading rate compared to earlier tests conducted under similar conditions with rice straw collected during the fall of 1987 (stored inside under cover) and used in the wind tunnel configuration trials described by Jenkins, et al. (1993a, b). A direct comparison of these two materials was conducted without emissions analysis during a test on 25 August 92. Results from this test confirmed earlier observations, and a more detailed test with some emissions analysis (excluded were VOC, PAH, CNL, and DRI samples) was conducted on 2 September 92. Another full suite of experiments on 21 and 23 October 92 was conducted using 1992 crop year rice straw harvested shortly before the tests.

Wheat straw of the Anza variety from the 1992 Yolo county crop was collected in bales during July 1992. The straw used included all shoot (stem and leaves) material upwards from the harvester cutting height 50 to 70 mm above ground level. Straw from a Yolo county Klages variety malting barley crop was obtained in a similar manner, but harvested in August 1992. Corn stover (Pioneer variety) was collected by hand from fields on the University farm of UC Davis, following machine shredding, a technique normally employed prior to field burning.

Almond (Nonpareil variety) and walnut (Hartley variety) tree prunings were collected in Yolo county during the 1992 fall pruning season. Prunings only were collected. No

material from orchard removals (e.g. roots and trunks) was included. Branches ranged in size up to 100 mm diameter, and for purposes of analysis were divided into the two size classes ≤ 50 mm (small branches) and > 50 mm diameter (large branches). Material in each size class was weighed and analyzed separately. The burns were conducted without segregation, using the approximate mix of sizes observed in the piles from which the materials were obtained.

Table 2.3.1. Fuels tested in the wind tunnel by test date and wind tunnel configuration.

	Fuel Type	Date of Test	Configuration*
1	Rice Straw (1991 crop year)	30-Apr-92	CRNF
2	Rice Straw (1991 crop year)†	9-Jun-92	CRNF
3	Rice Straw (1991 crop year, aborted)†	8-Jul-92	CEWF
4	Rice Straw (1991 crop year)	10-Jul-92	CEWF
5	Rice Straw (1991 crop year)	14-Jul-92	CRNF
6	Wheat Straw (1992 crop year)	11-Aug-92	CRNF
7	Wheat Straw (1992 crop year)	13-Aug-92	CEWF
8	Rice Straw (1987/1991 crop comparison)	25-Aug-92	CEWF
9	Rice Straw (1987/1991 crop comparison)	2-Sep-92	CEWF
10	Barley Straw (1992 crop year)	15-Sep-92	CEWF
11	Barley Straw (1992 crop year)	17-Sep-92	CRNF
12	Corn Stover (1992 crop year)	7-Oct-92	CRNF
13	Corn Stover (1992 crop year)	9-Oct-92	CEWF
14	Rice Straw (1992 crop year)	21-Oct-92	CEWF
15	Rice Straw (1992 crop year)	23-Oct-92	CRNF
16	Walnut Prunings (1992 crop year)	12-Nov-92	Pile
17	Almond Prunings (1992 crop year)	6-Apr-93	Pile
18	Ponderosa Pine Slash	29-Apr-93	Pile
19	Douglas Fir Slash	30-Apr-93	Pile

*CRNF=ceiling retracted, no auxiliary floor, CEWF=ceiling extended, with auxiliary floor, see section 2.1.3. †total filters installed improperly.

Ponderosa pine and Douglas fir slash were collected in April 1993 at the Blodgett experimental forest operated by the University of California in El Dorado county. The slash had been produced during commercial contract harvest of plots in the forest during the spring and summer of 1992, and left unprotected in the field for later piling and removal. The Ponderosa pine slash was divided into four size categories for analysis: large branches > 50 mm diameter, medium branches 25 to 50 mm diameter, small branches < 25 mm diameter, and a needle fraction. The largest branches collected were not over about 125 mm diameter. The medium branch size class was included principally because the segregation of the rather large needle fraction required separation of the smaller branches, and left the medium size class as a residual. The Douglas fir slash included a very small component of needles, and only two size classes were separated: large branches > 50 and up to about 125 mm diameter, and small branches ≤ 50 mm diameter. Material in each size class was weighed and analyzed separately. The burns were conducted without segregation. No litter or duff was included in any of the slash burns. Although litter and duff can contribute in important ways to the emissions from prescribed burns and wildfires, these tests were intended to collect information on pure fuels only.

Table 2.3.2. Average fuel compositions.

	Cereals				Woods			
Fuel Type	Barley Straw	Corn Stover	Rice Straw	Wheat Straw	Almond	Douglas Fir	Ponderosa Pine	Walnut
Ultimate Analysis (% dry weight)								
C	44.85	44.78	38.06	44.28	49.16	51.64	52.41	48.23
H	5.85	5.88	5.28	5.77	6.24	6.24	6.20	6.00
N	0.61	0.49	0.64	0.49	0.06		0.06	0.66
Elemental Analysis								
(% dry weight)								
N	0.77	0.58	0.72	0.62	0.49	0.27	0.30	0.60
P	0.12	0.08	0.07	0.05	0.03	0.02	0.02	0.04
K	2.50	1.76	1.71	1.89	0.29	0.17	0.16	0.30
Ca	0.26	0.17	0.27	0.11	0.28	0.35	0.35	1.33
Mg	0.11	0.38	0.20	0.11	0.12	0.03	0.06	0.28
Na	0.1700	0.0100	0.0983	0.0550	0.0008	0.0001	0.0003	0.0100
Cl	0.20	0.36	0.48	0.29	0.03	0.01	0.00	0.13
(mg/kg dry weight)								
S	1,300	596	894	1,835	208	166	202	372
B	7	12	14	6	15	5	4	30
Zn	12	18	24	14	16	19	14	10
Mn	66	53	693	22	12	118	66	33
Fe	128	285	265	251	1,329	245	175	225
Cu	4	4	9	3	4	2	3	3
Si					427	401	741	
Total (% dry weight)	54.96	54.08	47.06	53.37	56.84	58.85	59.63	56.99
Proximate Analysis (% dry weight)								
Ash	7.61	6.12	18.59	9.38	1.33	0.55	1.22	3.67
Volatiles	78.06	77.33	68.77	76.24	82.28	82.95	81.51	82.96
Fixed Carbon	14.33	16.55	12.64	14.38	16.39	16.50	17.27	13.37
Higher Heating Value								
(MJ/kg dry weight)	17.80	17.97	15.43	17.34	19.47	20.39	20.66	19.28

Properties of the fuels are listed in Table 2.3.2. Values shown are averages over all tests for each fuel type, and for the wood fuels, integrated by weight fraction over all size classes and representing total fuel composition. The ultimate elemental analyses for carbon (C), hydrogen (H), and nitrogen (N) were conducted at the Microanalytical laboratory of the College of Chemistry, UC Berkeley. Elemental analyses for nitrogen (N) through silicon (Si) were performed at the Division of Agriculture and Natural Resources (DANR) analytical laboratory, UC Davis. Proximate composition and heating value determinations were made at laboratories of the Biological and Agricultural Engineering Department, UC Davis. The same types of analyses were done on residual materials (ash, partially burned materials) from the test burns by the same laboratories, and are reported separately in the results section. Nitrogen analyses were conducted at both Berkeley and Davis, but by two different techniques. The Berkeley analysis utilized a combustion technique and is considered less accurate than the digestion analysis employed by the Davis laboratory. The Berkeley N analyses are in general low in comparison to the Davis N analyses, and recoveries by the Berkeley technique appear to be poor for fuels containing low amounts of nitrogen (slash). Since both laboratories calibrate on standard reference materials, the reasons for the discrepancies are not entirely clear. The carbon and hydrogen analyses compare well with previous analyses of similar materials (Jenkins and Ebeling, 1985). Analyses for samples from individual test dates and size categories are given in the results section. Moisture contents were selected to be as representative of field conditions as possible, and are listed for each test in the results section.

2.4. General burning procedures

The burning techniques employed in the two classes of fires (spreading and pile) were common among fuels in each class. Outlined below are the general procedures followed in conducting the tests. More detailed descriptions of the individual tests appear in the results section.

2.4.1. Spreading fires

As described above, spreading fires were conducted by advancing the wind tunnel conveyors at a speed equal to the fire spreading rate so as to maintain the fire stationary in the tunnel. Prior to the tests on each date, the ceiling and auxiliary floor were positioned to give the required wind tunnel configuration.

Fuel loading was done manually. The feed belt was marked in 2 m^2 sections, each section 1.64 m long on the 1.22 m wide belt. Fuel for each section was weighed into a large tared container on a platform scale in an amount sufficient to provide the yield or loading rate (g m^{-2}) desired. The fuel loading rates were selected to be similar to published yields for each crop from field studies (Knutson and Miller, 1982). The approximate yields utilized are listed in Table 2.4.1. Some loss occurred at the junction of the two conveyors, and actual moisture content was not known prior to the tests, so there was some deviation from the desired dry matter loading rates at the fire. Specific loading rates for each test are listed in the results section.

An attempt was made to avoid segregation of the fuels by size class when loading (e.g., loss of fines). The fuels were spread in a uniformly thick layer on the belt to a depth typical of that observed in the field, normally 75 to 100 mm but not exceeding 150 mm, which was the minimum clearance under the blower. Results of the tests suggest some influence of fuel bed density on spreading rate, but a parametric investigation of this effect was not undertaken. Some possible effects on emissions are discussed later.

Table 2.4.1. Approximate dry matter loading rates for fuels burned in spreading fires.

Fuel	Yield (g m^{-2})	Yield (tons $acre^{-1}$)
Barley straw	400	2
Corn stover	900	4
Rice straw	600	3
Wheat straw	400	2

Fuel was loaded into the tunnel in a continuous bed extending from the feeding table to about the center of the combustion test section. With all instrumentation operating and the sampling systems ready to operate, the blower was started and the wind speed set at the desired test value. The speed was determined from the stack anemometer. The fire was then ignited in a line across the fuel bed using a propane torch. The fire was allowed to develop and spread up to the second window in the first door approximately 2 m downstream of the combustion test section entrance. The conveyors were started, and the conveyor speed set with the motor controller to match the fire spreading velocity. The fire position was maintained at the second window and the conveyor speed adjusted as necessary to match the spreading velocity. Some time before the ash reached the bin, the ash bin auger was started. The auger was operated continuously to move ash from the bin into the sealed collection bag at the end of the auger.

The sampling equipment was started after the fire had achieved a steady spreading velocity and the stack thermocouple indicated at least a quasi-steady temperature. Typically the stack gas velocity increased somewhat over the initial setting due to the buoyancy created by the fire. This was accommodated partially by setting the initial velocity lower than the setpoint velocity for the test. In general, stack gas velocity was controlled to within about 0.5 m s^{-1}.

The total filter/PAH, cascade impactor, and VOC sampling systems were positioned at the first traverse point, started simultaneously, and operated continuously for 48 minutes in most tests. The probe inlets were left at each of the traverse positions (Figure 2.1.3) for 2 min. With some fuels, a shorter sampling time was necessary due to higher particulate matter concentrations which led to filter clogging earlier than 48 minutes. In these cases, a 24 minute traverse was typical, with 1 min at each traverse point. The DRI and CNL samplers were started during the traversing period, and operated typically for 30 and 10 min, respectively. Fires with higher particulate matter loading also required shorter sampling times for these systems. Up to six grab samples of stack gas were collected during the traverse period, normally at 8 to 10 min intervals. At least one background grab sample was collected prior to the start of any tests. The time of loading for each batch of fuel placed on the feed conveyor was recorded on paper by the operators. This log was later compared against the conveyor travel recorded on the datalogger to check for consistency in the fuel weight measurement. Fuel samples in amounts of 200 to 500 g were collected at the feed table at intervals of approximately 1 h and bagged in plastic.

At the end of the first traverse, the pumps were shut off, and the total filter probe, XAD-2 resin trap, and cascade impactor removed. The total filter probe and resin trap were replaced, and the cascade impactor reloaded. DRI filters were capped, bagged in plastic, and replaced in the insulated container on ice. During this time, the fire was sometimes extinguished to conserve fuel. This was done by moving the fire downstream on the conveyor, opening the first door, and separating the fuel bed to open a gap between the

fire and the incoming fuel. The fire was allowed to burn the remaining available fuel. With the fire extinguished, the conveyor was stopped, but the blower left running. The continuous gas analyzers were recalibrated as necessary during this time. When the sampling systems were ready for the next run, the fire was ignited in the same manner as before, and allowed to develop prior to sampling. Two replicates were usual, a third was completed for the tests of 30 April 92, 9 June 92, 14 July 92, 25 August 92, and a fourth for the experiment on 2 September 92. In these cases, a field blank for the total filter was not obtained. The tests of 25 August and 2 September 92 did not include PAH analysis, and were conducted to investigate gross differences associated with the two rice straw fuels described earlier.

At the end of all tests on each date, the sampling systems were disassembled. Each impinger flask and the desiccant canister in the total filter/PAH line was reweighed. The impinger train was reassembled and sealed. The impingers, teflon lines, total filter probes, and XAD-2 resin traps were delivered to the Facility for Advanced Instrumentation for analysis. The ash bin was cleaned into a bag, and all ash weighed. Ash samples were collected and bagged in plastic. Any fuel material lost through the gap in the conveyors at the transfer point near the combustion test section entrance was collected, weighed, and sampled. The length of unburned fuel bed remaining on the conveyors was recorded, and this unburned fuel unloaded from the conveyors and replaced in storage if needed for subsequent tests. Calibration on the continuous gas analyzers was checked. The DRI sampling system and the gas sample inlet and lines were disassembled and removed to a clean laboratory for cleaning. DRI filters were placed in a freezer at -10°C, held overnight (in some cases, over the weekend), and then shipped to DRI by one day delivery service. CNL filters were capped and boxed, and delivered to CNL for analysis. Fuel moisture was determined by placing samples in an air oven at 100°C to constant weight (typically 24 h). Dried samples were then milled through 20 mesh, bottled, and sent for analysis as described above under section 2.3. Ash samples were pulverized with mortar and pestle by hand, bottled, and sent for analysis.

2.4.2. Pile fires

Orchard prunings are most commonly burned in piles near the edge of the orchard. Forest slash is burned in two principal ways--broadcast burns and pile burns. The fires conducted in the wind tunnel with the four wood fuels were all pile burns. The conveyors were not operated during any of the pile fires. The first burn with walnut prunings was conducted by building the piles directly on the conveyor below the stack. All other tests were conducted by erecting the piles on the burning platform described in section 2.1.5. This platform was positioned directly beneath the stack, just above the conveyor.

The blower was not operated during any of the pile burns. Instead, air was supplied naturally to the fires by opening the doors about halfway as shown in Figure 2.1.4. All six doors along the combustion test section were opened, although the doors on either side of the platform were not always opened as far as the center doors to reduce ash blowing. Combustion products flowed freely up the stack past the sampling equipment, and no smoke leakage was observed to occur through the doors. A fine mesh stainless steel screen kept fuel ash from falling through the platform to the wind tunnel floor below. The pile support method meant that air was available to the pile from below.

The piles were ignited with a propane torch by setting alight small wood pieces at the base of the piles. Ignition was quite rapid with the Ponderosa pine due to the large population of needles. The fuel composition most likely contributed to the faster ignition of the pine wood as well. Burning profiles are shown in the results section as weight loss over time, and the ignition periods can be clearly seen.

Due to the size of the wind tunnel, the piles were small, not exceeding about 1.5 m in height and length, and 1.2 m in width. Total pile weight was 34 to 45 kg, although total fuel consumption was higher when the pile was stoked as described below. Individual fuel pieces ranged in size up to about 125 mm diameter and 1.5 m in length. The actual weight fraction in each size class is given in the results section. Two tests were conducted with each fuel. The piles were constructed by randomly piling fuel elements onto the platform in such a manner as to maintain a proper size distribution throughout the pile. Only for one test in Douglas fir was the piling method varied. In this case, the pile was constructed more as a fuel crib to determine if differences in emission factors could be observed.

Sampling procedures and instrumentation were essentially the same as for the spreading fires, except that a continuous CO_2 gas analyzer was added after the walnut pruning burns. With walnut prunings and almond prunings, the first sampling traverse extended over most of the burn period except for a small amount of residual smoldering at the end. A second test was conducted in which the fire was frequently stoked during the traverse, in order to prolong the flaming stage and observe changes in emission factors associated with stoking that often occurs with orchard fires. The fires in Ponderosa pine and Douglas fir were not stoked, and traverses were made during both the flaming and smoldering stages. When stoking, the weight of fuel added to the fire was recorded manually. After each test, ash was allowed to cool on the screen, then bagged and weighed as a check against the final weight obtained from the burning platform. All samples were handled as previously described for the spreading fires.

2.5. Data reduction

Each spreading fire experiment resulted in one data file containing sensor responses at 1 min intervals. The pile burns, with the exception of the tests with walnut prunings, also generated a second file containing weight data from the burning platform at 30 s intervals. Values of stack gas temperature, impinger outlet temperature, ambient air temperature and relative humidity (later replaced by the continuous CO_2 analyzer output), conveyor speed and conveyor travel (not utilized for the pile burns), stack gas velocity, combustion test section inlet air temperature, and the unconverted voltage outputs from the continuous analyzers (CO, NO, NO_x, SO_2, CO_2, THC, and total S) were included in the first data file. For the purposes of computing stack gas velocity by carbon balance, the weight data were subsampled at 1 min intervals and combined with the first data set beginning at the appropriate time. All gas analyzer data were converted to concentration units by the calibration coefficients determined for each instrument. All sensor data were plotted against time. These plots appear in the results section for each experiment.

Average response values from each instrument or sensor were computed over each traverse period. The data files were searched for times during each traverse when the gas analyzer inlet filter was changed or the original CO analyzer zero was being checked. Such times had been noted in the log book for each run, and were evident in the data files by the sudden reduction in concentration. For these times, the analyzer response(s) were excluded from the averaging. In general this meant the exclusion of data for a single minute.

2.5.1. Spreading fires

For each traverse, the total conveyor travel during the traverse was determined from the data set. The moist fuel loading rate at the fire, r_w (g m^{-2}), was determined by reducing

the loading rate at the feed table by the fraction of fuel lost at the conveyor gap during the test. The dry fuel loading rate at the fire, r_d (g m^{-2}), was computed on the basis of the moist fuel loading rate and the wet basis moisture content of the fuel, M (decimal), determined for that traverse, i.e.,

$$r_d = r_w (1 - M) \quad [1]$$

The total moist fuel consumption, m_{fw} (g), and dry fuel consumption, m_{fd} (g), for the traverse were then computed from the total travel and the loading rate:

$$m_{fw} = r_w D L \quad [2]$$

$$m_{fd} = r_d D L \quad [3]$$

where D is the conveyor travel (m) and L is the width of the fuel bed (= 1.2 m). The residual ash generation during the traverse, m_a (g), was computed from the total moist fuel consumption for the traverse and the ash mass fraction, y_a (decimal), determined from the weight of ash collected at the end of the test and the total moist fuel consumed in the fire during the test:

$$m_a = m_{fw} y_a \quad [4]$$

The mass of fuel volatilized during the traverse, m_{fv} (g) was computed as the difference between the moist fuel consumption and the ash generation:

$$m_{fv} = m_{fw} - m_a \quad [5]$$

The average rates of fuel consumption ($\dot{m}_{fw}$ and $\dot{m}_{fd}$, g s^{-1}), ash generation ($\dot{m}_a$, g s^{-1}), and fuel volatilization ($\dot{m}_{fv}$, g s^{-1}) were obtained by dividing the total values by the duration time of the traverse period, t (s).

Average stack gas density, $\bar{\rho}_g$ (kg m^{-3}), was computed from the equation of state using the average stack gas temperature measured during the traverse and a pressure of 1 standard atmosphere. The pressure assumption was considered adequate given the experimental uncertainty associated with the concentration and velocity measurements. The average stack gas flow rate, V_g (m^3 s^{-1}), was computed from the average stack gas velocity, $\bar{u}$ (m s^{-1}) and the stack area, A_s (= 1.49 m^2) as

$$V_g = A_s \bar{u} \quad [6]$$

and the average stack gas mass flow rate, $\dot{m}_g$ (kg s^{-1}) as:

$$\dot{m}_g = \bar{\rho}_g V_g \quad [7]$$

The average inlet air mass flow rate was the difference between the average stack gas mass flow rate and the average fuel volatilization rate, and was close to the value of the stack gas mass flow rate because fuel volatilization normally accounted for no more than a few tenths of a percent of the total stack flow. The overall air fuel ratio (wet or dry fuel basis) was computed as the quotient of the average inlet air mass flow rate and the average fuel consumption rate (wet or dry basis).

Emission factors, f_i, (% of fuel dry mass) for the gaseous species were computed in two ways. Properly, the emission factor is computed on the basis of the total mass of pollutant emitted while burning a mass of fuel, and was found by integrating the pollutant mass flow over the duration of the traverse using the instantaneous (1 min) values of stack gas velocity, u, stack gas density, ρ_g, and concentration, C_i (ppmv), of species i as,

$$f_i = \frac{1}{m_{fd}} k \int_{t_o}^{t_f} \rho_g A_s u C_i \frac{W_i}{W_s} dt \qquad [8]$$

where k is a unit conversion coefficient (= 10^{-1} for the units given), W_i the molecular weight (kg kg-mol^{-1}) of species i, W_s the molecular weight of the stack gas (kg kg-mol^{-1}), and the integral taken over the time from the start of the traverse, t_o, to the end, t_f. Because the stack gas consisted almost entirely of air, W_s was taken to be that of standard air, which, like the assumption for stack pressure, was assumed to be adequate.

An alternative average emission factor, $\bar{f}_i$, was computed from the average concentration and stack gas mass flow rate over the traverse as:

$$\bar{f}_i = \frac{1}{\dot{m}_{fd}} k \bar{\rho}_g A_s \overline{u C_i} \frac{W_i}{W_s} \qquad [9]$$

where $\overline{C_i}$ is the average concentration (ppmv) of species i. Strictly speaking, the average emission factor given by equation [9] should equal the integrated emission factor given by equation [8] only in the case of constant concentration, velocity, and density during the entire traverse. The extent to which the average emission factor approximated the integrated emission factor was indicative of the steadiness of the fire.

Average emission factors for methane were derived from GC determinations. Emission factors for non-methane hydrocarbons (NMHC) were determined from both the hydrocarbons analyzed by gas chromatography and the THC continuous analyses, in each case by subtracting the average CH_4 emission factor. All hydrocarbon emission factors are reported as equivalent methane.

For particulate matter, an emission factor, f_{PM} (% of fuel dry mass) was computed as:

$$f_{PM} = \frac{1}{\dot{m}_{fd}} k V_g C_{PM} \frac{T_i}{T_s} \qquad [10]$$

where C_{PM} is the concentration of total particulate matter (mg m^{-3}), T_i is the absolute impinger outlet temperature (K), T_s is the absolute stack gas temperature (K), and k is the unit conversion coefficient used above. The ratio T_i/T_s approximately corrects the sample flow rate determined with the dry test meter to stack conditions. Equation [10] gives the same result as integrating the velocity to obtain total volume and dividing by the total fuel mass consumed. Emission factors for PM10 and PM2.5 were also calculated by equation [10], with concentrations adjusted accordingly. The concentrations for PM10 and PM2.5

were determined from the concentration of total particulate matter (PM) and from the particle size distribution determined with the cascade impactor. Cumulative weight fraction was plotted against particle size, and the weight fractions at 2.5 and 10 μm used to scale the total particulate matter concentration. The mass median aerodynamic particle diameter (MMAD, μm) and geometric standard deviation (σ) were also computed using a log-normal distribution model (Raabe, 1968).

2.5.1.1. Carbon balance

Carbon, nitrogen, sulfur, water, and energy balances were computed for each test to evaluate closure and check for consistency. The carbon transfer to the stack was determined from the difference between the fuel carbon and ash carbon. The stack carbon determined in this manner was compared against the carbon contained in the major gas species CO_2, CO, THC (as CH_4), and particulate matter (PM) to determine closure. The carbon concentration for particulate matter used in the carbon balance was that determined from the PM10 analyses of the DRI filters. From the carbon transfer to the stack, a maximum CO_2 emission factor was calculated for comparison to the actual CO_2 emission factor. An estimated stack gas velocity was also computed from the stack gas concentration measurements for comparison with the velocity measured with the stack anemometer.

The fuel carbon rate, $\dot{m}_{fC}$ (g s^{-1}), was determined from the dry fuel consumption rate and the dry fuel carbon concentration, C_{fC} (decimal), from the ultimate analysis,

$$\dot{m}_{fC} = \dot{m}_{fd} C_{fC} \qquad [11]$$

with the ash carbon rate, $\dot{m}_{aC}$ (g s^{-1}), computed from the ash carbon concentration, C_{aC} (decimal):

$$\dot{m}_{aC} = \dot{m}_{a} C_{aC} \qquad [12]$$

The carbon release to the stack, $\dot{m}_{sC}$ (g s^{-1}), was:

$$\dot{m}_{sC} = \dot{m}_{fC} - \dot{m}_{aC} \qquad [13]$$

A maximum CO_2 emission factor was determined as:

$$f_{CO_2,\max} = \frac{\dot{m}_{sC}}{\dot{m}_{fd}} \frac{W_{CO_2}}{W_C} \qquad [14]$$

An estimated average stack gas velocity, $\hat{\bar{u}}$ (m s^{-1}) was computed from the stack carbon transfer and the concentrations of CO_2, CO, THC (as CH_4), and particulate matter (PM),

$$\hat{\bar{u}} = \frac{\dot{m}_{sC}}{\bar{\rho}_g A_s} \frac{W_s}{W_C} \frac{k'}{(C_{CO_2} + C_{CO} + C_{THC} + C_{PMC})} \qquad [15]$$

where W_C is the molecular weight of carbon, k' is a unit conversion coefficient (= 10^3 for the units given), and the concentrations C_i are given in ppm. The stack carbon concentration due to particulate matter, C_{PMC}, was computed as:

$$C_{PMC} = \frac{1}{\overline{\rho}_g} C_{PM} C_{pC} \frac{W_s}{W_C} \frac{T_i}{T_s} \quad [16]$$

where C_{pC} (decimal) is the carbon mass concentration in the particulate matter determined as total organic and elemental carbon from the DRI thermal-optical carbon analysis.

The approach to closure, γ_C (%), for the carbon balance was computed as the mass of carbon accounted for in the stack gas (including particulate matter) relative to the stack carbon transfer computed from the difference in carbon between the fuel and ash,

$$\gamma_C = \frac{1}{\dot{m}_{sC}} \dot{m}_{fd} (f_{PM} C_{pC} + W_C \sum_i \frac{f_i}{W_i}) \quad [17]$$

in which the summation is taken over the species CO_2, CO, and THC (as equivalent CH_4).

2.5.1.2. Nitrogen balance

The nitrogen balance was computed in a manner similar to the carbon balance. Mass fractions for ash, NO_x, and PM nitrogen were determined relative to fuel carbon. Nitrate (NO_3^-) and ammonium (NH_4^+) ion concentrations were the only nitrogen containing species analyzed in the particulate matter, and thus were the only contributors to PM nitrogen in the nitrogen balance.

The fuel, $\dot{m}_{fN}$, and ash, $\dot{m}_{aN}$, nitrogen rates were:

$$\dot{m}_{fN} = \dot{m}_{fd} C_{fN} \quad [18]$$

$$\dot{m}_{aN} = \dot{m}_a C_{aN} \quad [19]$$

where C_{fN} and C_{aN} are the nitrogen concentrations (dry basis) from the elemental analysis. The mass flow rate of nitrogen in NO_x was computed as

$$\dot{m}_{N,NO_x} = \frac{1}{k''} f_{NO_x} \dot{m}_{fd} \frac{W_N}{W_{NO_2}} \quad [20]$$

NO_x was reported as equivalent NO_2, and k'' is a unit conversion coefficient (= 10^2 for the units given). W_N and W_{NO_2} are the molecular weights of N and NO_2, respectively. The computation was done separately using the average and integrated emission factors.

The nitrogen rate for particulate matter was computed as:

$$\dot{m}_{N,PM} = \frac{1}{k''} f_{PM} W_N (C_{pNO_3^-} \frac{1}{W_{NO_3^-}} + C_{pNH_4^+} \frac{1}{W_{NH_4^+}}) \dot{m}_{fd} \quad [21]$$

in which the C_i and W_i are the concentrations in the particulate matter and molecular weights of NO_3^- and NH_4^+.

2.5.1.3. Sulfur balance

The sulfur balance included sulfur in fuel, ash, SO_2, and particulate matter. The sulfur concentration from the total S analyzer was not used due to the uncertainty associated with this measurement in the presence of high CO_2 concentrations. The PM sulfur concentration was that from the DRI elemental analysis.

The fuel and ash sulfur rates were

$$\dot{m}_{fS} = \dot{m}_{fd} C_{fS} \quad [22]$$

$$\dot{m}_{aS} = \dot{m}_a C_{aS} \quad [23]$$

in which C_{fS} and C_{aS} are the sulfur concentrations (dry basis) from the elemental analyses. The sulfur rate as SO_2 was

$$\dot{m}_{S,SO_2} = \frac{1}{k''} f_{SO_2} \dot{m}_{fd} \frac{W_S}{W_{SO_2}} \quad [24]$$

and was computed for the average and integrated emission factors. The sulfur rate for particulate matter was

$$\dot{m}_{S,PM} = \frac{1}{k''} f_{PM} C_{pS} \dot{m}_{fd} \quad [25]$$

in which C_{pS} is the concentration of total sulfur in the particulate matter.

2.5.1.4. Water balance

A water balance was computed to estimate the stack gas humidity at the point of sampling and to check the weight gain by the impingers and desiccant. From the ambient air temperature, the saturation vapor pressure, p_s (Pa), was computed from the correlation given by ASHRAE (1989):

$$p_s = \exp(\frac{-5800.2206}{T_s} + 1.3914993 - 0.04864039 T_s + \ldots$$
$$\ldots 4.1764768 x 10^{-5} T_s^2 - 1.4452093 x 10^{-8} T_s^3 + 6.5459673 \ln(T_s)) \quad [26]$$

The vapor pressure, p_v (Pa), was obtained as $\phi\, p_s$, where ϕ is the ambient air relative humidity (decimal). The dew point temperature, T_{dp} (°C) was determined by the correlation given by ASHRAE (1989):

$$T_{dp} = 6.54 + 14.526\ln\left(\frac{p_v}{1000}\right) + 0.7389\ln\left(\frac{p_v}{1000}\right)^2 + \ldots$$
$$\ldots 0.09486\ln\left(\frac{p_v}{1000}\right)^3 + 0.4569\left(\frac{p_v}{1000}\right)^{0.1984} \quad [27]$$

The volume fraction, x_w (decimal) and mass fraction, y_w (decimal) of water vapor in the inlet air were computed as:

$$x_w = \frac{p_v}{p_t} \quad [28]$$

$$y_w = x_w \frac{W_{H_2O}}{W_a} \quad [29]$$

where p_t is the total pressure and W_{H_2O} and W_a are the molecular weights of water and air respectively. The moisture evaporated from the fuel during combustion, $\dot{m}_{w,e}$ (g s^{-1}), was:

$$\dot{m}_{w,e} = \dot{m}_{fw} M \quad [30]$$

The water released by combustion of the fuel, $\dot{m}_{w,c}$ (g s^{-1}) was estimated from the difference in hydrogen concentration of the dry fuel and ash, assuming complete conversion to water:

$$\dot{m}_{w,c} = (\dot{m}_{fd} C_{fH} - \dot{m}_a C_{aH}) \frac{W_{H_2O}}{W_{H_2}} \quad [31]$$

Where C_{fH} and C_{aH} are the concentrations of hydrogen in the fuel and ash respectively. All outlet hydrogen was assumed to exit the stack in the form of water, other forms were neglected. The total water added to the stack flow from the fuel was $\dot{m}_{w,f}$ (g s^{-1}),

$$\dot{m}_{w,f} = \dot{m}_{w,e} + \dot{m}_{w,c} \quad [32]$$

The total stack water vapor flow rate, $\dot{m}_{w,s}$ (g s^{-1}) was the sum of the inlet air water vapor and that added by evaporation and combustion:

$$\dot{m}_{w,s} = \dot{m}_{air} y_w + \dot{m}_{w,f} \quad [33]$$

in which $\dot{m}_{air}$ (g s^{-1}) is the inlet air mass flow rate.

The stack water vapor mass and volume fractions were computed from the total stack gas flow and the stack water vapor flow as:

$$y_{w,s} = \frac{\dot{m}_{w,s}}{\dot{m}_g} \quad [34]$$

$$x_{w,s} = y_{w,s} \frac{W_a}{W_{H_2O}} \quad [35]$$

which yielded the stack vapor pressure, $p_{v,s}$ (Pa),

$$p_{v,s} = x_{w,s} p_t \quad [36]$$

The stack gas saturation pressure, $p_{s,s}$ (Pa) was determined from the stack gas temperature by equation [26], and the stack gas relative humidity computed as:

$$\phi_s = \frac{p_{v,s}}{p_{s,s}} \quad [37]$$

The stack gas dewpoint temperature was computed from equation [27] using $p_{v,s}$ from equation [36].

The water content of the stack gas was used to estimate the weight gain, Δm_w, of the impingers and desiccant from the mass of gas sampled, equal to $V_s \rho_s$, assuming complete dehydration of the gas:

$$\Delta m_w = V_s \rho_s y_{w,s} \quad [38]$$

with V_s the sample gas volume from the dry test meter and ρ_s the sample density. This value was compared against the actual weight gain.

2.5.1.5. Power balance

The total energy release due to combustion was determined from the difference in total heating value of the fuel and ash. The average energy release rate, $\dot{E}$ (kW), was

$$\dot{E} = \dot{m}_{fd} Q_f - \dot{m}_a Q_a \quad [39]$$

where Q_f and Q_a are the specific heating values (MJ kg^{-1}) of the dry fuel and ash, respectively. The total heat release, $\dot{Q}_s$ (kW), was estimated from the value of $\dot{E}$ less the energy in products of incomplete combustion, given individually by

$$\dot{q}_i = f_i \dot{m}_{fd} Q_i \quad [40]$$

for the products CO, THC, and carbon in particulate matter. Q_i are the mass basis heating values (MJ kg^{-1}) for each of the products. The fireline intensity, I (kW m^{-1}), was calculated simply by dividing $\dot{Q}_s$ by the width of the wind tunnel. The total heat release was compared against the enthalpy of the stack gas determined from the stack gas mass flow rate and stack gas temperature rise above inlet. The difference was attributed to the heat transfer across the walls of the wind tunnel (tunnel dissipation).

2.5.2. Pile fires

Data analysis for the pile fires differed from that for the spreading fires in two ways. For all but the tests with walnut prunings, the instantaneous fuel consumption, ash generation, and fuel volatilization rates were determined from the burning platform weight measurements and not from the conveyor speed as for the spreading fires. The availability of continuous CO_2 concentration and fuel weight data also permitted instantaneous (one minute) approximations of stack gas velocity by carbon balance over the initial stage of the fire (CO_2 concentrations and rates of weight loss during the later stages of the fire were sufficiently low to cause the instantaneous carbon balances to become essentially useless under these conditions, as shown later). In the case of the walnut prunings, only average values from initial and final weight measurements were determined. These results were later compared against the more detailed results of the subsequent burns.

The estimated instantaneous stack gas velocity was computed in the same manner as the estimated average stack gas velocity given by equation [15], except that the average density, concentrations, and stack carbon transfer were replaced by the values obtained at each one minute interval:

$$\hat{u} = \frac{\dot{m}_{sC}}{\rho_g A_s} \frac{W_s}{W_C} \frac{k'}{(C_{CO_2} + C_{CO} + C_{THC} + C_{PMC})} \qquad [41]$$

To solve equation [41], several assumptions were made regarding the value of $\dot{m}_{sC}$ since the actual amount of carbon volatilized in each minute could not be determined simply from the weight loss. During the flaming stage of combustion, the carbon volatilization was assumed to be simply that resulting if the organic matter in the fuel were completely gasified along with the fuel moisture. By defining the total moist fuel mass (m_t) to be the sum of the masses of inorganic ash (m'_a), moisture (m_w), and volatile dry fuel organic matter (m_v), the mass of dry fuel (m_d) associated with the observed weight change could be found. With

$$m_t = m'_a + m_w + m_v \qquad [42]$$

$$m_d = m_v + m'_a \qquad [43]$$

$$m_w = M m_t \qquad [44]$$

$$y'_a = \frac{m'_a}{m_d} \qquad [45]$$

the dry fuel mass attributed to the volatile mass $m_v + m_w$ was

$$m_d = \frac{\Delta m}{(1 - y'_a) + \frac{1}{\frac{1}{M} - 1}} \qquad [46]$$

where Δm is the weight loss (g) measured over 1 min and y'_a is the original fuel ash mass fraction, dry basis. The carbon volatilization (g s^{-1}) was then simply

$$\dot{m}_{sC} = \frac{1}{60} m_d C_{fC} \qquad [47]$$

This analysis was used only for unstoked fires. The computation of an estimated instantaneous stack gas velocity was not attempted during stoking as the weight change due to fuel volatilization was not adequately known.

When a traverse was made during the smoldering phase of the fire, the carbon balance was calculated under the assumption that the remaining fuel at the start of smoldering consisted only of carbon and ash, and that the total mass of ash was constant throughout. The ash and carbon concentrations of the final residual material were known from the proximate and ultimate analyses. The carbon concentration at the start of smoldering, $C_{aC,o}$ (decimal) was then computed as:

$$C_{aC,o} = 1 - \frac{m_f}{m_o}(1 - C_{aC,f}) \qquad [48]$$

in which m_o is the total mass at the start of smoldering, m_f the mass at the end of smoldering, and $C_{aC,f}$ the carbon concentration (decimal) of the residual matter (ash) at the end of smoldering. Application of this analysis to each minute past the start provided an estimate of the stack carbon transfer for computing stack gas velocity. However, the low CO_2 concentrations prevailing during smoldering, along with the low rates of weight loss and the rather poor knowledge of actual stack carbon transfer caused substantial variation in the estimated stack gas velocity determined in this manner. Anemometer measurements of stack gas velocity appear more reliable during smoldering due to the lower thermal radiation load on the anemometer, and were used to determine total fire emission factors.

3. Results

In what follows, results for individual experiments are presented by fuel type and in roughly chronological order. Summary results for all fuels appear at the end of this section.

3.1. Rice straw

A total of eight experiments with rice straw were conducted. The first two on 30 April and 9 June 92 used rice straw from the 1991 crop year, later referred to as type 2 straw. Both tests were conducted in the CRNF wind tunnel configuration at approximately 2 m s^{-1} wind speed. Two companion trials, one in the CEWF configuration at 3 m s^{-1} wind speed, and one in the CRNF configuration, were conducted on 10 and 14 July 92 using straw from the same source as the trials of 30 April and 9 June 92. Differences in fire spreading rates between these experiments and earlier experiments with rice straw from a different source (later called type 1 straw) led to direct comparisons of the two straw sources in repeated tests of 25 August and 2 September 92. The final two experiments on 21 and 23 October 92 were conducted with a third source of straw from the 1992 crop year. These, like the tests of 10 and 14 July 92, were companion tests in the CEWF and CRNF configurations.

3.1.1. Rice straw, CRNF, 30 April 92

This preliminary test was conducted with the wind tunnel ceiling retracted and without the auxiliary floor (CRNF configuration). The straw used was harvested during the autumn of 1991 and stored in bales inside under cover until the date of the test. This test did not include sampling for total hydrocarbons by continuous analyzer, or particulate matter composition using the CNL and DRI samplers. The air temperature and relative humidity probes were installed in the wind tunnel duct just downstream from the blower, rather than outside near the blower inlet as in later tests. For this reason, temperature and relative humidity changed dramatically following blower start-up and shut-down. The thermocouple near the inlet of the combustion test section was retained in place. Elemental analyses were not completed on the fuel samples but were deferred to the test of 9 June 92 with the same fuel. Moisture, proximate, and heating value analyses were completed. The test was otherwise conducted in the same manner as described in section 2.4.1.

The fire was ignited shortly before 1300 h and burned continuously until shortly before 1700 h. Three traverses of 48 min each were completed, with the second and third nearly contiguous. Part of the test involved an evaluation of the appropriate sampling time to acquire sufficient sample for VOC analysis. The first VOC sample was taken over the first 48 min traverse, and the second sample collected over the full 96 min of the second and third traverses. The 48 min sampling period was found after analysis to provide ample sample. Total filter and cascade impactor samples were collected during the first two traverses only. The CO analyzer was subject to zero drift and about half way through the test a two way valve was added in the CO analyzer inlet line connecting it to a zero air source. This permitted frequent and rapid zero checking on the CO analyzer without disturbing the other analyzers. The plumbing arrangement described under section 2.2.2.1 was added immediately following this test. Higher CO concentrations in the stack during the first half of the test are believed to be due principally to the uncorrected zero drift of the instrument rather than to any inherent changes in fire behavior. Following this test, the CO analyzer was disassembled and the sample cell thoroughly cleaned, which improved analyzer performance in later tests. CO concentrations measured during the first traverse were not used in computing the global average concentration discussed later. All other analyzers appeared stable.

Operating conditions and gas concentrations are displayed in Figures 3.1.1.1 through 3.1.1.12. Air temperature and relative humidity from the probes just downstream of the blower are shown in Figure 3.1.1.1. Actual weather conditions obtained from the nearby CIMIS station appear in Figures 3.1.1.2 - 4. Combustion test section inlet air temperature, stack gas temperature, and impinger outlet temperature are shown in Figure 3.1.1.5. The stack gas temperature averaged about 60°C, about 30 K higher than the inlet air temperature. The traverse periods are evident in the low temperature regions for the trace of impinger outlet temperature.

Conveyor and stack gas velocities appear in Figure 3.1.1.6. As discussed above, for the CRNF configurations, the stack gas velocity was set to approximately 2 m s^{-1} as one of the extreme cases from the previous study (Jenkins, et al., 1993a, b). The conveyor speed was adjusted frequently to between about 0.5 and 1 m min^{-1} to maintain the fire location in the tunnel. A smoothed plot of conveyor speed obtained as a 10 point (or 10 min) rolling average appears in Figure 3.1.1.7. The speed increased consistently during the first half of the test, later showing an oscillatory behavior around 0.7 m min^{-1}. The reason for the difference between the two periods is not known, but is perhaps due to warming of the wind tunnel. Inlet air temperature remained nearly constant throughout

the test, and loading rate was not varied. As discussed later, rice straw of the same variety and moisture content from different sources was observed to burn at different rates, although the reasons for this are not completely understood. Differences observed in this test may also be due in part to changes in the physical conditions of the straw from different bales.

Conveyor travel is given in Figure 3.1.1.8. The fire spread through approximately 170 m of fuel. Gas concentrations from the CO, NO_x, SO_2, and total S continuous analyzers are shown in Figures 3.1.1.9 - 12, respectively.

Results of fuel and ash analyses are included in Table 3.1.1.1. The proximate composition and heating value for the fuel are very similar to those determined for the experiments of 9 June 92, 10 July 92, and 14 July 92, all using the same fuel. Elemental analyses are given in the results for 9 June 92 and 14 July 92. Compositions from both dates are seen to be quite similar.

The ash produced in all rice straw tests was black. For 30 April 92, the carbon concentration in the ash was about 7% of dry weight. The inorganic fraction (listed as "ash" under the proximate analysis) was about 87%. The volatile portion of the proximate analysis, conducted by holding the sample in an inert environment at 950°C for 6 min, is subject to loss of inorganic constituents, and should be considered to yield primarily qualitative results for these ash samples. As shown later, loss of inorganics during the volatile analysis can cause fixed carbon values, computed by difference, to become negative. The residual heating value of 3 MJ kg^{-1} agrees roughly with the carbon concentration observed for the sample, in that small amounts of organics remain as suggested by the hydrogen concentration of 0.7%.

Average values of wind tunnel operating conditions and stack gas and particulate matter concentrations are listed in Table 3.1.1.2. For all three traverses, the spreading rate was around 0.7 m min^{-1}, with an average stack gas velocity of slightly under 2 m s^{-1}. The concentration values for hydrocarbons, listed as HC, were obtained as equivalent methane from the GC derived concentrations of methane, ethane, ethylene, acetylene, and propane. The concentrations for non-methane hydrocarbons (NMHC) were obtained as the difference between HC and CH_4. As mentioned under section 2.2.2.1, the total sulfur analyzer was sensitive to the presence of CO_2, and the values reported are subject to considerable uncertainty.

Total particulate matter concentrations were 12 to 13 mg m^{-3}. The concentrations of PM10 and PM2.5 were derived from the total PM concentrations and the mass fractions at 10 and 2.5 μm obtained from the results of the cascade impactor. The particle size distributions from the first and second traverses are given in Figures 3.1.1.13 and 3.1.1.14. As shown, PM10 represents about 95% of total particulate matter mass, with PM2.5 in the range of 80 to 88% of total PM. These results were largely consistent with earlier studies (Jenkins, et al., 1993a, b). The PM2.5 mass fractions are slightly lower on average.

Results of the mass balances for each of the three traverse periods are listed in Table 3.1.1.3. In each case, the fire spread through about 30 m of fuel during the traverse. The actual fuel loading rates were 610 - 620 g m^{-2} dry basis, with fuel moisture between 8 and 11% wet basis. The total ash fraction was about 21% of the moist fuel burned, which agrees with the proximate and elemental analyses. The dry fuel consumption rates were 8 to 9 g s^{-1}, with 7 to 8 g s^{-1} gasified and emitted through the stack. The mass ratio of air to fuel was in the range of 300 to 400.

Emission factors for major species are listed in Tables 3.1.1.4 and 5. The values are given as % of fuel dry weight. Table 3.1.1.4 lists the integrated values computed by equation [8] for species analyzed continuously (CO, NO, NO_x, SO_2, and total S as SO_2). Shown for comparison in Table 3.1.1.5 are the average values computed by equation [9]. Emission factors for hydrocarbons and CO_2 were computed by equation [9], and for particulate matter by equation [10] in both instances. Also listed are the ratios of SO_2 to total S, as well as the values of mass median aerodynamic particle diameter (MMAD) and geometric standard deviation (σ) from the log-normal fit of the particle size distribution. Although the units for the emission factors are in percent of fuel weight, they do not add to 100% because of the incorporation of atmospheric oxygen into the emission species, especially CO_2.

The agreement between the integrated and average factors is quite good, indicating good stability in fire conditions. The CO emission factor for the first traverse is likely inflated due to the problem with zero drift during this time as described above. Overall, the results are consistent with those obtained in the original wind tunnel study of Jenkins, et al. (1990), although the CO emission factors are somewhat lower here.

Results of carbon balances are listed in Table 3.1.1.6. The average PM concentration from traverses 1 and 2 was assumed to apply to traverse 3, as no direct PM measurement was made during this traverse. Because no PM carbon concentration was available, that from the subsequent run on 9 June 92 was assumed to be representative. Closure for the first and third traverses was reasonably good at 94 and 87% respectively. The second traverse shows a poorer closure due to the lower CO_2 emission factor obtained. The measured value of 96% is well below the theoretical maximum of 133% determined from the difference in fuel and ash carbon. The low CO_2 yield is also evident in the estimated stack gas velocity of 2.48 m s^{-1} for the second traverse. The good agreement between measured and estimated stack gas velocities for traverses 1 and 3 suggest an error in the determination of average CO_2 concentration for traverse 2, rather than in stack velocity.

The results of nitrogen balances are given in Table 3.1.1.7. Because the amount of molecular nitrogen emitted from the fuel could not be measured, the closure was not expected to be good. The results show this to be true. The total fuel nitrogen accounted for in ash, NO_x, and particulate matter (obtained from NO_3^- and NH_4^+ concentrations in PM from the experiment of 9 June 92), amounts to about 30%. The average distribution of fuel nitrogen among the products is shown in Figure 3.1.1.15. Nitrogen as NO_x is in a ratio of about 17% to fuel nitrogen, although the source of the NO_x was not determined. How much NO_x originates via fuel, thermal, or prompt mechanisms is unknown, although most is suspected to arise from fuel nitrogen for these fires. About 11% of fuel nitrogen was retained in the ash. The fraction titled ND (not determined) in the figure represents fuel nitrogen not allocated to ash, NO_x, or particulate matter, although the nitrogen for NO_x and particulate matter is not necessarily fuel derived.

Results of sulfur balances are listed in Table 3.1.1.8. Here the closure is relatively good, and calls into question the total S concentrations obtained. The sulfur balances made use of the SO_2 concentrations, rather than total S, as these were thought more reliable. The good closure on traverse 2 is consistent with the earlier observation that the poor closure on the carbon balance for this traverse is due to an error in the CO_2 determination, rather than to an error in stack gas velocity. The average distribution of sulfur among the products is illustrated in Figure 3.1.1.16. SO_2 accounts for the largest fraction of fuel sulfur, about 72%, followed by sulfur in the ash at 21% and sulfur in particulate matter at 6%. About 1% of fuel sulfur was not accounted for in the ash, particulate matter, and

SO_2. The ratio of SO_2 to total S (as SO_2) was shown in Tables 3.1.1.4 and 3.1.1.5 to be about 0.7. Closing the sulfur balance on SO_2 alone suggests most of the fuel sulfur is present in this form, while the total S values suggest the presence of other forms. The total S instrument response was observed to underestimate SO_2 concentrations in the presence of high CO_2, which implies that the total S measurements of stack gas should be biased low, if at all. Overall, the total S and SO_2 concentrations can be construed as indicative that much of the gas phase sulfur is emitted as SO_2, but cannot be used to establish the presence of other forms.

Water balances were also completed as shown in Table 3.1.1.9, but actual weight gains for the impingers and desiccant were not measured. Weight gains were measured in all subsequent tests. Estimates of stack gas humidity show the gas to be far from saturation, with relative humidities in the range of 10%. The total estimated weight gain for the impingers and desiccant was 9 g over the first two traverses. The total PM sampling system was not used during the third traverse.

Results of power balances are given in Table 3.1.1.10. The average heat release rate was about 120 kW, with a fireline intensity of about 100 kW m^{-1}. The thermal dissipation by the tunnel walls was estimated at 40 - 50 kW.

VOC concentrations are listed in Table 3.1.1.11. Only benzene, toluene, styrene, and xylene were quantified for this experiment, due to the availability of standards. Although only four compounds were quantified for this test, the total ion chromatogram (TIC) indicated the presence of additional species. Emission factors (mg kg^{-1}) were computed from the concentrations for the four species, and are listed in Table 3.1.1.12. No PAH samples were collected during this test. Results from samples submitted for chlorinated dioxins and furans identified detectable amounts of only three species: 1,2,3,4,6,7,8-HpCDD, 1,2,3,4,6,7,8,9-OCDD, and 1,2,3,4,6,7,8,9-OCDF. These analyses were carried out on filter and sorbent samples including field blanks by Triangle Laboratories of RTP, Inc., Durham, North Carolina. Detection limits for filter samples ranged from 0.003 to 0.005 ng for 7 chlorinated dioxin species and 10 chlorinated furans. Detection limits for sorbent samples ranged from 0.01 to 0.03 ng. The actual amounts found and the emission factors were as follows:

Analyte	Filter (ng)	XAD Sorbent (ng)	Total Emission Factor (μg kg^{-1})
1,2,3,4,6,7,8-HpCDD	0.05	not detected	0.037
1,2,3,4,6,7,8,9-OCDD	2.40	0.06	1.840
1,2,3,4,6,7,8,9-OCDF	0.04	not detected	0.030

No 2,3,7,8-TCDD or -TCDF was identified in the samples. Due to the expense of the analysis and the small levels detected, no further samples were evaluated.

3.1.2. Rice straw, CRNF, 9 June 92

This test was a replicate of the test of 30 April 92, but included the DRI particle sampling system and PAH analysis. Unfortunately, the total filters loaded at FAI were later found (aborted run of 8 July 92) to have been installed improperly, and the PM concentrations were therefore erroneous. Results from the cascade impactor, which were in fair correspondence with the mass concentrations determined from the DRI filter samples, were used to estimate the total particulate matter concentrations for this test. The total hydrocarbon analyzer was not yet installed for this and the succeeding two tests, and hydrocarbons were determined by GC only.

The fire was ignited at 1120 h and burned nearly continuously until 1630 h. Three stack traverses of 48 min each were completed. Between 1500 h and 1520 h, the wind tunnel doors were opened to clear a straw accumulation on the side of the conveyor. This event is reflected in the stack gas temperature, velocity, and concentrations. Only two PAH sorbent tubes were available, and were used on the first two traverses.

Operating conditions are shown in Figures 3.1.2.1 through 3.1.2.12. Air temperature and relative humidity at the wind tunnel site (Figure 3.1.2.1) were measured under a gill radiation shield outside the wind tunnel, and were not substantially different from the values obtained at the CIMIS site (Figure 3.1.2.2). Ambient temperature increased about 10 K during the test, which was reflected in increasing stack temperature throughout the course of the experiment. Stack temperature was again about 30 K above inlet temperature, except during the last traverse when the temperature differential increased to 40 K (Figure 3.1.2.5). Consistent with this stack temperature rise was an increase in fire spreading velocity (Figures 3.1.2.6, 7), which for the last 2 h was in excess of 1 m min^{-1}. The total fire spreading distance was just under 300 m (Figure 3.1.2.8).

Fuel and ash analyses are given in Table 3.1.2.1. The ash carbon concentration was slightly elevated over that of the 30 April 92 experiment, but the compositions were overall quite similar. Average operating conditions and concentrations are listed in Table 3.1.2.2. Stack gas velocity was approximately 2 m s^{-1}, as before. With the exception of CO_2, stack gas concentrations were similar for all three traverses. The average CO_2 concentration was lower for the first traverse than for the second and third.

The PM concentrations listed in Table 3.1.2.2 are those obtained from the total filters, but are erroneous due to the filter loading problem mentioned above. Total masses from the cascade impactor give stack PM concentrations during the first, second, and third traverse as 11.65, 9.5, and 15.06 mg m^{-3}, respectively. No DRI filter samples were taken during the first traverse period, but results from the second and third traverses give PM mass concentrations of 9.36 and 13.69 mg m^{-3}, which are in good agreement with the results from the cascade impactor. All PM, PM10, and PM2.5 emission factors were therefore recomputed using the concentrations from the cascade impactor. The revised results are listed in Table 3.1.2.3.

Particle size distributions from the cascade impactor are shown for the three traverses in Figures 3.1.2.13 - 15. The distributions are similar, although the profile for traverse 3 shows lower PM10 and PM2.5 concentrations than the other two.

Results of the mass balances are listed in Table 3.1.2.4. The faster spreading rate compared to the test of 30 April 92 is evident in the longer spreading distance (conveyor travel) for each traverse. Fuel moisture was 8 to 9% wet basis. Overall air-fuel ratios were 200 to 250, or somewhat lower than in the previous test, again due to the faster spreading rate of the fire.

There were no significant differences observed in fuel moisture or loading rate among the three traverses. New bales of straw were started at 1140, 1220, 1252, 1325, 1400, 1427, 1446, 1510, 1545, and 1609 h. After loading, fuel required 20 to 30 min to travel the 20 m to the fire. The increase in stack temperature and spreading rate beginning around 1430 h and continuing to the end of the test suggests that straw from the bales loaded at 1400 h and after in some way differed from the straw loaded previously. The same operator loaded the straw, and there were no changes in the manner in which straw was loaded onto the feed conveyor. As discussed later, some differences in chemical

composition between rice straw from different sources exist, but repeated analyses from the same source are in quite good agreement. Physical differences in color and texture have been observed for straw from the same and different sources, which may be relevant to the observed changes in spreading rate. A parametric investigation of these effects has not been undertaken, although differences in behavior for two separate straw sources under the same wind tunnel conditions have been confirmed, as shown later.

Emission factors for major species are listed in Table 3.1.2.5 using the integrated approach for continuously monitored species, and in Table 3.1.2.6 using the average approach. The two results are again in good agreement. The ratios of SO_2 to total S are similar to those obtained in the earlier experiment. CO and PM emission factors are lower than for the previous test, with NO_x emission factors slightly higher.

Closure on the carbon balances ranges from 80 to 115% (Table 3.1.2.7), with an average around 90%. The high value for traverse 2 is due to a higher CO_2 emission factor than can be accounted for by the carbon concentration of the fuel and ash and the measured stack velocity.

Nitrogen balances (Table 3.1.2.8) show the ratio of nitrogen in the ash, NO_x, and particulate matter to be about 30% of that in the fuel. This result is similar to that obtained in the test of 30 April 92. The distribution of nitrogen among the products is shown in Figure 3.1.2.16.

Closure on the sulfur balances (Table 3.1.2.9) is good, ranging from 90 to 94% on an integrated basis. The average distribution of sulfur among the products shown in Figure 3.1.2.17 yields a higher proportion in ash than in the previous test, but the undetermined fraction is somewhat higher (ND = 8%).

Water balances (Table 3.1.2.10) yield an estimated impinger and desiccant weight gain which is 80% of the measured value. The stack humidity was still well away from saturation. The water from evaporation of fuel moisture and released by combustion was sufficient to raise the stack dewpoint temperature 3 - 4 K above ambient dewpoint, but still below temperatures in the sample line. The impingers failed to cool the gas to the dewpoint, leaving a fair amount of absorption in the desiccant.

Heat release rates (Table 3.1.2.11) were 50 to 100 kW higher than in the previous test due to the higher spreading rates encountered. Wall dissipation was in the range of 50 - 80 kW.

Results of chemical and elemental analyses on the DRI particulate matter samples are given in Tables 3.1.2.12 - 17. Concentration units are mass fraction in percent. The values are blank subtracted and include propagated uncertainties based on analytical precisions and standard deviations of blanks. The analytical precisions are derived from counting statistics for the XRF, the precisions for the other techniques are based on replicates or minimum detection limits (Chow, 1987).

DRI samples were collected during the second and third traverse periods. Filters labeled ABTT005 and ABTQ005 (Tables 3.1.2.12 -14) are the 2.5 μm size cut teflon and quartz filters, collected during the second traverse period. ABTT006 and ABTQ006 are the corresponding 10 μm samples taken at the same time. Filters 7 and 8 (Tables 3.1.2.15 - 17) were collected during the third traverse period. Mass concentration fractions are given in Tables 3.1.2.12 and 3.1.2.15 for each of the two sets of filters. The sums of measured species do not include $SO_4^=$, Cl^-, K^+, organic high temperature carbon

(C(oht)), or elemental high temperature carbon (C(eht)), as these are subsets of the corresponding total elemental concentrations. Analysis flags appearing at the top of each table were assigned by the DRI analyst and were defined in Table 2.2.1.3.1 above. The flags indicating separation of the teflon membrane filter from the support ring suggest some problem in filter loading. Appearing along with the mass concentration fractions are analytical uncertainties, and the ratio of each compound in the 2.5 μm size fraction to that in the 10 μm size fraction.

Tables 3.1.2.13 and 16 give ratios of some of the compounds analyzed. Chloride ion and potassium ion concentrations are about 80 and 60% respectively of the total chlorine and potassium measured. The near unity ratio of Cl/K along with other observations of filter samples from the wind tunnel when burning rice straw suggest that at least a portion of the chlorine and potassium may be present as a KCl salt.

Emission factors for each of the species analyzed were computed from the mass fractions and the emission factors for particulate matter in each size range. The results are listed in Tables 3.1.2.14 and 17. The PM10 and PM2.5 emission factors derived from the cascade impactor results were used in computing the individual species emission factors, rather than the DRI mass concentrations, which were obtained without traversing the stack. In subsequent experiments, the emission factors computed on the total filter mass concentrations were used. The values are listed at the top of each table, along with the ratio of the DRI teflon filter mass concentration to the PM10 and PM2.5 mass concentrations derived from the cascade impactor. These ratios range from 77% to 97%. In computing the emission factors, the species concentration was normalized to the sum of the species so as to produce a sum of individual species emission factors equal to the total PM10 or PM2.5 emission factor, which can be seen at the bottom of each table. The magnitudes of the concentrations and emission factors between the two sets of filters are in fair correspondence. The composition of the particulate matter is dominated by carbon, potassium, and chlorine.

VOC concentrations are listed in Table 3.1.2.18 and emission factors in Table 3.1.2.19. The concentrations are higher than measured during the previous experiment, although the relative rates of emission are consistent. Benzene was present in highest concentration, followed by toluene, styrene, and xylene in that order. The magnitudes of the emission factors are subject to considerable uncertainty, but show good repeatability among the three traverses.

PAH emission factors are listed in Table 3.1.2.20. Shown are the results for the total filters, XAD-2 sorbent, tubing, and impinger rinse, along with totals. These values are suspect due to the improper loading of the filters, as mentioned above. Very little PAH was found in the impinger rinse, indicating little or no breakthrough. Total PAH emission factor averaged about 5 mg kg^{-1}, about 95% of it captured in the sorbent. Naphthalene accounts for roughly two-thirds of the total. The fraction of each species found on the total filter is shown in Figure 3.1.2.18. Around molecular weight 200 (Fluoranthene, molecular weight 202), the fraction of PAH found in the particle phase begins to increase. This is consistent with later tests.

3.1.3 Rice straw, CEWF, 10 July 92

This test was conducted with the same fuel used in the tests of 30 April and 9 June 92, and in the aborted run of 8 July 92. The wind tunnel was configured with the ceiling extended to the forward edge of the fire, and the auxiliary floor was installed blocking ventilation from below. The stack gas velocity was set to approximately 3 m s^{-1}.

The fire was ignited at 1006 h and burned until 1338 h, with short interruptions from 1114 to 1130 h, and from 1250 to 1315 h. Two main traverses of 48 min each were conducted. The second traverse was interrupted to correct a high pressure drop on the total filter line due to excess glass wool packing at the inlet to the XAD-2 resin trap, and then restarted. Sampling after the second traverse was done to collect filter samples for biogenic silica fiber analysis, and accounts for the lower impinger temperatures occurring after the second traverse was completed.

Operating results from this test are given in Figures 3.1.3.1 through 3.1.3.12. Stack gas temperature (Figure 3.1.3.5) was consistently about 20 K above inlet air temperature. Spreading rate (Figures 3.1.3.6 and 7) was less variable than in previous trials, and stayed at about 1 m min^{-1}. Ash composition is given in Table 3.1.3.1. The composition is quite similar to that for the previous test.

Average results for the two traverses are listed in Table 3.1.3.2. Results of the mass balances (Table 3.1.3.3) show an average fuel consumption rate of 11 to 12 g s^{-1} dry basis, with an overall air-fuel ratio of about 400. Particle size distributions are shown in Figures 3.1.3.13 and 14. The distributions are not as regular as in previous experiments. The PM concentration from the second traverse was one third of that from the first. This result is corroborated by the total mass concentrations from the cascade impactor, which yield 4.0 mg m^{-3} for the first traverse and 2.1 mg m^{-3} for the second traverse. The mass concentrations from the DRI teflon filters taken during the first traverse period were 3.4 and 3.9 mg m^{-3} for the PM2.5 and PM10 fractions respectively. No DRI filter samples were collected during the second traverse. The reasons for the difference in concentrations between the first and second traverse are not clear. The high pressure drop in the total filter line during the second traverse may have had some influence on the mass concentration for the total filter, but would not have affected the cascade impactor. Although total mass concentrations determined from cascade impactors are known to be unreliable, the general correspondence between these and the total filter results shows them to be valid indicators of trends in concentration.

Emission factors computed by the integrated and averaged techniques appear in Tables 3.1.3.4 and 5. The magnitudes are quite similar, indicating relatively stable fire conditions. The ratio of SO_2 to total S is in this case greater than unity, due to low total S concentrations. The concentrations on this test were approximately one fifth the concentrations of the previous test, although the stack gas flow rates were on average only 50% higher. SO_2 concentrations were lower by about one third compared to the previous experiment.

Carbon balances (Table 3.1.3.6) show an excess closure for both traverses, due likely to error in the determination of the average CO_2 concentration. The fuel carbon concentration used in computing the carbon balances was that from the analysis of the test of 14 July 92 with the same fuel. The carbon concentration matches that from the analysis of 9 June 92 to within 0.1%.

Nitrogen balances (Table 3.1.3.7) yield a somewhat lower ratio of ash, NO_x, and PM nitrogen to fuel nitrogen than on the previous test. In this case the ratio is about 25%, about 5% absolute lower than previously. The distribution among products is shown in Figure 3.1.3.15. The proportion of nitrogen in NO_x is lower than before. The proportions in ash and PM are roughly the same.

Sulfur balances (Table 3.1.3.8) yield a much larger undetermined fraction (35%) than in previous experiments. Ash and PM sulfur fractions are very similar to previous experiments, as shown by Figure 3.1.3.16, but the fraction as SO_2 is reduced.

Water balances (Table 3.1.3.9) show only 1% difference between estimated and measured impinger and desiccant weight gain. Stack relative humidities were 8%, with water release again sufficient to raise dewpoint temperature about 3 K above ambient. Power balances (Tables 3.1.3.10) yield total heat release rates of 160 to 170 kW, with tunnel dissipation at about 80 kW.

Results of the DRI analyses on PM2.5 and PM10 samples collected during the first traverse period are listed in Tables 3.1.3.11 - 13. Carbon, potassium, and chlorine are again the dominant elements, but nitrogen as ammonium contributes substantially as well (9%). The ratio of Cl to K is here twice the value obtained in the previous experiment, due mostly to lower K concentrations than before. Included in Tables 3.1.3.14 and 15 are concentration values and ratios for the DRI filter samples collected during the aborted test of 8 July 92. This test was conducted in the same manner, and with the same fuel and wind tunnel configuration, as the test of 10 July 92. The NH_4^+ concentrations are high in these samples as well, and K concentrations lower than those obtained in the experiments of 9 June and 10 July 92. The reconstructed masses show good recovery for filter sets from both 8 and 10 July 92.

Two CNL filter samples were collected, one each during the two traverses. Results from the filter collected during the first traverse (filter ID AG-28) are shown in Tables 3.1.3.16 and 3.1.3.17. Concentrations of hydrogen were determined by PESA, all others by PIXE. Concentration values are listed in Table 3.1.3.16 in ng m^{-3}, and converted to emission factors (mg kg^{-1}) in Table 3.1.3.17. These results can be compared against the emission factors for matching species from the DRI analysis in Table 3.1.3.13, using the PM10 values, which should approximate total PM values. In general the results compare within the same order of magnitude, and in roughly the same relative proportions. Results for the CNL filter sample from the second traverse period (Tables 3.1.3.18 and 19) show fair repeatability, and somewhat better correspondence to the DRI emission factors for certain species, particularly K and Cl. A comparison of average concentration values from both the CNL and DRI analyses for the various fuel types appears later.

Distributions of elements among various size fractions using PIXE/PESA analyses on DRUM sampler strips are set out in Tables 3.1.3.20 - 27. These analyses are useful primarily from a qualitative perspective in ascertaining the relative abundance of various species in each size fraction. The tables include computed abundances for species relative to potassium in the same size range, and relative to the same species in the first size range of 10 to 15 μm. Results of the latter analysis are summarized in Figure 3.1.3.17 for the major elements Si, Cl, K, Ca, and Fe. Both Si and Fe are shown to be present principally in the large size fractions, dropping off a hundred fold in the finest sizes. Ca remains nearly constant in concentration, but was not detected below 2 μm by the PIXE analysis, and no conclusions can be drawn about its presence in the fine particle range from these results. Both K and Cl are greatly enriched in the range 0.5 to 1 μm relative to their concentrations in the coarse fractions. The qualitative nature of these results is apparent from the lack of consistent detection of elements among the various size fractions.

Results of VOC analyses are listed in Tables 3.1.3.28 and 29. The analysis here differs from the previous analysis in that the MS library was automatically searched for appropriate species matches, and concentrations scaled from peak areas relative to

toluene. A wider range of compounds was identified. The listing of dimethyloxirane is done tentatively as this represents a possible mismatch. The concentrations for benzene, toluene, and xylene are similar to those from the experiment of 9 June 92. Styrene concentrations are somewhat lower, and closer to those from 30 April 92. Other compounds identified include naphthalene, phenol, benzonitrile, benzaldehyde, and benzofuran.

PAH emission factors are listed in Table 3.1.3.30. The filter fraction from the second test shows almost no PAH present. This appears to be an analysis error. The data from this second test are excluded from the average values reported later. The sorbent tube from the second test yields about the same levels as the from the first test. The impinger rinsate shows only low levels of PAH, as do the back-up filter and tubing. The total from the first test is higher than the previous experiment in rice straw, being about 15 mg kg^{-1}. The paritioning of PAH to the filter fraction is shown in Figure 3.1.3.18.

3.1.4. Rice straw, CRNF, 14 July 92

This was the companion test to 10 July 92, conducted under the alternate wind tunnel configuration (CRNF). Average wind speeds were about 2.5 m s^{-1}. The fuel used was the same as that of the three previous tests. The fire was first ignited at 0931 and was extinguished between sampling periods.

Operating results are summarized in Figures 3.1.4.1 - 12. Three traverses of 48 min each were completed, although the cascade impactor was not used with the third traverse. Stack gas temperatures were 20 to 25 K above inlet air temperatures. Fire spreading velocity was again about 1 m min^{-1}, increasing slightly with increasing inlet air temperature (Figures 3.1.4.6 and 7). Results of fuel and ash analyses are listed in Table 3.1.4.1. The compositions are quite similar to those from previous experiments.

Average results are listed in Table 3.1.4.2. Gas and PM concentrations were fairly stable over all three traverses. Mass balances (Table 3.1.4.3) show the overall air-fuel ratio to be higher during the first traverse (about 350) than for the latter two (approximately 300). The change is due to the increasing fire spreading velocity from about 0.9 to 1.1 m min^{-1} with nearly constant air flow. Particle size distributions in Figures 3.1.4.13 and 14 have similar appearances to those from the previous CRNF experiments on 30 April and 9 June 92.

Emission factors for major species computed by the integrated and averaged techniques appear in Tables 3.1.4.4 and 3.1.4.5 respectively. The agreement between the two techniques is, as before, fairly good. The ratio of SO_2 to total S is less than unity and closer to the values obtained in the previous CRNF tests, although the emission factors for both are less than those of the tests of 30 April and 9 June 92. Hydrocarbon emission factors as determined from GC analyses of grab samples are also lower compared to the two previous CRNF tests. PM emission factors are nearly the same as for 9 June 92, but both tests show lower values than for the test of 30 April 92.

Closures on carbon balances in Table 3.1.4.6 are 73 to 89%. The CO_2 emission factors appear somewhat low compared to maximum values, and indicate a possible error of 10 to 25%. Stack velocities estimated by closing the carbon balance with the measured CO_2 concentrations are over 3 m s^{-1} for the second and third traverses, and reflect the sensitivity to the average CO_2 concentrations.

Nitrogen balances (Table 3.1.4.7) show the total ratio of ash, NO_x, and PM nitrogen to fuel nitrogen to be similar to what it was in the previous CRNF experiments, but the distribution among products (Figure 3.1.4.15) is different than in the previous tests, with more nitrogen in the ash and less appearing as NO_x. The undetermined fraction is about the same at 70%.

Closure on the sulfur balances (Table 3.1.4.8) is quite poor at 55 - 65%, with an undetermined fraction (38%) similar to that found in the CEWF test of 10 July 92. The distribution of sulfur among products (Figure 3.1.4.16) is also similar to that of the prior test, although the ash sulfur fraction is somewhat depressed.

Water balances (Table 3.1.4.9) show good agreement between estimated and measured weight gains for the impingers and desiccant. Stack humidities were higher than in previous tests due to the higher ambient humidities encountered, but still well below saturation. Impinger outlet temperatures were below calculated stack gas dewpoint temperatures. Average heat releases were 170 to 200 kW (Table 3.1.4.10).

Results of DRI analyses on the filter samples collected during the first traverse period are listed in Tables 3.1.3.11 - 13. The teflon filter mass concentrations were well below those obtained on the total filter. The analysis flag for the quartz filters (ABTQ019) indicates an inhomogeneous sample deposit (flag i1). The reasons for inhomogeneities in deposit or low sample masses are not known. All filters were handled and samples collected in the same manner as previous tests. Only very minor adjustments were needed to maintain flow rate through the filters. The Cl/K ratio approaches unity, as in the CRNF test of 9 June 92. Mass concentrations for C, Cl, and K are similar as well, although the emission factors for Cl and K (Table 3.1.4.13) decreased.

PIXE/PESA results from CNL filters collected during each of the first two traverses are given in Tables 3.1.3.14 - 17. Concentrations for Cl and K were lower in the second sample, and emission factors for these two elements were half the values of the first sample. The Cl and K emission factors from the first CNL filter are in fairly good agreement with those from the DRI PM10 samples collected on the same traverse. Emission factors for Si, Fe and Mn from the CNL analysis are intermediate to the PM2.5 and PM10 values from the DRI analysis.

DRUM sampler results are given for the eight stages in Tables 3.1.4.18 - 25. Results for Si, Cl, K, Ca, and Fe are summarized in Figure 3.1.4.17. The trends are similar to those observed in the CEWF test of 10 July 92, although the enrichment of Cl and K in the finer size fractions is not as evident and more variable. Differences may be due to the analysis procedure described above in which the deposits on the DRUM tape were not analyzed at the same location, giving variable deposit density.

VOC concentrations are listed in Table 3.1.4.26 with computed emission factors in Table 3.1.4.27. Emission factors for benzene, toluene, styrene, and xylene are reduced relative to the CEWF test of 10 July 92. Naphthalene and benzaldehyde were identified in all three traverses, butane in the second and third traverses.

PAH emission factors from the first two traverses are listed in Table 3.1.4.28. The totals are quite similar to the previous experiment, with an average of 15 mg kg^{-1} over both traverses. Mass fractions of speciated PAH on the primary filters are shown in Figure 3.1.4.18.

3.1.5. Rice straw, spreading rate comparisons, CEWF, 25 August 92

Spreading velocities observed in the preceding tests were consistently higher than observed during the earlier comprehensive study of rice straw fires and effects of wind tunnel configurations (Jenkins, et al., 1993a, b). Whereas spreading rates in the previous study using a M202 variety straw harvested in the autumn of 1987 were consistently 0.5 to 0.7 m min^{-1}, spreading rates for the tests from 30 April 92 through 14 July 92, also with a M202 variety straw were 0.7 to 1.1 m min^{-1}, with all three of the latter tests in this group near 1 m min^{-1}. The fuel moistures and loading rates were not different between the two studies. To investigate whether the differences in spreading rates were due to differences in the fuels or to differences in the ambient or wind tunnel conditions at the time of the experiments, the two types of straw were tested on the same date under the same conditions.

The CEWF wind tunnel configuration was used, with an average wind speed of 3 m s^{-1}. Fuel moisture for both types was 7 to 8% wet basis. The 1987 crop year straw, referred to here as type 1 straw, was fed during the first 97 min and the last 84 min of the test. The 1991 crop year straw, or type 2 straw, was fed during the intermediate 68 min of the test. The fuel beds were contiguous, with no interruption of fuel supply at any time. Paper markers were inserted in the fuel bed indicating the change in fuel type. No emissions sampling was performed for this test. The results of the experiment are included in Figures 3.1.5.1 through 3.1.5.8, and in Table 3.1.5.1. Unfortunately, ambient conditions were not constant, and the results were not conclusive. Some influence due to fuel type was apparent, however.

The average spreading rate for the type 1 straw (Table 3.1.5.1) was 0.46 m min^{-1} during the first period, and 0.59 m min^{-1} during the final period. The fire in the type 2 straw spread at an average rate of 0.63 m min^{-1}, which was not substantially different than the average spreading rate for the type 1 straw in the final period, and lower than observed during the other CEWF trial with this straw on 10 July 92. As shown in Figure 3.1.5.7, however, the spreading rates were by no means uniform. During the first period, the fire slowed somewhat in the type 1 straw, but immediately started spreading faster upon reaching the type 2 straw. However, about 15 min later, the spreading rate, after reaching a high of 0.66 m min^{-1}, decreased to about 0.56 m min^{-1}. It then rapidly increased again to a peak value of 0.78 m min^{-1}. Immediately after reaching the second load of type 1 straw in the final period, the spreading rate dropped again to about 0.58 m min^{-1}, and then slowly increased, reaching a final value of about 0.64 m min^{-1} before the test was terminated. Observations of the color and texture of the straws showed the type 2 straw to be darker in color, and finer stemmed than the type 1 straw, which may relate to important differences in weathering which we believe to be responsible for the differences in burning rate.

3.1.6. Rice straw, spreading rate comparisons, CEWF, 2 September 92

The inconclusive nature of the test of 25 August 92 led to a second trial on 2 September 92 to compare the two types of straw. The test was conducted as in the previous test, except with selected emissions sampling and running two 48 min traverses on type 1 straw followed by two traverses on type 2 straw. The results were still not entirely conclusive due to changes in ambient temperature and relative humidity during the experiment, but some apparent differences in spreading rate due to fuel type were observed. Influences due to ambient conditions may also be present, and are discussed later.

Results of the experiment are included in Figures 3.1.6.1 - 21, and in Tables 3.1.6.1 - 10. No VOC or PAH samples were collected, and no DRI or CNL filter samples were taken. Only the total filter, cascade impactor, continuous gas analysis (now including a continuous hydrocarbon or THC analyzer), and grab samples were used. The fire was extinguished after the second traverse to reload the total filter probes. The high conveyor speeds seen in Figures 3.1.6.6 and 7 at the end of the second traverse are not natural spreading rates, but are due to the operators moving the fuel bed downstream at high speed to locate the intersection of the type 1 and type 2 straw.

As shown in Table 3.1.6.1, differences exist in the major elemental compositions of the two types of fuels. Potassium concentration in the type 2 straw is about half that of the type 1 straw. Sulfur concentration is slightly lower in the type 2 straw, and chlorine concentration is is roughly a fifth of that in the type 1 straw. Larger differences exist in the residual ash composition (Table 3.1.6.1). The carbon concentration of the type 1 ash is higher than the type 2 straw (12.5% vs. 8.5%), which is reflected in the higher heating value for the type 1 ash (4.2 vs. 2.8 MJ kg^{-1}). The potassium concentration is lower in the type 2 ash, being only a third that of the type 1 ash. A similar result is obtained for chlorine.

Ambient conditions changed by 10°C in temperature and 40% in relative humidity over the full duration of the experiment (Table 3.1.6.2). Temperature elevations in the stack relative to inlet were 15 and 16 K for the first and second traverses, but only 14 and 11 K for the third and fourth traverses. Stack gas velocity was approximately 3 m s^{-1} during the first two traverses, increased to nearly 4 m s^{-1} during the third traverse, and declined to 3.5 m s^{-1} over the fourth traverse. Measured stack gas velocities are supported by the carbon balances (Table 3.1.6.6) , which show good agreement except for the first traverse where an apparently low CO_2 concentration causes a high estimate of stack gas velocity. The fire spreading rates were 0.37 and 0.43 m min^{-1} for the first two traverses in type 1 straw, and 0.71 and 0.55 m min^{-1} for the final two traverses in type 2 straw. The substantial difference in spreading rate for the third traverse is apparent in Figure 3.1.6.7. The spreading rates are essentially constant throughout each of the traverses. The spreading rate in the third traverse is higher than in the fourth even with increased inlet temperature and decreased humidity during the fourth traverse. Lower inlet air temperatures are probably responsible for the lower spreading rates of the type 2 straw compared with the tests of 9 June and 10 and 14 July 92. Moisture contents were identical for the two types.

Several important differences emerge from the emission factor determinations (Tables 3.1.6.4 and 5) for the four traverses. CO was reduced in the third traverse, closely approaching the values seen with this fuel in the earlier trials. CO in the fourth traverse was essentially the same as that observed in the first and second traverses. NO_x was higher in the third traverse than the others, SO_2 slightly elevated, hydrocarbons and PM reduced. The THC emissions were on average higher with the type 1 straw than the type 2 straw, although this is the result principally of a high THC emission in the first traverse. Note that the THC concentrations determined by continuous analyzer were higher than obtained from GC analyses. The continuous analyzer consistently gave higher concentrations than the GC analysis, in many cases by about a factor of 2.

The relative emission levels for the four traverses suggest a more thorough burn during the third traverse, which appears consistent with the faster spreading rate. The PM emission factor, however, remained low for the fourth traverse, and was only slightly elevated compared to the third traverse. The PM emission factors for the type 1 straw are

both higher, and better match the emission factors observed in the earlier study (Jenkins, et al., 1993a, b). Differences in PM emission factor between the two types of straw are not thought to be due to fine materials in the fuel (e.g. dirt, dust, or fine fuel particles). To the contrary, the operators observed that the type 2 straw appeared in some respects to be "dustier" to handle, although this was not quantified.

Nitrogen balances (Table 3.1.6.7 and Figures 3.1.6.18 and 19) did not reveal significant differences in nitrogen accounting or in product distribution. The fraction of nitrogen in NO_x is higher for the type 2 straw on average, due primarily to the higher NO_x in the third traverse. Sulfur distributions (Table 3.1.6.8 and Figures 3.1.6.20 and 21) show some difference, but the average undetermined fraction is higher with the type 1 straw and perhaps masks true differences between the fuels. The distribution for the type 2 straw is similar to the results of the tests of 10 and 14 July 92, although, like these two tests, different from the results of 30 April and 9 June 92 due to the larger undetermined fraction. Water balances overestimate impinger and desiccant weight gain by about 30%, but do not reveal any gross errors in humidity or flow rate measurements.

We have recently discovered that leaching rice straw with water dramatically alters its combustion characteristics (Jenkins, et al., 1995). The differences in burning rates between the two types of straw are believed to be due largely to the differences in chlorine and alkali metal (especially potassium) concentrations. Halogens are known fire retardants, and the lower chlorine concentrations for the type 2 straw are consistent with the improved ignition and burning characteristics observed for this straw. We have also shown that the removal of alkali metals by leaching results in kinetic shifts and slower rates of reaction, however, the reduction in chlorine concentration appears to more than compensate for any such reductions due to the catalytic effects of alkali salts. Any amount of precipitation on the straw prior to harvesting would have resulted in at least partial leaching of alkali and chlorine from the straw. This may occur simply as a result of condensation (dew) as well. The differences in burning characteristics and emission rates seen here suggest some amount of variation in field burning emissions from prior weathering of the straw and the loss of alkali metals, chlorine, and possibly other elements as well. Spring burns may result in substantially improved ignition and reduced emissions compared to fall burns due to the reductions in chlorine concentration by leaching through precipitation.

3.1.7. Rice straw, CEWF, 21 October 92

The tests of 21 October 92 and the following companion tests of 23 October 92 were conducted with a 1992 crop year rice straw, also of the M202 variety. This first experiment employed the CEWF wind tunnel configuration with a wind speed of around 3 m s^{-1}. Two stack traverses of 48 min each were completed. Operating results are shown in Figures 3.1.7.1 through 3.1.7.13. Particle size distributions appear in Figures 3.1.7.14 and 15. .

Results of fuel and ash analyses are listed in Table 3.1.7.1. The straw is distinguished by a very high ash content. The residual ash produced from the test was also higher in carbon, and had a composition more closely resembling the type 1 straw used in the test of 2 September 92.

Average results are listed in Table 3.1.7.2. The fuel loading rate at the fire was somewhat reduced compared to earlier tests due to a higher gap loss with this fuel. The fire spreading rates were reduced compared to the tests using the 1991 (type 2) straw, and more closely resembled the rates obtained with the type 1 straw of the previous study.

Partly this may be the result of the moderately high relative humidities, but the tests of 14 July 92 were conducted at similar humidities with faster spreading rates. Inlet air temperatures appear to have greater influence on spreading rates. Correlations of spreading rates against various external parameters are described later. The slower spreading rates are reflected in the stack temperature differentials, running only 7 to 10 K above inlet temperature.

Typical of all the tests were the higher total hydrocarbon concentrations determined by continuous analyzer compared to the sum of the five hydrocarbon species analyzed by GC. As mentioned above, THC concentrations in general were found to be about double the C_1 - C_3 hydrocarbon concentrations from GC.

Emission factors for major species by the integrated technique are listed in Table 3.1.7.4 and for the averaged technique in Table 3.1.7.5. Emissions of CO, hydrocarbons, and particulate matter are higher compared to the earlier test of 10 July 92, and again more closely resemble the results obtained on the type 1 straw.

Carbon balances (Table 3.1.7.6) are reasonably well closed. Nitrogen balances (Table 3.1.7.7 and Figure 3.1.7.16) show larger fractions of nitrogen in ash and particulate matter and a lower undetermined fraction than in the previous CEWF experiment. Sulfur balances (Table 3.1.7.8 and Figure 3.1.7.17) reveal a much larger fraction of sulfur retained in the ash than on the previous trial (compare Figure 3.1.3.16). To some extent, the larger undetermined fraction in the earlier test may mask similarities in this regard. Compared to all other tests using the 1991 type 2 straw, the fraction of sulfur in ash from this test is much larger.

Water balances (Table 3.1.7.9) show good agreement between estimated and actual impinger and desiccant weight gain. Water from combustion and evaporation of moisture was sufficient to increase dew point temperature in the stack only about 1 K above ambient due to the low spreading rates. Total heat release rates (Table 3.1.7.10) were 60 to 80 kW, with tunnel dissipation around 30 kW.

Results of the DRI filter analyses are given in Tables 3.1.7.11 - 13. The concentration of potassium in the particulate matter is low and ranks fourth in total concentration behind ammonium ion. The reconstructed mass is low for both PM2.5 and PM10 (87 and 82% respectively), which possibly contributes to the low potassium. However, the fuel and ash analyses show that 91% of the fuel potassium is accounted for in the ash, indicating less potassium release than in earlier tests. Potassium retained in ash accounts for 78 and 54% of fuel potassium in the tests of 10 and 14 July 92, respectively. The ratio of Cl to K in the particulate matter of this test (Table 3.1.7.12) is also consistent with that from the test of 10 July 92. Several discrepancies do appear in the data, however. The concentration of K^+ is higher than for elemental K. The same is true for chloride ion and elemental chlorine, and sulfate ion (as sulfur) and elemental sulfur (Table 3.1.7.12). These represent analysis errors.

Results of PIXE and PESA analyses on two filter samples analyzed by CNL are given in Tables 3.1.7.14 - 17. Comparison of the DRI and CNL computed elemental emission factors for traverse 2 (Table 3.1.7.13 and Table 3.1.7.17) show them to be in good agreement for Si, Cl, K, Mn, Fe, As, and Br, and rather poorer agreement for Cu and Na (Na^+ is analyzed by DRI, not elemental Na).

DRUM sampler results are listed in Tables 3.1.7.18 - 25, and summarized for major elements in Figure 3.1.7.18. The results suggest enrichment of K and Cl in the smaller

size fractions in a manner similar to the tests of 10 July 92. The other elements also follow trends similar to the earlier experiments.

VOC concentrations and emission factors are listed in Tables 3.1.7.26 and 27. The concentrations are higher in this test than in the previous CEWF test of 10 July 92. The slower spreading rates in combination with these higher concentrations yield greater emission factors than found previously, perhaps reflecting poorer burning conditions.

PAH emission factors are listed in Table 3.1.7.28. The totals are quite high, with very high emission rates of 2-methylnaphthalene. The average total emission factor is 39 mg kg^{-1}. The mass fractions of PAH on the filters are shown in Figure 3.1.7.19.

3.1.8. Rice straw, CRNF, 23 October 92

This was the companion test to that of 21 October 92, employing the alternate wind tunnel configuration and wind speed, but the same fuel. Two traverses of 48 min each were completed. Results are given in Figures 3.1.8.1 - 19 and Tables 3.1.8.1 - 28. Conducted at the same time of day as the test of 21 October 92, the ambient conditions were somewhat warmer and drier. Loading rate and fuel moisture were quite similar.

A significant feature of this test was the increase in spreading rate relative to the CEWF experiment conducted two days earlier. The average spreading rates were 0.97 and 1.13 m min^{-1} for the first and second traverses, respectively. These are double the rates observed in the CEWF test. This trend was not seen with the CEWF and CRNF tests of 10 and 14 July 92. As shown later in the discussion, the difference appears to be due almost entirely to the differences in inlet air temperature. The inlet temperatures were 5 K higher in the tests of 23 October 92 than in the tests of 21 October 92. The inlet temperatures for both experiments on 10 and 14 July 92 were nearly the same, and similar to those of 23 October 92. Later analyses on all rice straw tests show spreading rate to increase about 0.05 m min^{-1} for each 1 K increase in inlet air temperature. The 5 K increase for 23 October over 21 October 92 suggests an increase of 0.25 m min^{-1}. The other major influence is due to inlet air mass flow rate (wind speed), which suggests an additional increase of 0.2 m min^{-1} in spreading rate for the CRNF configuration of 23 October over the CEWF configuration of 21 October 92.

The emission factors for CO, total hydrocarbons, and particulate matter in this test were lower by approximately 20, 40, and 20%, respectively, compared with the CEWF configuration. NO_x and SO_2 were higher by 20% and 100%. The lower particulate matter emission for this test compared to the CEWF test contrasts with the results from the earlier comprehensive study (Jenkins, et al., 1993a, b). That study showed a consistent reduction in PM emission factor with increasing wind speed. The presence of the auxiliary floor was also observed to reduce PM emission factor. Clearly, the results of Table 3.1.8.4 show a cleaner burn for this CRNF test compared to its companion CEWF test of 21 October 92.

The carbon (Table 3.1.8.6) and water (Table 3.1.8.9) balances show good closure. Nitrogen balances (Table 3.1.8.7 and Figure 3.1.8.16) show a decrease in ash nitrogen fraction consistent with the increase in NO_x nitrogen fraction relative to the CEWF test of 21 October 92. Sulfur balances (Table 3.1.8.8 and Figure 3.1.8.17) show a higher fraction of sulfur in SO_2 and a lower fraction in ash compared to the CEWF test. Heat release rates (Table 3.1.8.10) were double those of the CEWF experiment, which follows directly from the increase in spreading rates.

Both DRI and CNL filter analyses show increased potassium emission for this experiment relative to its companion CEWF experiment (Tables 3.1.8.13 and 15). Both analyses are in relatively good agreement for major elements. A second filter sample analyzed by CNL (Tables 3.1.8.16 and 17) shows somewhat lower emission factors for most species. The distribution of species as a function of particle size from PIXE/PESA analyses of DRUM filter strips (Tables 3.1.8.18 - 25 and Figure 3.1.8.18) yield results similar to those obtained earlier, although without the apparent depletion in K and Cl around 2 μm diameter seen in Figure 3.1.7.18 for the CEWF configuration.

VOC concentrations (Table 3.1.8.26) were reduced relative to the CEWF configuration for most species identified in both tests. Emission factors (Table 3.1.8.27) were correspondingly reduced. Benzaldehyde and pentene, which were tentatively identified in the CEWF samples, were not identified (at least at threshold concentrations) in the CRNF samples. Dimethylbutane was listed for the CRNF configuration, but not for the CEWF configuration.

PAH emission factors are listed in Table 3.1.8.28. Like VOC, the levels were reduced compared to the companion CEWF configuration, and comparable to values obtained on earlier experiments. Emission factors for fluorene, phenanthrene, and 2-methylnapthalene are negative in certain filter samples due to blank subtraction. The reasons for these compounds appearing on the blank are unknown. Filter fractions of PAH are shown in Figure 3.1.8.19.

3.2. Wheat straw

Two companion experiments were conducted with wheat straw. The first, on 11 August 92, was conducted using the CRNF wind tunnel configuration with a wind speed of approximately 2 m s^{-1}. The second on 13 August 92 utilized the CEWF configuration at 3 m s^{-1}.

3.2.1. Wheat straw, CRNF, 11 August 92

This test was conducted with the wind tunnel ceiling retracted and without the auxiliary floor. The air flow was set to give an average wind speed of 2 m s^{-1}. Fuel loading rates for wheat straw were about 400 g m^{-2} and roughly a third lower than those used for rice straw. Two traverses of 48 min each were conducted. Results are given in Figures 3.2.1.1 - 19, and in Tables 3.2.1.1 - 26.

Results of fuel and ash analyses are listed in Table 3.2.1.1. The inorganic ash fraction of the straw was approximately 9%, but ash recovered from the burns amounted to about 15% of fuel dry weight. The carbon and hydrogen concentrations in the ash were fairly high at 18.85 and 1.25% respectively, but don't quite account for the difference in recovered ash fraction and inorganic ash fraction from the proximate analysis. Sulfur concentrations in this fuel were higher than observed in any of the rice straw fuels.

The tests were conducted earlier in the day to avoid extreme inlet air temperatures caused by ambient wind tunnel heating in an attempt to better match field conditions, although the humidity during the first traverse was higher than desired. Fuel moisture was nearly identical for both traverses at about 7% wet basis. Fire spreading rates were 0.3 to 0.4 m min^{-1} (Table 3.2.1.2), and in the lower range of those observed for rice straw. The reduced loading rate is thought to be a major factor in the slower spreading rates observed.

Emission factors for major species are listed in Tables 3.2.1.4 and 5 for the integrated and averaged techniques. CO, THC, and PM emission factors are smaller for the second traverse, while NO_x and SO_2 are increased. The second traverse shows a cleaner burn, probably as a result of the higher inlet air temperature, with possible influences from lower relative humidity. Although the spreading rates were slower by a third to a half compared to the rice straw tests, the emission factors on average were not found to be substantially different.

Carbon balances (Table 3.2.1.6) demonstrate good closure. Computed stack gas velocities are in good agreement with measured values. Nitrogen balances (Table 3.2.1.7 and Figure 3.2.1.16) show a distribution among products similar to rice straw. Sulfur balances (Table 3.2.1.8 and Figure 3.2.1.17) show much of the sulfur retained in the ash (58%), with about 20% as SO_2. Water balances (Table 3.2.1.9) give good agreement between measured and estimated impinger and desiccant weight gain. The low heat release rates of 40 to 50 kW (Table 3.2.1.10) follow directly from the low fire spreading rates.

Results of analyses from the DRI filter samples (Tables 3.2.11 - 13) show carbon, chlorine, and potassium as major elements, as was the case with rice straw. Mass fractions and emission factors are also similar to those from rice straw. PIXE analyses of filter samples collected during the second traverse (Tables 3.2.1.14 and 15) are in rather poor agreement for K and Cl with the DRI samples of the first traverse, being one-third to one-half lower. Results from DRUM sampler analyses (Tables 3.2.1.16 - 24) are rather sparse. Major elements are not found consistently. Although K appears to be enriched in the smaller particle size fractions (Figure 3.2.1.18), no data were obtained for Cl, Ca, or Fe.

VOC concentrations and emission factors are listed in Tables 3.2.1.25 and 3.2.1.26 for benzene, phenol, toluene, benzaldehyde, styrene, xylene, benzofuran, naphthalene, and an unidentified compound at 8.5 min retention time. Emission factors are similar to those for rice straw.

PAH emission factors are listed in Table 3.2.1.26. PAH in the filter fractions were consistent between the two traverses, but the sorbent fraction from the first traverse shows and extraordinarily high level of naphthalene (669 mg kg^{-1}). The second traverse has a much reduced naphthalene emission level, but other species are comparable. Naphthalene, as discussed later, has been occasionally observed at high concentration, and may be a breakdown product of the XAD-2 resin under high acidity, as when NO_x or SO_2 levels are high. The very high level of naphthalene for the first traverse may therefore be an an artifact of the sampling. The naphthalene analysis in general, however, is not thought to suffer in this regard. Mass fractions of speciated PAH are shown in Figure 3.2.1.19.

3.2.2. Wheat straw, CEWF, 13 August 92

This experiment was conducted at a wind speed of 3 m s^{-1} with the ceiling extended and the auxiliary floor installed. Loading rate and fuel moisture were the same as the previous test of 11 August 92. Two traverses of 48 min each were completed, both at somewhat higher humidities than the previous test. Results are presented in Figures 3.2.2.1 - 19 and Tables 3.2.2.1 - 26.

Fuel and ash compositions are listed in Table 3.2.2.1. The ash from this test had a slightly lower carbon concentration and heating value, and a higher inorganic

concentration, compared to the CRNF experiment. The fuel carbon concentration was also lower, although the same source of fuel was used. The concentration differences most likely reflect sample inhomogeneities, rather than consistent differences in average fuel composition. Ambient air temperatures (Table 3.2.2.2) were 2 to 5 K cooler than the previous test, with somewhat higher relative humidities. Mean spreading velocities were lower, reflecting the lower air temperatures and higher wind speeds. Overall air-fuel ratios (Table 3.2.2.3) were very high due to the low spreading rates and reduced loading rates.

Differences in burning characteristics between this and the CRNF test of 11 August 92 are evident in the emission factors shown in Tables 3.2.2.4 and 5. CO emissions were nearly three times greater than those for the CRNF test, and NO_x about half. Hydrocarbon emissions were increased, as were particulate matter emissions. SO_2 emissions, like NO_x, were about half those for the CRNF test. With the high wind speed, and low fuel loading rate, flame length was very short and the flame was blown over giving a very shallow flame angle. Differences between the integrated and averaged emission factors for traverse 2 suggest greater variability in burning conditions for this test. This is also reflected in the carbon balances of Table 3.2.2.6, showing poor closure for traverse 2 as a result of low CO_2 concentration. Methane, then, for traverse 2, may also be low because it, like CO_2, was determined by GC from grab samples. The trend towards lower methane is consistent with lower CO, THC, and particulate matter emissions for the second traverse, however. These three species were not subject to aliasing in concentration caused by grab sampling.

Nitrogen balances (Table 3.2.2.7 and Figure 3.2.2.16) show 9% of fuel nitrogen to be retained in the ash, compared with 5% in the CRNF test. The undetermined fraction is over 80%. Sulfur balances are only somewhat better than half closed. The reason for the poor closure is not entirely clear. Three major possible sources for error exist: the determination of SO_2 concentration, the use of SO_2 in the balance rather than total sulfur, and the stack gas velocity measurement. Figure 3.2.2.11 shows the SO_2 concentration to be at the bottom of the calibration range. SO_2 is about 90% of total S as listed in Table 3.2.2.4, implying no large amounts of sulfur in other forms, although the total S analyzer was also operating at the bottom of its calibration range. The lower CO_2 concentrations should have reduced interference in the total S measurement for this test. The carbon balances suggest that error in stack gas velocity is insufficient to account for the undetermined fraction in the sulfur balance. Other errors are possible in fuel and ash sulfur determinations, and in measurements of fuel consumption and ash production rates. The lower ash recovery (11%) compared to that for the CRNF test (14%), coupled with high retention of sulfur in ash, may account for some of the discrepancy in the sulfur balance.

Supporting the stack gas velocity measurements are the water balances (Table 3.2.2.9), which show good agreement between estimated and actual weight gains by the impingers and desiccant. Of the errors influencing the sulfur balance discussed above, those associated with the stack gas velocity measurement and the determination of fuel rate most strongly affect the water balance. Neither the carbon nor water balances support large errors in this regard. Lack of closure on the carbon balance appears to due to low CO_2 concentrations. For the most part, the results suggest that the poor closure on the sulfur balance is due to errors in the determination of SO_2, or to errors in total ash production rate. Due to the low spreading rates and low fuel loading rate, the average heat release rate was about 30 kW (Table 3.2.2.10).

Analyses of the DRI filter samples (Tables 3.2.2.11 - 13) show carbon to make up roughly two-thirds of the particulate mass. The total carbon is not quite double the

concentration found in the CRNF results, and most of the difference appears to be in the concentrations of organic carbon rather than elemental carbon. The emission factors for K and Cl from both the DRI and CNL filter samples (Tables 3.2.2.14 and 15) are in fair agreement, and the ratio of Cl to K is quite similar in both cases. Enrichment trends seen in DRUM sampler results (Tables 3.2.2.16 - 23 and Figure 3.2.2.18) are similar to other experiments, especially the CEWF test in rice straw on 21 October 92. Although the data are rather sparse, both Cl and K show enrichment below 1 μm diameter, with some possible depletion around 2 μm. Si, Fe, and Ca appear consistent with other analyses showing depletion in the smaller size fractions.

A third VOC sample set was collected following the two main traverses. Results of all three sets are listed in Tables 3.2.2.25 and 26. Benzofuran, listed in the previous CRNF test results, was not identified in the CEWF test at levels above the threshold for the automatic search routine. An unidentified compound at 8.51 min retention time was listed. Whether this is the same compound found at 8.5 min in the previous test is not known. Emission factors are in fair correspondence between the two tests, with the exception of traverse 2 in the run of 11 August 92 (CRNF) where lower emission strengths were found for phenol, benzaldehyde, and naphthalene.

PAH emission factors are listed in Table 3.2.2.26. The emission levels are fairly consistent between traverses, and the totals are high, running 76 mg kg^{-1} on average. The impinger rinsate contained rather higher levels of lower molecular weight species, especially fluoranthene, indicating some breakthrough of the sorbent. The mass fractions of PAH on the filters (Figure 3.2.2.19) begin to increase at lower molecular weight (starting at fluorene), reflecting the lower stack gas temperatures for these experiments.

3.3. Barley straw

Like wheat straw, two companion experiments were conducted with barley straw. The first, on 15 September 92, was conducted using the CEWF wind tunnel configuration with a wind speed of approximately 2 m s^{-1}. The second on 17 September 92 utilized the CRNF configuration at a wind speed of 2 m s^{-1}.

3.3.1. Barley straw, CEWF, 15 September 92

This test in barley straw on 15 September 92 was conducted with the ceiling extended and with the auxiliary floor installed. The fuel was initially loaded at a rate of 400 g m^{-2} to simulate field conditions. The wind speed was set for 3 m s^{-1}, the usual speed for this configuration. However, the fire would not spread under these conditions, even with fuel moisture between 6 and 7% wet basis, and air temperatures similar to those with wheat straw. To prevent extinction, the wind speed was first decreased to 2 m s^{-1}, but fire spread was still very erratic. The fuel loading rate was then increased to 500 g m^{-2}, which gave a more uniform fire spread. These conditions of wind speed and loading rate were maintained throughout this and the subsequent CRNF experiment with barley straw. Results are included in Figures 3.3.1.1 - 19 and Tables 3.3.1.1 - 26.

Two stack traverses were completed, the first of 48 min duration, the second of 24 min duration. The sampling time at each traverse point was initially set to 2 min, which was the duration used for all previous tests. However, the cascade impactor loaded up and was shut down 31 min into the first traverse, and the total filter began to clog during the last minute of the traverse. Due to the early clogging of the filters experienced during the first traverse, the sampling time at each traverse point was reduced to 1 min during the

second traverse. Particle size distributions for the two traverses are shown in Figures 3.3.1.14 and 15. There is very little difference between the distributions despite the difference in total mass collected.

Fuel and ash compositions are listed in Table 3.3.1.1. The inorganic ash fraction of the fuel was about 8%. The amount of ash recovered from the ash bin amounted to 10% of fuel mass (Table 3.3.1.2). The carbon concentration of the recovered ash was 24%, which is consistent with the difference between recovered ash and inorganic ash. The high carbon concentration is reflected in the high heating value (8 MJ kg^{-1}) of the ash for this test.

Fire spreading rates were 0.35 and 0.47 m min^{-1} during the two traverses, respectively. The increase in spreading rate from the first to the second traverse period is most likely due to the increase in air temperature and decrease in relative humidity. The stack gas concentrations (Table 3.3.1.2) were fairly consistent between the two tests. Both CO and NO_x increased somewhat during the second traverse. Although the fuel contained substantial amounts of sulfur (1,330 mg kg^{-1}), the stack SO_2 concentration was extremely low and essentially in the noise range of the instrument at 10 to 20 ppbv. The total S analyzer also showed stack gas sulfur levels to be extremely low. With the reduced wind velocity, the overall air-fuel ratios (Table 3.3.1.3) were between 800 and 1200.

Emission factors computed by both the integrated and averaged techniques are listed in Table 3.3.1.4 and 5. The agreement between the two is good. The emission factors for CO and particulate matter are high and reflect the observed "smoky" character of the fire. The results are similar to those of the CEWF burn in wheat straw on 13 August 92. The mass median aerodynamic particle diameter (MMAD) of 0.3 μm is on average higher than observed with any other fuel.

Carbon balances (Table 3.3.1.6) come within about 20% of being closed. Nitrogen balances (Table 3.3.1.7) show 12% of fuel nitrogen retained in the ash, and a 78% undetermined fraction. Although the SO_2 concentrations in the stack gas were observed to be very low, the sulfur balances are within 10 to 20% closed (Table 3.3.1.8). The distribution of sulfur among products (Figure 3.3.1.17) shows a large proportion (22%) in particulate matter. The large fraction of sulfur in particulate matter is unique to this fuel among the four cereal crop residues burned.

Impinger and desiccant weight gain estimated from water balances (Table 3.3.1.9) is only 64% of measured. Whether the difference is due to experimental error or other compounds condensing along with water is not known. Power balances (Table 3.3.1.10) give total heat release rates in the range of 50 to 70 kW.

The results of the DRI particle analyses from filters collected during traverse 2 are listed in Tables 3.3.1.11 - 13. Carbon is a major component of the particulate matter, accounting for 64% of PM10 mass. Unlike rice and wheat straw, the particle analyses show relatively little Cl present, and the Cl to K ratios are only about 0.15. Sulfur is present in greater concentration than chlorine. The results are consistent with the lower chlorine concentration in the fuel compared to other fuels (Table 3.3.1.1 and Table 2.3.2), but the fuel and ash compositions show about 1,000 mg kg^{-1} of Cl volatilized. The DRI analyses of Table 3.3.1.13 show that Cl in particulate matter can account for only about 140 mg kg^{-1}, and the results of the CNL analyses on filter samples are in agreement with this value (Tables 3.3.1.14 and 15). HCl was not analyzed in the stack gas, but clearly not all chlorine can be accounted for in the particulate matter and ash.

Although Cl concentrations are low compared to other fuels, enrichment is still apparent in the smaller particle sizes, as the results of DRUM sampler analyses reveal (Tables 3.3.1.16 - 23 and Figure 3.3.1.8). Potassium is also enriched at the smaller sizes. Results in Table 3.3.1.1 show that better than 90% of the potassium stayed in the ash. Five percent of potassium is accounted for in the particulate matter, and the potassium balance is nearly closed. The data for Si, Ca, and Fe are quite sparse, but these elements appear to be depleted at the smaller sizes in the manner observed with other fuels.

VOC concentrations and emission factors are listed in Tables 3.3.1.24 and 3.3.1.25. In addition to benzene, toluene, styrene, xylene, and naphthalene, which are found in almost every test, the analysis shows the presence of hexane, dimethylfuran, benzaldehyde, and trimethylpentane. The emission factors are similar to those for rice and wheat straw, except for much higher concentrations of styrene.

Total PAH emission factors (Table 3.3.1.26) are quite high, averaging 217 mg kg^{-1}, with both traverses giving nearly identical totals. Naphthalene constitutes are large fraction of PAH, but acenaphthylene and phenanthrene are also present in quantity. Levels in the impinger rinsate are comparatively low, although some higher molecular weight compounds found in the impingers were not observed on the sorbent. The particle phase (Figure 3.3.1.19) show large mass fractions beginning with fluoranthene, in a manner similar to the wheat straw experiments.

3.3.2. Barley straw, CRNF, 17 September 92

This companion test to the run of 15 September 92 was conducted with barley straw from the same source loaded at 500 g m^{-2} and a wind speed of 2 m s^{-1}. In this case, the ceiling was retracted and the auxiliary floor removed. Two stack traverses of 24 min were completed. The reduced sampling time was in anticipation of filter cloggin problems such as experienced in the CEWF barley straw test of 15 September 92. Results of the experiment are included in Figures 3.3.2.1 - 20 and Tables 3.3.2.1 - 34.

Fuel and ash compositions (Table 3.3.2.1), operating conditions (particularly inlet air temperature and relative humidity), and fire spreading rates (Table 3.3.2.2) were all very similar to those of the experiments using the CEWF wind tunnel configuration. As a result, overall air-fuel ratios (Table 3.3.2.3) were not markedly different.

Emission factors for major species (Tables 3.3.2.4 and 5) reveal several differences between this and the previous experiment. CO, hydrocarbon, and particulate matter emission strengths are reduced relative to the CEWF test. SO_2 emission factors are unchanged. NO_x is increased slightly, as is CO_2. The median particle diameters (MMAD) are still quite high in comparison to other fuels, and only slightly different from those obtained in the CEWF test.

The carbon balances (Table 3.3.2.6) are on average nearly closed, which reflects the higher CO_2 concentrations determined for these tests. Nitrogen balances (Table 3.3.2.7 and Figure 3.3.2.16) are not substantially different from those of the CEWF tests, and show about 15% of fuel nitrogen retained in the ash. Sulfur balances (Table 3.3.2.8 and Figure 3.3.2.17) show an even greater fraction of sulfur in the particulate matter compared to the CEWF configuration. The fraction of SO_2 is still low at 2%.

Water balances (Table 3.3.2.9), like those of the previous barley straw test, yield impinger and desiccant weight gains only half measured. As before, the reason for the discrepancy is not clear. Neither the carbon nor sulfur balances suggest large errors in

stack gas velocity measurements or fuel consumption rates, and results of fuel moisture analyses were very similar for the two experiments. Heat release rates were similar to those obtained during the CEWF trial.

Results of particle analyses on DRI filter samples in Tables 3.3.2.11 - 13 show greater emission rates for chlorine and potassium from these tests compared to the CEWF configuration. Carbon concentrations are reduced. The ratios of Cl to K are about double those from the CEWF tests. Particulate sulfur, as mentioned above, is high. The DRI filter sample results for S, Cl, and K are supported by the PIXE results from the CNL samples (Tables 3.3.2.14 and 15).

Two DRUM samples were collected during this experiment. The results of the first are given in Tables 3.3.2.16 - 23 and summarized in Figure 3.3.2.18 for major elements. Results for the second sample appear in Table 3.3.2.24 - 31, and are summarized in Figure 3.3.2.19. Although the data are somewhat sparse, the results of the two analyses are in fair agreement. Potassium enrichment begins to occur at a smaller particle size in the second sample compared to the first. Trends for Si, Fe, and Ca are similar to those observed previously.

VOC analyses (Tables 3.3.2.32 and 33) yield fewer identified compounds compared to the CEWF results. Not included were hexane, dimethylfuran, and trimethylpentane, although benzofuran was identified. Emission strengths for styrene remain enhanced, although somewhat below those for the CEWF configuration.

PAH emission factors (Table 3.3.2.34) were lower for this experiment compared to the CEWF experiment, but still quite high. The total values are comparable to the CEWF experiment in wheat straw, although naphthalene does not make up as much of the total. Mass fractions on filters are shown in Figure 3.3.2.20.

3.4. Corn stover

Experiments with corn stover were conducted on 7 and 9 October 92, the first using the CRNF configuration with a wind speed of 2 m s^{-1}, and the second in the CEWF configuration at 3 m s^{-1}.

3.4.1. Corn stover, CRNF, 7 October 92

Corn stover was initially loaded at 800 g m^{-2} and the first of two traverses were conducted with this loading rate. The fire spread irregularly at this loading rate, even with high air temperature and low ambient humidity. The loading rate was increased to 1,000 g m^{-2} for the second traverse. The fire spread was more uniform, and this loading rate was used for the subsequent tests. A standard 48 min traverse was attempted, but 24 min into the first traverse, the filters began to load and only 1 min was spent at each of the 12 remaining sampling positions. The total time for the first traverse was 36 min. The cascade impactor was shut off 29 min into the traverse. The second traverse was conducted with 1 min at each position and a total duration of 24 min. Both the total filter and cascade impactor completed this traverse without clogging. Results of the tests are given in Figures 3.4.1.1 - 19 and Tables 3.4.1.1 - 26.

The inorganic material content of the fuel (Table 3.4.1.1) was about 6%, and about 8% of the fuel was recovered as ash after the tests (Table 3.4.1.2). The carbon concentration of the ash was 8%. The influence of the increased fuel loading rate was apparent in the spreading rate, which increased from around 0.5 to 0.7 m min^{-1}. Average stack gas

velocities were only slightly different between the two traverses. Fuel moisture was 9% wet basis, and the overall air-fuel ratios were around 500 for the first traverse and 250 for the second.

Although the fuel loading rates in the two traverses differed by 200 g m^{-2} and the fire spread was more uniform during the second traverse, the emission factors (Tables 3.4.1.4 and 5) were not markedly different between the two tests. The major difference was in the emission factor for total hydrocarbons, which was higher by 30% in the first traverse. CO_2 was higher by 17% in the first traverse, which is contrary to the expected average concentration based on fuel consumption rate and air flow rate. The carbon balance for the second traverse is only 83% closed (Table 3.4.1.6), and indicates that the lower CO_2 emission may be the result of an error in the CO_2 determination for this traverse. The carbon balance for the first traverse gives 103% closure.

Nitrogen balances and sulfur balances are presented in Tables 3.4.1.7 and 8, with summaries in Figures 3.4.1.16 and 17. The ash retains only about 5% of fuel nitrogen. The sulfur balance shows a large undetermined fraction (48%). Results of the total S analyzer do not indicate serious errors in the SO_2 determination. Sulfur retention in the ash is lower than found for the subsequent CEWF experiment with corn stover, and suggests some possible error in sulfur determination in the ash. Errors may also exist in the fuel sulfur determinations, which were completed at the same time. The fraction of sulfur in particulate matter is similar to the result for rice and wheat straw, and substantially lower than found for barley straw.

Water balances (Table 3.4.1.9) yield a total estimated impinger and desiccant weight gain that is half that measured. Such discrepancies were observed only for barley straw and corn stover.

Average heat release rates for the two traverse periods were 120 and 230 kW respectively. The heat release during the second traverse was substantially higher because of the higher loading rate for this fuel.

Carbon, chlorine, and potassium make up the majority of the particulate mass as shown by the DRI analyses of filter samples collected during the second traverse (Tables 3.4.1.11 - 13). Ammonium ion concentration was the fourth largest at about 6%. Results from the CNL filter samples (Tables 3.4.1.14 and 15) yield emission factors for Cl and K that are double those of the DRI analyses. The PIXE results are higher for all major elements, although this may reflect to some extent the shorter sample time for these filters compared to the DRI filters. Relative abundances of elements from the DRUM samples (Tables 3.4.1.16 - 24 and Figure 3.4.1.18) repeat previous observations of potassium and chlorine enrichment at the smaller particle sizes.

Listed in Tables 3.4.1.24 and 25 are VOC concentrations and emission factors. Identified were propanone, benzene, phenol, dimethylfuran, toluene, styrene, naphthalene, and an unknown compound at a retention time of 6.7 min. The relative emission strengths for styrene were reduced compared to those observed with barley straw.

PAH emission factors (Table 3.4.1.26) were much lower than those for wheat and barley straw, averaging 8 mg kg^{-1} total. Many higher molecular weight compounds are absent. Mass fractions on the primary filters are shown in Figure 3.4.1.19.

3.4.2. Corn stover, CEWF, 9 October 92

This experiment was the companion to the previous CRNF experiment. Two traverses were completed, the first of 24 min, the second of 48 min duration. The duration of the first traverse was set based on the previous trial in which the filters loaded prior to 48 min. The filter and cascade impactor pressure drops were not observed to change much during the first traverse, and the filters removed from the continuous analyzer inlet line were not as heavily loaded as before. For these reasons, the length of the second traverse was increased to 48 min and completed without clogging the filters. Results of the experiment are included in Figures 3.4.2.1 - 18 and Tables 3.4.2.1 -19.

The test differed from any other tests in that part of the fuel consumed in the first traverse was left on the conveyor from the previous test of 7 October 92. The final test on that date ended with approximately half the feed conveyor loaded. The fuel was left on the conveyor inside the flow development section of the wind tunnel for approximately 44 h prior to ignition. Fuel samples were collected from the conveyor prior to the burn for moisture analysis. Before the start of the test, the conveyor was fully loaded with fuel from covered storage beside the wind tunnel. Although the fuel samples collected from the conveyor showed fuel moistures nearly identical to the those from the test of 7 October 92, the fire was observed to spread at a much slower rate through the material which had been left on the conveyor. There appeared to be more smoldering as well. The sudden increase in stack temperature around 0850 h in Figure 3.4.2.5 occurred at the same time the fire encountered the freshly loaded fuel. Associated with the poor fire spread were higher particulate matter concentrations than observed in the second traverse with freshly loaded fuel, as shown later. Fuel temperature, although not measured, may have been influential in the difference in spreading rate observed for the two traverses on this date. Also possible is undetected amounts of surface moisture contributed to the low rate of fire spread. Surface moisture can be lost in handling of fuel samples during preparation for moisture analysis, in which exposures to ambient laboratory air for two to three minutes prior to weighing is common. Equilibrium moisture contents for the prevailing night time outside air conditions are above the 9% observed, but the fuel was not directly exposed to ambient conditions and achievement of such levels was not detected in the moisture analyses. Both air temperature and fuel moisture were observed to influence fire spread, as discussed later, and some combination of these influences probably caused the low fire spreading rate seen during the first traverse.

Examination of the fuel compositions in Tables 3.4.1.1. and 3.4.2.1 shows them to be nearly identical. The ash from this test was higher in carbon and potassium, and considerably higher in iron. The high iron concentration may indicate contamination from the wind tunnel structure, possibly due to flaking and spalling of mild steel surfaces in the ash bin or tunnel. The level is six times higher than that observed in the previous test. In both instances, the absolute yield of iron in the ash is higher than the iron in the fuel. This is not a general result for all fuels, however, but suggestive of iron contamination with increased use, which was anticipated.

Of note is the negative value of fixed carbon from the proximate analysis of the ash. Fixed carbon is computed by difference from the determinations of ash and volatile material. When the sum of ash and volatiles exceeds 100%, the fixed carbon value becomes negative. Negative values for fixed carbon were encountered with ash from several fuels. The first proximate analysis of the ash from the previous CRNF experiment yielded a value of fixed carbon equal to -1.77%. Because of this, the proximate analysis was repeated yielding the value of 6.34% shown in Table 3.4.1.1. This value is not likely correct, either. A duplicate analysis of the ash from this CEWF experiment yielded a value for fixed carbon of -9.38%, very close to the initial value.

High temperature processing is known to result in losses of alkali metals, and possibly other compounds. Such loss in the volatile analysis, which is performed at 950°C, would overestimate the volatile content (intended to represent organic species), and cause a negative value of fixed carbon when the total inorganic content of the sample is high, as it is here. The values of fixed carbon and volatile matter from the proximate analyses were not used for any computations in this study. Any use of these values should be done cautiously. The values are suspect even for fuels, although because the total ash content is frequently low, the error is not usually as large.

The spreading rate for the fire during the first traverse was 60% that of the second traverse and both were lower than the spreading rates of the CRNF configuration. Flame length was observed to be substantially shorter under the higher wind speed, and the flames were blown over with shallow flame angle. Differences in spreading rate between the two traverses reflect possible changes in the fuel condition and inlet air temperatures, as mentioned above.

Emission factors for particulate matter (Tables 3.4.2.4 and 5) on average are roughly twice those determined with the CRNF configuration. However, the increase is due largely to the PM emission of the first traverse, which was three times that of the second. That from the second was approximately equal to the emission factors obtained during the CRNF experiment. The much higher value from the first traverse can be attributed to the poor burning conditions. Differences in the length of sampling time are not thought to be responsible based on the results of the previous experiment. The higher particulate matter concentrations for the first traverse are consistent with greater smoldering, but this is not particularly well supported by the CO and THC emission factors. CO emission factor was reduced in the first traverse, while THC was nearly the same. NO_x and SO_2 emission factors are lower for the first traverse, which is consistent with greater smoldering.

Stack carbon flows do not entirely balance the fuel carbon loss. The undetermined fraction (Table 3.4.2.6) is higher for the second traverse. The average CO_2 concentration determined for this traverse was low in comparison to that of the first. The emission factor is also well below the maximum CO_2 emission factor derived from the carbon balance (Table 3.4.2.6). Nitrogen balances (Table 3.4.2.7 and Figure 3.4.2.16) are quite similar to those obtained on the previous trial, showing a greater fraction of nitrogen distributed to particulate matter, but still with a large undetermined fraction (compare Figure 3.4.1.16). Sulfur flows are somewhat better balanced, but still only 70% closed (Table 3.4.2.8 and Figure 3.4.2.17). Differences between this experiment and the previous CRNF experiment are due largely to a greater fraction of sulfur accounted for in the ash. The water balance (Table 3.4.2.9) is somewhat improved compared to the previous test, although the estimated impinger and desiccant weight gain is still only 70% of measured. The slower spreading rates are reflected in the lower heat release rates (Table 3.4.2.10) for this trial compared to the previous one (Table 3.4.1.10).

Results of the particle analyses on the DRI and CNL filter samples resemble the results from the CRNF configuration quite closely. Major species determined in the DRI analyses (Tables 3.4.2.11 - 13) are carbon, chlorine, potassium, and ammonium ion. The Cl to K ratio is approximately 1.7 and compares well with the value of 1.6 from the previous test. PIXE results (Tables 3.4.2.14 and 15) again give emission factors for Cl and K in particulate matter which are higher than the XRF values from the DRI analysis. Only samples from two stages of the DRUM sampler could be analyzed: stage 5 (0.56 - 1.15 μm) and stage 8 (< 0.24 μm). The data from these analyses were quite sparse, and no conclusions regarding relative abundance of elements could be made.

The VOC analyses (Tables 3.4.2.18 and 19) show three additional compounds to those obtained from the CRNF test. These are 2-methyl-2-cyclopenten-1-one, 2-chlorophenol, and benzaldehyde. The unlabeled compound at 6.7 min retention time seen in the CRNF test was not found here. The concentrations of compounds identified in both experiments are for the most part fairly similar given the uncertainty that exists with this analysis.

PAH emission factors (Table 3.4.2.20) are significantly elevated in the first traverse (119 mg kg^{-1}) over the second (7 mg kg^{-1}). The difference in total PAH emission is due primarily to large amounts of high molecular weight material captured on the primary filter during the first traverse, including high levels of benzo[a]pyrene (29 mg kg^{-1}). The results of the second traverse bears a fair resemblance to those from rice straw with more robust burning conditions. Both traverses show higher mass fractions of lighter species on the filter (Figure 3.4.2.18), but for the second traverse this is at least partly due to the lower total amounts of these materials in the sorbent phase.

3.5. Walnut tree prunings, Pile burns, 12 November 92

The first of the wood fuel experiments was conducted with walnut tree prunings on 12 November 1992. Two pile burns were completed, with one stack traverse made during each burn. Results of the tests are included in Figures 3.5.1 - 22 and Tables 3.5.1 - 33.

The first pile was allowed to burn to completion without stoking. The first traverse of 48 min between 0904 and 0952 h covered virtually the entire burn. Two stack traverses were actually completed, with 1 min at each sampling position. This was done in anticipation that the filters might begin to load early with this type of fire. When particulate sampling was stopped, only a few small embers were still glowing and very little smoke was apparent. Although particulate matter sampling stopped 48 min into the test, continuous stack gas analysis continued until 1026 h by when CO concentration had returned to near pre-burn levels. The test was intended to produce emission factors integrated over the entire burning history of the fire. Results for the traverse alone and the full test are presented.

During the second traverse, the fire was stoked at regular intervals to maintain a steady flaming stage. Shortly after starting the traverse, the VOC pump was found to be providing inadequate flow, and had failed to do so during the first traverse as well. The traverse was stopped and the fire allowed to burn down while a new pump was obtained. The fire was restoked, and the traverse continued after steady flaming resumed. The pump for the cascade impactor was shut off after 24 min (1 min at each traverse point) due to high pressure drop and inability to hold isokinetic conditions. The pump for the total filter was shut down after 39 min for the same reason. After completing the test, the fire was allowed to burn out before recovering ash.

Before burning, the fuel was classified into two size categories. Any material with a maximum diameter greater than 50 mm was lumped into a large branch category, with the remainder classified as small branches. Fuel in each class was weighed, and representative samples collected for analysis. When loading into the pile for burning, care was taken to match the fractions of small and large material to those observed for the total fuel supply. The branches ranged in length from about 0.5 to 2 m. Ash was recovered on a fine mesh stainless steel screen placed beneath the pile prior to loading. Ash was removed after completing each burn.

Results of the fuel and ash analyses are listed in Tables 3.5.1 and 2. The compositions of the small and large branches were not substantially different. The inorganic fraction was

3 to 4% dry weight and indicative of younger tissues (stem wood is often less than 1% ash). Results of the ash analyses for the two burns are quite similar. Values of fixed carbon are negative due to the problems in completing the proximate analysis with high ash materials as discussed above under section 3.4.2. The proximate analyses yield organic fractions of 2 to 3%, whereas the carbon, hydrogen, and nitrogen analyses suggest organic fractions in the range of 8 to 9%. Heating value analyses only support the presence of low amounts of organic materials. The heating values were determined by blending the ash with benzoic acid in an attempt to burn out any organic material remaining in the ash. The low or negative values obtained are indicative of the low organic fractions in the ash as well as the difficulties in completing these analyses. The carbon concentrations observed may represent the presence of carbonates in the ash, rather than elemental carbon. The ash at the end of each test was white and visually did not suggest the presence of much carbon.

Total fuel concentrations are listed for selected elements in Table 3.5.2. As shown, the small branches accounted for about two thirds of the fuel weight. Fuel moisture averaged 33%, with the larger material somewhat drier than the small material.

Average operating results are listed in Table 3.5.3. The first pile was constructed with a total of 34 kg of fuel. 1.2 kg of ash were recovered, accounting for 5.3% of dry weight. This is somewhat more than the average 3.7% ash in the fuel determined by proximate analysis. The difference may be due to errors in weighing the ash or to inherently larger amounts of ash in the fuel burned compared to the sample taken for analysis. The second test burned a total of 150 kg, but not all during the second traverse. The amount of ash recovered was 6.5% of dry weight, and was again higher than that determined by proximate analysis.

Peak stack gas temperature (Figure 3.5.5) reached 100°C shortly after ignition of the second pile. On average, the stack temperatures were considerably lower, being 32 and 50°C respectively during the two traverses. Over the full 83 min of the first test, the stack gas temperature averaged only 14 K above inlet temperature.

The tests were conducted without the blower running. The doors were left half open for free air flow to the fire. Average velocities measured in the stack ranged from 2 to 3 $m\,s^{-1}$ (Table 3.5.3).

Average stack gas concentrations for CO_2, CH_4, and hydrocarbons by GC were computed as time averages using trapezoidal integrations of grab sample concentrations. The concentrations are shown in Figures 3.5.14 and 15. All other gas concentrations were determined in the usual manner from continuous analyzer data. The particle size distributions for traverses 1 and 2 were not substantially different, as Figures 3.5.12 and 13 demonstrate.

Fuel consumption rates are listed in Table 3.5.4. Based on observations of the amount of material remaining when the first traverse was stopped, and burning rates during the flaming stage from the second test, the fuel consumption during the first traverse was taken as 95% of the total fuel consumption measured for the entire first test. The fuel consumption rate for the second traverse was an average value from measured stoking rates. Because the instantaneous fuel composition during burning was not known, several assumptions were made in computing the element balances. For the first traverse, the 5% unreacted fuel mass was assumed to consist only of carbon plus ash under the further assumption that the fuel volatiles would be given off during the flaming stage. For the element balances of the second traverse, stoked fuel was assumed to react completely

leaving only ash behind, essentially as an approximation to the continuous burnout of both stoked fuel and fuel loaded initially.

Emission factors for major species computed by the integrated and averaged techniques are listed in Tables 3.5.5 and 6. The values listed are derived from the measured stack gas velocities. Differences between the two tables reflect the non-steady nature of these fires. No particulate matter emission factors are listed for test 1. The values listed for traverse 1 account for nearly all of the fuel, and are perhaps indicative of the entire test, although the release during the small amount of smoldering may be enhanced for certain species. The PM emission factors for traverse 2 during the flaming stage are lower than those for traverse 1 due to the rapid burning and larger fuel consumption rate during this stage compared to smoldering. This is also true for NO_x, although in both cases the average stack gas concentrations for these species were well above the average concentrations for the entire burn as measured during the first test. The results also show the flaming stage to produce lower emission rates for CO and hydrocarbons than the fire as a whole, which is also apparent in the stack gas concentrations for these species (Table 3.5.3).

Results of carbon balances (Table 3.5.7) are varied. Measured stack carbon flows for the first traverse account for more carbon than fuel consumption rates justify. To some extent this suggests that the amount of fuel burned during the traverse was in excess of 95% of total weight. It also suggests that the assumption of carbon concentration for the ash at the end of the traverse is too high. The major error appears to lie in the determination of average CO_2 emission factor, which at approximately 220% is above the maximum emission factor of 175% determined for the entire test based on known weights and carbon concentrations. The value obtained for the second traverse appears to underestimate the CO_2 emission, as evidenced by the poor closure. The measured stack velocity for this traverse may also be low for the reasons discussed above under section 2.2.5. Some combination of errors associated with the velocity and CO_2 concentration measurements is likely responsible for the poor closure.

Nitrogen balances are presented for all three cases in Table 3.5.8 and Figures 3.5.16 - 18. The rates shown are averages over the duration of each traverse or test. Little nitrogen remains in the residual ash, and the ratio of nitrogen in NO_x to fuel nitrogen is 19 to 27%. The ratio for nitrogen in particulate matter, at least as ammonium and nitrate, is about 1%. Note that in computing the nitrogen distribution for test 1, the PM emission factor was set equal to that for traverse 1. This is also the case for the carbon and sulfur balances.

Sulfur balances are listed in Table 3.5.9 and distributions of sulfur in products appear in Figures 3.5.19 - 21. The results for traverse 1 and test 1, which are quite similar, show a fraction of about 30% undetermined. The rest is divided about equally among ash, SO_2, and particulate matter. The results for traverse 2 show a lower undetermined fraction, and more sulfur allocated to SO_2, which is not unexpected but uncertain because of the assumptions made.

The water balance (Table 3.5.10) is fairly well closed, giving an estimated weight gain for the impingers and desiccant that is 86% of measured. This was a significant improvement over the results from the tests with barley straw and corn stover. The inlet air and stack gas flow rates used in this case were computed from the measured stack gas velocities.

Average heat release rates during the second traverse period were more than 100 kW greater than during the first. The lower average heat release rate for test 1 in comparison

to traverse 1 is due to the rather lengthy smoldering period at the end of the test with little fuel consumption.

Carbon balances in Table 3.5.7 showed that the stack gas velocity might differ from the measured values by about 1 m s^{-1} or roughly one-third. The emission factors have a linear dependence on velocity. To demonstrate the effect on the emission factors, they were recomputed using the stack gas velocities obtained by closing the carbon balances. The results are given in Tables 3.5.12 - 16. The stack gas velocity for traverse 1 was reduced from the measured 2.97 m s^{-1} to 1.88 m s^{-1} as given by the carbon balance. The velocity for traverse 2 increased from 2.66 to 3.99 m s^{-1}, and for test 1 as a whole decreased from 2.33 to 1.91 m s^{-1}. The stack gas and inlet air flow rates changed accordingly (Table 3.5.13). The recomputed emission factors are shown in Table 3.5.14. Because instantaneous CO_2 concentration data were not available, only the average basis results are shown. The effect on the water balance is indicated in Table 3.5.16. The difference between the ratio of estimated to measured weight gain using the velocities from the carbon balance and using the measured velocities is small due to the counteracting effects of the velocity decrease for traverse 1 and the velocity increase for traverse 2.

Results of the analyses from the DRI filter samples are listed in Tables 3.5.17 - 19 for the set taken during the first traverse period, and in Tables 3.5.20 - 22 for the set taken during the second traverse period. Carbon is the dominant species, accounting for 70% of mass in both PM2.5 and PM10 for the first set, and 52 and 83% respectively in PM2.5 and PM10 for the second. Following carbon in decreasing concentration are K, Cl, S, NH_4^+, and NO_3^-. The mass recovery for PM2.5 in the second set is rather poor. The others show good recovery. The difference in explained masses for these filters (48 and 49) is the reason for flagging these data as suspect. This also accounts for the larger emission factors for some elements in the PM2.5 fraction than in the PM10 fraction. The discrepancy arises because the concentrations were normalized to reconstructed mass in computing the emission factors.

Four filter samples were collected for analysis by CNL at the times indicated on Tables 3.5.23 - 3.5.30. The first filter sample was collected during the first test. The three remaining filter samples were collected during the second test. The emission factors for major elements are generally in good agreement with those determined from the DRI samples. The DRUM sampler was unavailable for this and all subsequent experiments.

Identified VOCs are listed in Tables 3.5.31 and 32, and include propanone, methylacetate, methylbutanone, furfural, benzene, toluene, benzaldehyde, styrene, xylene, and naphthalene. The emission factors listed in Table 3.5.32 are at the low end of the range observed for the cereal crop residues.

PAH emission factors were also computed on the basis of themeasured stack gas velocities and those derived by carbon balance. The results are listed in Tables 3.5.33 and 3.5.34. The average total is both cases is about 25 mg kg^{-1}, although the second test gives lower amounts of PAH compared with the first test by the measured stack gas velocities than by the carbon balance method. Mostly lower molecular weight species were observed, which is reflected in Figure 3.5.22 giving the mass fractions of PAH on the primary filters.

3.6. Almond tree prunings, Pile burns, 6 April 93

Two tests with almond tree prunings were conducted on 6 April 93 in essentially the same manner as those for walnut tree prunings. The first pile was allowed to burn to completion without stoking. The second was stoked and then allowed to burn out. Two stack traverses were completed. The first was of 48 min during the first fire and encompassing most of fuel burnout. The second was of 24 min taken while the fire was stoked to maintain a continuous flaming stage. These tests were conducted with the weighing platform in place and continuous CO_2 monitoring. CO was also continuously monitored by the same instrument used to monitor CO_2 (a dual channel infrared analyzer). The ambient air temperature and relative humidity sensors were not used in order to record CO_2 concentrations. Instead, ambient data were obtained from the nearby CIMIS weather station. The wind tunnel doors were open to allow free flow of air to the fires. Results are included in Figures 3.6.1 - 21 and Tables 3.6.1 - 35.

Prior to burning, the fuel was segregated into two size categories in the same manner as the walnut tree prunings. On a moist basis, about 60% of the fuel weight was in branches having a maximum diameter less than 50 mm. The small branches were drier than the larger branches, and the overall moisture was less than that of the walnut tree prunings (18% as opposed to 33%). As before, the fuel was loaded with the appropriate proportions of small and large branches. Ash compositions were quite similar between the first and second tests. The inorganic material concentrations of the residual ash as determined from the proximate and ultimate elemental analyses were in better agreement than in the case of walnut tree prunings. The problem of negative fixed carbon values for the ash in the proximate analyses recurred, due to substantial overestimates for volatile matter. Both tests produced a white ash.

Records of weight loss are given in Figure 3.6.14. Profiles of residual weight from ignition on are shown in Figure 3.6.15. Burning rate profiles are shown individually in Figures 3.6.16 and 3.6.17. The first pile was loaded to 35 kg and ignited at 0944 h. The first stack traverse ended with 8% residual weight. The maximum burning rate of approximately 0.1% s^{-1} occurred about 20 min after ignition. The second pile was also loaded to 35 kg, and then stoked for an hour following ignition. The second traverse was made around 1200 h, with stoking keeping the weight at about 75% of the initial weight. A total of 55 kg of fuel were burned during the second test, with 23 kg burned during the period of the second traverse (Table 3.6.5).

Average operating conditions are listed in Table 3.6.3. Four periods of time are included in this table and those that follow. In addition to the periods of the two traverses, conditions were monitored over the total duration of the first burn (Test 1). Conditions were also monitored over an extended time period of 3.5 h after the second traverse. The results from this low smoldering period are included under the heading of "Test 2-final". The average stack gas velocity during the second traverse was substantially higher than velocities measured during the other time periods. This is thought to be the result of a grounding fault with the anemometer when a ground strap was not replaced after an instrument check.

Average gas and particulate matter concentrations are listed in Table 3.6.4. Particle size distributions for the two traverses are given in Figures 3.6.12 and 3.6.13. CO concentrations were more stable during extended sampling, without the long term zero drift seen in the results with the previous analyzer.

Mass balances are listed in Table 3.6.5. Because instantaneous fuel composition was not known, the dry fuel consumption rates were computed from the weight loss measurements for the first and second traverses under the assumption of complete combustion (weight loss measurements give the mass volatilized, not dry fuel consumed). The moist fuel consumption was found by adding to the total weight loss an amount of ash giving the total ash fraction listed in Table 3.6.2. In the case of the second traverse, the fuel consumption was based on the weight loss during the traverse period, plus the weight of fuel stoked, again assuming an ash fraction as measured. For test 1 as a whole the fuel consumption was measured directly. For the final period of test 2, the fuel consumption was based on weight loss following the end of the second traverse and the weight of ash. The moisture content of the fuel for the final period of test 2 was arbitrarily assumed to be zero based on the assumption that moisture would have evaporated by this time. The very slow burning rates for this period are evident in the large overall air-fuel ratio.

Emission factors computed from the integrated and averaged techniques and using the measured stack gas velocities are listed in Tables 3.6.6 and 3.6.7. CO, NO_x, SO_2, THC, CO_2, and PM emission factors were all elevated for traverse 2 over traverse 1. The higher CO emission rate for test 1 than traverse 1 shows the effect of smoldering. The CO emission for the final smoldering period of test 2 is also high, but the total fuel consumption during this time was low in comparison to the flaming stage, being only about 1 g s^{-1} compared to 16 g s^{-1} for flaming. The integrated CO_2 emission factor for the final stage of test 2 is higher than the time averaged value. The result is sensitive to small changes in CO_2 concentration and gas velocity due to the low rate of fuel consumption.

Results of carbon balances are listed in Table 3.6.8. The high stack gas velocity for traverse 2 and the high CO_2 emission factor for the final period of tests 2 are evident in the excessive closures. The results for both traverse 1 and test 1 are improved with respect to those for traverse 2 and test 2, but the integrated values still yield excess closure.

Nitrogen balances in Table 3.6.9 show a low retention of nitrogen in the ash, and a fairly high ratio of nitrogen as NO_x to fuel nitrogen. Only the results for test 1 as a whole are shown in Figure 3.6.18, representing the distribution over the entire burn. The results are quite similar to those obtained for walnut tree prunings (Figure 3.5.18). Results of sulfur balances (Table 3.6.10) show good closure for all but traverse 1. The trends are somewhat surprising given the results of the carbon balance suggesting possible errors in measurements of stack gas velocity for traverse 2. The distribution of sulfur among products for test 1 (Figure 3.6.19) shows about half of it in particulate matter, and a third in ash. The large proportion in particulate matter resembles the results for barley straw.

The water balance (Table 3.6.11) is 73% closed. In computing the water balance, the ash hydrogen concentration was assumed to be zero, which was consistent with the assumption of complete fuel conversion used to compute the fuel consumption rate. Even with this assumption the estimated weight gain of the impingers and desiccant is less than measured.

Power balances (Table 3.6.12) yield average heat release rates similar to those observed for walnut tree prunings. The values of tunnel heat dissipation shown for traverses 1 and 2 and test 1 were computed using the stack gas velocities derived by closing the carbon balances. For traverse 2 and the final period of test 2, the measured stack velocities yield stack gas enthalpies higher than energy release. The carbon balance for the final period

of test 2 yields a higher stack gas velocity than measured, which further exacerbates the problem. The major difficulty in computing the balances for the final period of test 2 is believed to lie with the rather low CO_2 concentrations prevailing at this time. The concentrations were closer to background levels than at any other time, and errors in either the determination of stack or background CO_2 concentrations would have greater impact on the results for this period.

If the gas velocities are adjusted according to the results of the carbon balances, the effects on operating conditions and emission factors are as listed in Tables 3.6.13 - 17. In computing the integrated emission factors for Table 3.6.15, instantaneous (1 min) carbon balances were used to give estimated stack gas velocity. The results of this analysis are shown in Figure 3.6.20. The estimated and measured velocities are not too different for the flaming stage of the first test, but the low CO_2 concentrations and low rates of weight loss during the last stages of the test lead to an underestimate of the stack gas velocity. The calculation is useless for the stoked period of test 2 because the weight gains and losses occurring simultaneously lead to an inaccurate estimate of effective fuel consumption rate. Later on, the very low weight loss rates combine with the CO_2 concentrations to give very high estimates of velocity, which are known to be erroneous. The difficulty again lies with the small CO_2 concentration differential above ambient. The failure of the analyses for the second test is obvious from the closure computed for the integrated technique listed in Table 3.6.17. The closure for the average basis is, of course, forced. Only for the period of traverse 1 does the integrated technique employing instantaneous carbon balances appear to offer any promise in testing the measured stack gas velocity.

On an average basis, the emission factors recomputed using the velocity from the carbon balance (Table 3.6.16) are in better agreement with those determined from the measured velocity. The effect of decreasing the gas velocity for traverse 2 is readily apparent in the reduced emission factors. The effect on the water balance was small, increasing the estimated weight gain by only 6 relative percent.

Results of DRI filter analyses for sets taken during the first and second traverse periods are listed in Tables 3.6.18 - 23. To compute the individual species emission factors, the particulate matter emission factors derived from the carbon balances were utilized. Once again, carbon is the major species, followed by K, S, Cl, and NO_3^-. Organic carbon makes up about two-thirds of total carbon. Results of CNL filter analyses are listed in Tables 3.6.24 - 31. Four samples were collected--two during the first traverse and two during the second. The average emission factors for K and Cl from the first traverse are in good agreement with the results of the DRI results. Results for K and Cl from both CNL samples collected during the second traverse are in excellent agreement with the DRI samples for the same traverse. DRI results for Al are substantially below the results of the PIXE analysis on CNL samples. Results for other elements are comparable. Zinc appears in concentrations sufficiently large that the total quantity of zinc emitted in particulate matter exceeds that found in the fuel (Table 3.6.1). Because no galvanized metals or other known sources of zinc were used in the wind tunnel structure or sampling systems, the source of the excess zinc is unknown. Field data from Ward, et al. (1989), show zinc concentrations about half those of the DRI analyses here, as discussed later.

VOCs found during the two traverses are listed in Tables 3.6.32 and 33. Compounds identified included furfural, benzene, phenol, toluene, benzaldehyde, methylphenol, styrene, xylene, benzofuran, and naphthalene. Relative emission strengths were very close for the two traverses except for methylphenol.

Total PAH emission factors were similar to those obtained for walnut prunings. Factors computed from both the measured stack gas velocities and the velocities derived via carbon balance are listed in Tables 3.6.34 and 3.6.35. More higher molecular weight species were identified compared to the walnut prunings. The total PAH emission factor computed with stack gas velocities derived from the carbon balances is lower for the stoked fire. The opposite is true for the measured velocities. As noted below, the velocities computed by closing the carbon balance are considered to be superior to the measured velocities due to the effects of flame radiation on the stack anemometer. Mass fractions of speciated PAH on the primary filters are lower compared to the cereal crop residues, most likely as a result of the higher stack gas temperatures at the time of sampling (Figure 3.6.21).

3.7. Ponderosa pine slash, Pile burns, 29 April 93

Ponderosa pine slash was burned in two identical tests. Neither of the fires was stoked. Approximately 45 kg of fuel was loaded onto the burning platform for each test and allowed to burn to completion. The fires burned very rapidly, with 90% of fuel mass consumed within 32 to 38 min, and 94 to 97% within 72 min. A 24 min traverse was conducted during the first test covering the flaming stage of the fire. A second traverse of 48 min was conducted during the second test covering the weakly flaming and smoldering later stages of the fire. Together the two traverses covered essentially the entire burning period. The results of the experiment are shown in Figures 3.7.1 - 20 and Tables 3.7.1 - 29.

The fuel was collected from the Blodgett Experimental Forest operated by the University of California in the Sierra Nevada mountains. Branches extended in diameter up to a maximum of about 125 mm. Prior to burning, the fuel was segregated into four size classes including large, medium, and small branches and needles. Large branches were classified as those having diameters exceeding 50 mm, medium branches as those with diameters between 25 and 50 mm, and small branches as those with diameters less than 25 mm. The weight fractions in large and medium branches, and small branches with needles attached were determined directly. The weight fractions of small branches and needles were determined by subsampling the small branches and stripping the needles. These samples were not used in the fires. The piles were constructed so as to provide representative proportions in each size class. The weight fractions are listed in Table 3.7.2 along with total values for selected fuel parameters. Needles accounted for 3% of total mass, with the other 3 classes divided roughly equally in proportion.

Individual compositions for each of the size classes are listed in Table 3.7.1. Blanks in the data set indicate that the element was not detected. The nitrogen results from the ultimate analysis are low in comparison to the elemental analysis. The ultimate analysis failed to detect N in two of the samples, whereas the alternate technique identified it at concentrations of 0.2 to 0.3% dry weight. The reasons for the discrepancies are unknown. Cl was present in very small concentrations. The inorganic (ash) fraction of the fuel increased in a very typical manner with decreasing size, reflecting the age of material. Total average fuel moisture was about 25%.

Collected at the end of each test was a residue consisting of white ash and some unburned carbon in the form of one or two short pieces of larger diameter material that were not burned fully. Small samples of the white ash were collected separately. The remaining residue was mixed, comminuted, blended, and split into multiple subsamples for analysis. Compositions of the residue and ash materials from the two tests are listed in Table 3.7.3. Although the residue from test 2 had a higher carbon content, the heating value for this sample was lower, possibly as a result of inhomogeneities in the sample. The problem

with volatile matter and fixed carbon recurred for the white ash samples from both tests. Iron concentrations were extremely high in three of the four samples, and likely indicate iron contamination from steel in the support platform or stainless steel mesh screen used to retain the ash.

Weight records for the two tests are shown in Figure 3.7.14, and residual weight profiles from time of ignition are given in Figure 3.7.15. Slightly more fuel was loaded in the first test than in the second. The small dips seen in the traces for residual weight are due to occasional poking of the fires by the operators as they shifted fuel into the center. Similar artifacts are seen in Figure 3.6.15. Rates of weight change for both tests are overlaid in Figure 3.7.16. The maximum rate loss of 0.2% s^{-1} during test 2 was a third higher than the maximum rate for test 1.

Average operating conditions for the tests are listed in Table 3.7.4. The average stack gas temperature during the flaming stage of traverse 1 was 40 K hotter than that of the second traverse during the smoldering stage. Overall average temperatures for both tests were quite similar, however. Measured velocities were around 2 m s^{-1}, and lower than those measured in the previous pile burns. Time averaged gas and particulate matter concentrations are given in Table 3.7.5. Concentrations for all species were substantial during the first traverse. Particulate matter concentrations in the second traverse were roughly a fourth those of the first traverse. Particle size distributions were distinctly different between the two traverses as well. The size distribution for the first traverse (Figure 3.7.12) shows a greater proportion of mass in the larger size fractions than does that for the second traverse (Figure 3.7.13). The total sulfur concentrations in the first traverse were suppressed relative to the SO_2 concentrations, apparently as a result of the high CO_2 concentrations which interfere with the total S analyzer.

Mass balances (Table 3.7.6) for the first and second traverses were computed under similar assumptions to those employed in the balances for almond tree prunings. For traverse 1, the fuel consumption rate was again based on the measured weight loss and the assumption of complete fuel conversion, giving an ash content equal to that measured by the proximate analysis. The fuel consumption rate for the second traverse during the smoldering stage of the fire was obtained from the measured weight loss, the ash content from the proximate analysis, and the total residual weight from test 2. The moisture content of the fuel burned during the second traverse was arbitrarily assumed to be zero under the assumption that fuel moisture would have evaporated during the flaming stage. Fuel consumption for tests 1 and 2 was determined directly. Burning rates and air-fuel ratios were quite similar for both tests.

The integrated and time averaged emission factors are listed in Tables 3.7.7 and 8, respectively. The results reveal trends similar those observed previously for the flaming and smoldering stages of combustion. The emission factor for CO in particular was about three times higher in the case of smoldering than in flaming, but the fuel consumption rate in smoldering was about one seventh that of the flaming stage. The two effects combine to give an overall result closer to the factor determined for the flaming stage alone. The values for hydrocarbons determined by GC and particulate matter for the complete tests 1 and 2 were computed as mass averages from the amount of fuel burned in traverse 1 and that burned in traverse 2. Results from the continuous analyzers were computed directly. Total results for the two tests compare quite well. The mass averaged values are, of course, identical for the two tests.

Results of carbon balances are given in Table 3.7.9. If the time averaged emission factors are used, the balances are only 60 to 75% closed. The closure is improved for three of the

four analyses when the integrated emission factors are used. The estimated stack gas velocities are in all cases higher than the measured velocities, with differences ranging from 0.7 to 1.2 m s^{-1}. The consistently low measured velocities and the reduced uncertainty in the CO_2 concentration with continuous monitoring suggests that the true stack gas velocities were higher than measured.

Nitrogen balances yield 2% retention in ash (Table 3.7.10 and Figure 3.7.17). The undetermined fraction in the sulfur balance (Table 3.7.11 and Figure 3.7.18) is quite large however, and suggest errors in the velocity measurements. The proportion of sulfur in the particulate matter is high and similar to the values obtained for walnut tree prunings, although the larger undetermined fraction makes comparison difficult.

The water balance (Table 3.7.12) does not provide much information relative to possible errors in measurements of stack gas velocity. The estimated weight gain for the impingers and desiccant is within 80% of measured, and use of the stack gas velocities which close the carbon balances reduces that to 75%.

The average heat release rate during the first traverse was over 400 kW (Table 3.7.13). For smoldering, the average value over the second traverse was 70 kW. Both tests yielded similar overall average heat release rates of around 150 kW.

For comparison purposes, emission factors were recomputed using the stack gas velocities given by closing the carbon balance. The results of these calculations are listed in Tables 3.7.14 - 18. The factors shown in Table 3.7.16 were computed using instantaneous (1 min) carbon balances as in the test with almond tree prunings of 6 April 93. The results are given in Figure 3.7.19. Peak gas velocities computed via the carbon balance are higher in both tests than measured values. They suggest that the stack anemometer was lagging in heating the sensing element and underestimated the true velocity. The computed velocities fall off to less than 1 m s^{-1} in the smoldering stage, whereas the stack anemometer indicates velocities above 1 m s^{-1}. Measurements of the stack anemometer made during this time with a handheld anemometer were in close agreement with the stack anemometer. As discussed above for the test on almond prunings, lower CO_2 concentrations coupled with low rates of weight loss reduce the utility of the carbon balance for estimating velocity in this region. The peak velocities measured by the anemometer quite possibly underestimate the true velocities during the flaming stage, however. The probable influence of flame radiation on the anemometer appears in the abrupt drop in stack gas velocity at the beginning of each traverse, which is quite distinct in Figure 3.7.19 for these rapidly burning fires. The carbon balances are confounded by the high values of CO_2 in the stack which exceed not only the span concentration (5,000 ppmv) but the range of the instrument as well (10,000 ppmv). The error in instrument response at such high levels is unknown.

Results of the DRI analyses on filter samples collected during the first traverse appear in Tables 3.7.19 - 21. Results of CNL PIXE analyses on two filter samples also collected during the first traverse period are given in Tables 3.7.22 - 25. No DRI or CNL filter samples were collected during the second traverse. The results of the DRI analyses show carbon to be the dominant species, with organic carbon again making up about two-thirds of the total carbon mass. Carbon is followed in decreasing concentration by K, S, Cl, Zn NO_3^-, Ca, Na, and Si. Chlorine is present primarily as chloride ion, and the ratio of elemental Cl to K is about 0.1. The emission factors computed from both the DRI and CNL analyses for K and Cl are in quite good agreement, poorer agreement exists for other elements. Zn emission exceeds total fuel zinc, indicating a probable source of contamination.

VOC concentrations for the first traverse were generally about twice the concentrations for the second traverse (Tables 3.7.26). Compounds identified included acetic acid, furfural, benzene, hexane, phenol, toluene, methylphenol, styrene, xylene, methoxymethylphenol, naphthalene, Δ3-carene, and limonene. Estimated emission factors (Table 3.7.27) were higher for the second traverse because of the very low fuel consumption rates, although it must be kept in mind that these emission factors are based on the actual amount of fuel burned during this time, not the original fuel mass loaded. Mass averaged values applicable to the entire fuel mass are presented later in Tables 4.5.1 and 4.5.2. The high VOC emission factors for this period may be due in part to heating of unburned or partially burned fuel near the periphery of the fire.

PAH emission factors are listed in Table 3.7.28 for the measured stack gas velocities, and Table 3.7.29 for the velocities determined via carbon balance. Both show that the emission factor is substantially increased during the weakly flaming and smoldering stages of the fire. Few higher molecular weight species were seen. Mass fractions of PAH on the primary filters (Figure 3.7.20) are low in comparison to the cereals, again likely due to the higher stack temperatures during sampling.

3.8. Douglas fir slash, Pile burns, 30 April 93

Two tests were conducted with Douglas fir slash. The first pile was arranged randomly, as was the case with all previous pile burns. Two stack traverses were completed during this test, one during the flaming stage and one later on during the smoldering phase of the fire. PAH analysis was not performed on the second traverse. The second pile was arranged more as a fuel crib, with branches laid crosswise to each other in a vertical stack. A third traverse was completed during the flaming stage of this fire. The ignition and burning times for this pile were more rapid than for the randomly loaded pile, although partly this appears to be the result of a better lighting technique for the fire. Neither fire was stoked. Results of the two tests are included in Figures 3.8.1 - 22 and Tables 3.8.1 - 28.

Prior to burning, the fuel was separated into two size categories and weighed. All branches with maximum diameters greater than 50 mm were classified as large branches, all others as small branches. There were few needles on this material, unlike the Ponderosa pine slash. Branch diameter extended up to a maximum of about 125 mm. Major element compositions of the large and small branches were seen to be similar (Table 3.8.1), although the small branches contained more calcium, sulfur, manganese, and iron. The ultimate analyses did not detect nitrogen; alternate elemental analyses found 0.2 to 0.3%. The discrepancies between the analyses for nitrogen duplicate those for Ponderosa pine. Mass fractions for the two size categories and total concentrations for selected elements are listed in Table 3.8.2. The total mass was split roughly equally between the small and large branches.

Only small amounts of residue remained at the end of each test, and no attempt was made to subdivide it as was done for the Ponderosa pine residue. The residue consisted primarily of white ash with a few small pieces of charcoal. The residue was mixed, comminuted, blended, and split to obtain samples for analysis. The remaining charcoal was obvious in the carbon concentrations, which were 25 and 31%, respectively, and reflected in the heating values. The inorganic fractions identified by proximate analyses were quite different at 74% for the residue from the first test and 37% for the residue from second test. Although these results are supported by the heating value determinations, the result for the second test suggests a higher carbon concentration than

the 31% detected by ultimate analysis. This may reflect the small sizes and inhomogeneities of the samples.

Weight loss from both fires appears in Figure 3.8.15. Piles were loaded to 45 - 46 kg, keeping the same proportions of large and small pieces observed for the fuel at large. The longer burning time for the first pile compared to the second is apparent in the graph. Residual weight profiles from ignition are given in Figure 3.8.16, where again the much longer burning time for the first pile is apparent. Fuel consumption reached 90% of initial weight 78 min after ignition in the first test, whereas only 48 min elapsed in the second test. The fire in the first test spread more slowly from the ignition points at the ends of the pile towards the center. Due to the way the fuel was loaded in the second pile, the pile became almost entirely involved within 10 min following ignition. Differential weight changes for both tests are plotted in Figure 3.8.17, and demonstrate the marked difference in burning rates between the two tests. The rapid burning at 2700 s into the second test is due to a rearrangement of the fuel on the platform by the operators. Unburned fuel at the periphery of the fire was moved into the center.

Although the burning rates for the second test were faster than the first, they were still lower than those observed for the Ponderosa pine fires. A comparison of the residual weight profiles for all Ponderosa pine and Douglas fir tests appears in Figure 3.8.18. The average fuel moisture contents (wet basis) were 25% for the Ponderosa pine and 30% for the Douglas fir. The dry needle fraction in the Ponderosa pine was quite obviously of benefit in promoting the spread of the fire through the pile. Although the volatile fractions from the proximate analyses were nearly the same for the two fuels, differences in volatile composition may have contributed to the differences in burning rates observed.

Average operating conditions are listed in Table 3.8.3. In addition to the three traverses, results for the total duration of tests 1 and 2 are given as well. Also listed are the observed durations of the flaming stages of the fires, and the weight loss associated with flaming. The flaming stage was considered to have ended when very few luminous flames were visible above the fuel bed, although the determination of this point was subjective and to some extent arbitrary. As indicated in the table, for both tests this point occurred at around 30% residual weight (70% weight loss).

Stack gas velocities measured with the hot film anemometer were all lower than observed in previous tests. As discussed later, results of the carbon balances suggest that the anemometer failed to respond properly to peak velocities during periods of rapid burning, with high heat release rate and flame radiation.

Average gas and particulate matter concentrations are listed in Table 3.8.4. The slow burning rates of the smoldering stage during traverse 2 are evident in the low concentrations. CO concentration was still quite high, however, and typical for fire smoldering. Results shown for the full tests 1 and 2 are direct results from the continuous analyzers.

In completing the mass balances (Table 3.8.5), similar assumptions were made to those for the tests in Ponderosa pine slash and almond tree prunings because instantaneous fuel compositions were not known. For the first and third traverses, the weight loss measured over each traverse interval was converted to fuel consumption by adding an amount of ash giving the total ash content determined by proximate analysis. The calculation assumes complete fuel conversion in the period. For the second traverse, the fuel consumption was based on the weight remaining at the beginning of the traverse, and the ash fraction remaining at the end of the traverse. The fuel moisture content was assumed to be zero. Fuel consumption for the total tests 1 and 2 was determined directly.

Emission factors are listed in Tables 3.8.6 and 3.8.7. The values for tests 1 and 2 which were not determined by continuous analysis were computed as mass averages of values from the flaming and smoldering stages. The fuel mass fractions converted during the two stages were used as weighting factors. These are listed for each of the two tests in the tables. The CO_2 concentrations suggest a somewhat different weighting than the subjective evaluations of flaming and smoldering. Using the integrated results of Table 3.8.6, the flaming stage conversion fraction giving the best fit for the total CO_2 emission factor from the individual traverse emission factors was determined. The best fits are 83% flaming conversion for the first test, and 88% for the second. The time averaged emission factors give best fits with 76 and 88% conversion (Table 3.8.7). These fractions are still somewhat arbitrary because of decisions made about when to sample. In general, however, they suggest about 80% fuel burn-up in the flaming stage for these fires.

Carbon balances (Table 3.8.8) are not well closed for the first and third traverses (ignition and flaming stage). Improved closure on the second traverse and the two complete tests suggest that the measured stack gas velocities are low for the rapid burning stages of the fires. The differences between the measured velocities and those estimated by closing the carbon balances are 1 m s^{-1} for the first traverse and 0.7 m s^{-1} for the second. These values resemble those from the Ponderosa pine experiments. Note also that for traverse 2, the carbon concentrations for both the fuel and the ash were estimated. The estimates were derived from the carbon analysis of the residual ash and the assumption that all mass in excess of the residual mass at the end was due to carbon alone. The same assumption was applied to the nitrogen and sulfur balances.

Nitrogen balances (Table 3.8.9 and Figure 3.8.19) yield a ratio of nitrogen as NO_x to fuel nitrogen equal to 16% averaged over the two tests. The sulfur balances are far from closed with the exception of traverse 2 (Table 3.8.10). The undetermined sulfur fraction (Figure 3.8.20) is greater than 70%. The undetermined fraction was higher than encountered with Ponderosa pine slash. The sulfur in particulate matter was lower than for other wood fuel experiments. Note that in computing the element balances, the concentrations in the particulate matter are all assumed equal to that in the DRI PM10 fraction (Tables 3.8.18 - 20). The DRI filters from the second traverse were all flagged invalid due to low deposit mass (apparently insufficient material was collected during this smoldering period). No DRI filters samples were collected during the third traverse. The assumption of equal concentrations represents a small source of error in the overall element balances.

Results of the PIXE analyses of CNL filter samples (Tables 3.8. 21 - 24) collected during the first two traverses show the PM sulfur yield from the second traverse (Table 3.8.24, smoldering) to be about half that from the first (Table 3.8.22, flaming). The emission factor for PM sulfur from the CNL filter sample taken during the first traverse (Table 3.8.22) is in turn about half that determined from the PM10 filter sample analyzed by DRI (Table 3.8.20).

Water balances (Table 3.8.11) show that about 73% of the weight gain by impingers and desiccant is accounted for under the assumptions made. Using the stack gas velocities computed by carbon balance does not improve the water balance (water released by evaporation and combustion has less effect on absolute humidity at higher gas flows).

The much greater average heat release rate for the flaming stage of the second test compared to the first is evident in the power balances shown in Table 3.8.12. The negative value of tunnel dissipation for traverse 2 implies heat transfer from the tunnel

structure to the gas. Cooling of the structure following flaming combustion would account for this transient effect.

Emission factors were recomputed using the gas velocities derived from carbon balances. The results are listed in Tables 3.8.13 - 17. Instantaneous (1 min) carbon balances were used for the integrated emission factors of Table 3.8.15. The velocities computed in this manner are displayed in Figure 3.8.21. The figure also displays measured velocities and stack temperatures. The carbon balance results are quite scattered. There is a general trend in the carbon balances suggesting that the velocity during the flaming stages of the fire was higher than measured.

The effect of using the velocities computed from the carbon balances is to increase the integrated emission factors for traverse 1 and 3 and substantially reduce them for traverse 2 (Table 3.8.15). Those factors determined as time averages (hydrocarbons determined by GC) or as integrated values (particulate matter) are changed in linear proportion to the change in velocity, and have the same values in both Table 3.8.15 and Table 3.8.16. The emission factors for the full tests derived from continuous analyzer results are changed moderately, increasing for test 1 and decreasing for test 2. Those for particulate matter and hydrocarbons by GC increase for both tests. Emission factors computed using only the average stack gas velocity obtained from the carbon balance are increased for all species in tests 1 and 2 (Table 3.8.16).

Particulate matter compositions determined from DRI and CNL filter samples are listed in Tables 3.8.18 - 24. Results for sulfur in particulate matter were discussed above. Results of the DRI PM10 analyses from traverse 1 for potassium give emission factors which are quite similar to the CNL filter samples from the same traverse. Cl in the DRI analysis is low in comparison to both CNL samples, but Ca and Si in the DRI PM10 fraction are similar to the CNL results.

VOC results are listed in Tables 3.8.25 and 26. The number of compounds identified in the samples from the second traverse was less than half that from the first traverse. The emission strengths were also substantially smaller. Conspicuous in the first traverse are the terpenes, including pinene which was not identified in the test with Ponderosa pine.

Total PAH emission factors (Tables 3.8. 27 and 3.8.28) also show a lower emission rate for traverse 3 compared to traverse 1, by a third to a quarter. Mass fractions of speciated PAH (Figure 3.8.22) are not entirely consistent between the two traverses, with traverse 3 yielding higher fractions of heavier compounds, although in both cases the quanities of these species are very small.

4. Discussion

4.1. Average emission factors, major species

Average emission factors for major species from the eight fuels are summarized in Tables 4.1.1 through 4.1.8. The results are also displayed in Figures 4.1.1 - 4.1.8. Average results for the spreading fires in the four cereal crop residues (barley straw, rice straw, corn stover, and wheat straw) are listed by wind tunnel configuration (CEWF and CRNF). A single average for the two configurations is also listed. For rice straw, an additional average is given for all tests. Results listed for the four wood fuels (almond tree prunings, Douglas fir slash, Ponderosa pine slash, and walnut tree prunings) include emission factors computed from direct measurement of stack gas velocity, as well as those determined through use of the velocity obtained by closing the carbon balance. Similar values are not shown for the spreading fires because no serious discrepancies

were found, and differences for the cereal fuels are thought to be primarily associated with CO_2 concentration measurements rather than velocity. For species analyzed continuously (CO, NO, NO_x, SO_2, total S, THC beginning 11 August 92, and CO_2 beginning 6 April 93), the values listed are those derived from the integrated technique of equation [8]. Those determined by GC (CH_4, HC, and CO_2 prior to 6 April 93) are derived from time averages of stack gas velocity using equation [9]. Non-methane hydrocarbons (NMHC) are determined as the difference between THC and CH_4, or HC and CH_4 in the case of the GC results. Emission factors for particulate matter represent integrated samples. PM emission factors for Ponderosa pine and Douglas fir are mass averages for the flaming and smoldering stages combined. All values are based on total dry fuel consumption.

4.2. Experimental uncertainties

Error in the emission factor determinations is introduced primarily through three important parameters, as equations [8], [9], and [10] show. The three are the species concentration, fuel consumption, and stack gas velocity. Error in stack gas density also contributes, but is much less important. In addition to these errors, the emission factors for particulate matter are subject to uncertainty arising from equilibration of filter samples prior to weighing and anisokinetic conditions at the time of sampling.

Determination of species concentration is subject to a number of analytical difficulties related to sampling, calibration, and interference from other species. For particulate matter, sampling errors are also related to the stack gas velocity measurements, as these were used to set sample flow rates to maintain isokinetic conditions. Fortunately, for these flows, even moderate deviations from isokinetic conditions do not have important consequences for most of the sample. Standard sampling techniques call for sample flows to be within 10% of isokinetic. The results listed in Table 4.2.1 show that sample flow rates for the total filter were maintained within 10% of isokinetic for most traverses, at least based on the measured stack gas velocities which were used to set flow rate. For spreading fires, the flow rates deviate more than 10% from isokinetic on seven occasions. The deviation is 11% for traverse 1 of 9 June 92, 10 July 92, and 7 October 92, 12% in traverses 2 and 3 of 9 June 92, 16% in traverse 2 of 13 August 92, and 23% in traverse 1 of 11 August 92. With the velocity computed from the carbon balance, the deviation is within about ± 20% with a few exceptions. Deviations beyond 10% of isokinetic for measured stack gas velocities occurred in 4 out of the 9 traverses with wood fuels. In two cases the deviation is rather severe. The second traverse of 6 April 92 is that for which the stack gas velocity was observed to be high in comparison to other tests. The anisokinetic conditions were largely due to the need to maintain pump flow above the design flow of 10 L min^{-1} with the nozzle employed. Results of the carbon balance suggest that the nozzle flow was closer to isokinetic than measured, although on this basis other large errors appear for different tests. The flow rate for the second traverse of 30 April 93 was well in excess of isokinetic, a result supported by the stack gas velocity computed from the carbon balance. The discrepancy in this case is due to operator error.

The error in particle concentration due to anisokinetic conditions can be assessed from a Stokes number analysis of the flow. When the probe velocity exceeds the stack velocity, particles with high inertia bypass the probe because they cannot follow the converging streamlines at the probe nozzle. This leads to an error in the concentration from under-sampling large particles. When the probe velocity is too low, the streamlines diverge at the nozzle, and larger particles are over-sampled, again leading to an error in concentration. Assuming the probe is adequately aligned to the flow, the ratio of the

sampled concentration, C_{PM}, to the actual concentration, C_{PMo}, with mismatching of probe velocity can be estimated as (Hinds, 1982):

$$\frac{C_{PM}}{C_{PMo}} = 1 + \left(\frac{u}{u_p} - 1\right)\left(1 - \frac{1}{1 + \left(2 + 0.62\frac{u_p}{u}\right)Stk}\right) \qquad [49]$$

where u is the stack gas velocity, u_p is the gas velocity in the probe nozzle, and Stk is the Stokes number,

$$Stk = \frac{\tau u}{D_p} \qquad [50]$$

with τ the particle relaxation time (s) and D_p the probe nozzle diameter (m). When Stk < 0.01, particle inertia is sufficiently low to cause minor error (~1%) by mismatching probe velocity to stack velocity. At higher Stokes numbers, the error is given by equation [49]. The analysis of Table 4.2.1 shows a maximum deviation of something under a factor 2 for the ratio of probe velocity to stack velocity. For u = 3 m s^{-1}, and D_p = 0.0095 m, the required particle relaxation time to avoid separation is about 3 x 10^{-5} s, which corresponds to a particle size of 3 μm or less. For 10 μm particles, the particle relaxation time is 3 x 10^{-4} s. Equation [49] gives C_{PM}/C_{PMo} = 0.92 for u_p/u = 2, and C_{PM}/C_{PMo} = 1.13 for u_p/u = 0.5. At 100 μm, the error caused by over- or under-sampling the flow by a factor of 2 is about ±100%. Maximum concentration errors of roughly ±20% may be expected for the PM10 size class, since error due to anisokinetic sampling would apply to both the total and cascade impactor probes. Concentrations for much larger particles would only be known within a factor of 2 or 3 for those tests with large deviation from isokinetic. Other errors, such as loss of particles to the wall of the probe, are not considered in this analysis.

Errors in gas concentration also arise from grab sampling. Aliasing is a particular problem with unsteady flows. Multiple grab samples were taken in an attempt to reduce this type of error, and seemed generally adequate for spreading fires. As a means of testing measured stack velocities by carbon balance, grab sampling clearly was inadequate for pile fires.

Frequent calibration was employed in an effort to reduce the error from drift and other changes in instrument response. Interference from CO_2 was a particular problem for the total sulfur determinations. Such interference makes the total S determinations largely qualitative.

Fuel consumption was subject to the least uncertainty of the three major parameters affecting emission factor. For the spreading fires, uncertainty in the fuel consumption arises due to possible errors in scale calibration, measurement of conveyor speed, moisture determination, and measurement of fuel loss prior to combustion. For the pile fires, errors are associated with load cell calibration, ash loss through the retaining screen, moisture determination, and assumptions used in estimating fuel composition to segregate emission factors for flaming and smoldering combustion. The latter source of error arises only for the species not determined by continuous analysis and where fully integrated

samples could not be obtained due to the length of burn or to heavy particulate matter loading on filters.

Stack gas velocity measurements were prone to errors associated with the nature of the flow. The stack environment was fairly harsh, and measurement of low velocities in such particle laden flows is difficult without more sophisticated equipment (e.g. laser doppler velocimetry). Attempts to measure stack gas velocity with standard S-type pitot tubes were unsuccessful because of the low and fluctuating velocity heads encountered. The hot film anemometer employed held up well in repeated calibrations, but could not be calibrated in-stack under actual flow conditions. Stack gas velocity measurements were tested by carrying out element balances to check for consistency. An estimated stack gas velocity was computed by closing the carbon balance. Error in the carbon balance arises principally from errors in the CO_2 concentration measurement and in gas velocity. Where burning intensity, flame heights, and stack gas temperatures were relatively low and steady, as in the case of the spreading fires, discrepancies in the carbon balances did not appear to be due to serious errors in the measurements of stack gas velocity. Flame radiation appears to have had an impact on the anemometer during the intense burning stages of the pile fires. These fires were built directly below the anemometer. Under flaming, the radiation received by the anemometer would have been well in excess of that received during the spreading fires. Radiation heat transfer would have reduced the transducer heating required to compensate for the convective heat loss, causing a low signal response and low velocity estimate. The very hot and rapidly burning fires in Ponderosa pine slash show this quite clearly, where a marked decline in measured velocity occurs shortly after ignition. Discrepancies in the carbon balances can likely be attributed in large part to errors in the measured stack gas velocities for the pile burns.

Velocities computed by closing the carbon balance are compared against measured velocities for all tests in Figure 4.2.1. The maximum difference of 2.3 m s^{-1} occurred for traverse 2 in the experiment of 6 April 93 with almond tree prunings. The fire was stoked to maintain steady flaming throughout this period. The measured velocity was consistently high during the experiment, which is thought to be the result of an instrument grounding problem when one of the ground straps was not reconnected following a calibration check.

The measured and computed velocities were compared by linear regression. Results are listed in Table 4.2.2. For all fires combined, the regression model is shown in Figure 4.2.1. The line has a slope of 0.5 and an intercept of 1.4, rather far from the ideal of slope = 1 and intercept = 0. The model fit is not good, having an r^2 of only 0.33. The 95% level confidence interval for the slope is 0.31 to 0.78, and 0.8 to 2.0 for the intercept. With the measured velocity of 5.3 m s^{-1} removed as an outlier, the slope and model fit are marginally improved, as shown in Figure 4.2.2. The maximum difference is about 1.2 m s^{-1}, and occurs for both pile and spreading fires. Forcing the model through zero intercept (Figure 4.2.3) reveals a slope error of about 10%, still with poor fit. Separate analyses of the spreading fire and pile fire data are given in Figures 4.2.4 and 4.2.5. Two models are shown in each case, one unconstrained and one constrained to zero intercept. The slope in the case of the unconstrained model for spreading fires is close to 1, with the intercept showing an offset of about 0.3 m s^{-1}. The constrained model shows a slope error again about 10%, with a slightly worse fit. The situation is quite different for the pile burns (with the measured velocity for traverse 2 of 6 April 93 included in the analysis). The unconstrained model yields a 0.3 slope with an offset of nearly 2 m s^{-1}. This is in large part due to the single measured velocity above 5 m s^{-1}. The fit of this model is quite poor. The constrained model yields a slope near unity, but the fit is also

quite poor. These results suggest that for spreading fires the anemometer on average produces a good estimate of the stack gas velocity. For both spreading fires and pile fires, the possible absolute error appears to be not better than 1 m s^{-1}. Uncertainties in the emission factors due to the stack gas velocity may typically be in the range of 30 to 50%.

Possible error in the particulate matter concentrations was also examined by comparing the results of the various particle samplers employed. Both the DRI and CNL samplers had inlets fixed in the stack and were not traversed. Particle mass concentrations could be either higher or lower than obtained from the stack traverse depending on the smoke distribution across the tunnel stack. Previous analyses using a 12 point traverse had shown the distribution to be nearly uniform (Jenkins, et al., 1993a). The 24 point traverse approached the stack walls more closely. Non-uniformity of particle concentration near the walls would have influenced a 24 point traverse more than a 12 point traverse. The closest approach to any wall was 100 mm (Figure 2.1.3) in the 24 point traverse. Stack velocity distributions from the traverses are quite uniform across all 24 points during periods of steady burning (spreading fires and stoked pile fires). Concentrations from the continuous analyzers were also fairly uniform under steady burning, but changes in fire behavior with time made it more difficult to assess the spatial uniformity under less stable conditions. Both velocity and concentration variations due to position are difficult to distinguish from variations in time with the rapidly burning pile fires. No direct measurements of concentration uniformity for particulate matter were made.

Assuming particle concentration is uniform across the stack, the total filter (combined with the mass of the back-up filter) would be expected to yield a higher mass concentration than any of the other three samplers. The impactor stages used on the DRI filters would exclude the larger particle size fractions. The long CNL inlet, combined with the anisokinetic inlet conditions, should also produce lower mass concentrations. Total mass concentrations obtained by reconstructing the mass from the individual stages of cascade impactors are known to be unreliable. The total particulate matter concentration from the total filter should therefore form a concentration ceiling for the other samplers, with their results following the total concentration trend. Such is the case in Figure 4.2.6 where concentrations from the DRI PM10 and PM2.5 stages, the CNL total filters, and the reconstructed mass concentrations from the cascade impactor are plotted against the total filter mass concentrations. The uncorrected total filter values from the tests of 9 June 92 have been included. The concentrations for the DRI, CNL, and cascade impactor samplers lying well above the 1:1 line in the figure around 3 and 5 mg m^{-3} total filter concentration are for this date. The cascade impactor results are surprisingly consistent with the total filter data. The CNL filter concentrations are generally lower than anticipated, although they vary over a broader range than the others. Comparative results for the individual traverses are given in Figures 4.2.7 through 4.2.12. Only results for the PM10 fraction from the DRI analyses are included in Figures 4.2.7 and 4.2.8.

4.3. Emission factors, major species by fuel type

For comparative purposes, emission factors for individual species were plotted by fuel type for each test. Also plotted were the NO/NOx and SO_2/total S ratios, and the MMAD. Data were further summarized for spreading fires as averages for each fuel type in each wind tunnel configuration, along with global averages for each fuel. Data for the pile fires appear with side-by-side comparisons for the measured and computed stack gas velocities. All values shown are integrated emission factors using the measured stack gas velocities. For the pile fires, additional sets of figures are given for the emission factors computed on the basis of the velocities estimated from the carbon balances.

4.3.1. Spreading fires

The spreading fire results for each test and each fuel type are compared in Figures 4.3.1.1 - 17. Summary results are given in Figure 4.3.18 - 31

The higher CO emission factors for barley straw in both configurations and wheat straw in the CEWF configuration are readily apparent in Figures 4.3.1.1 and 4.3.1.18. The values are about twice those for corn and rice, and wheat in the CRNF configuration. The apparently poorer combustion in the barley and CEWF wheat straw tests is reflected in some of the emission factors of the other species. Both hydrocarbons and particulate matter emissions are enhanced for these tests. NO_x appears to be reduced relative to peak values obtained for rice straw, but on average NO_x emission factors are similar for all fuels, with corn reduced slightly in comparison to the others (Figure 4.3.1.19). For the spreading fires, the NO mass emission ranges from 40 to 60% of total NO_x expressed as NO_2 (Figure 4.3.1.4). The very low SO_2 emissions observed for barley straw are distinct in Figures 4.3.1.5 and 4.3.1.21. The results for total S follow closely those for SO_2 (Figures 4.3.1.12 and 28).

Total hydrocarbon emissions (from the continuous analyzer results only) vary over about one order of magnitude (Figure 4.3.1.6). The CEWF configuration produced higher THC emissions for barley and wheat straw, and with the 1992 crop year rice straw. Average THC emission factors for corn were not different between the two configurations. The GC results, although yielding concentrations well below the continuous analyzer, are consistent with higher hydrocarbon emission factors in the CEWF configuration (Figure 4.3.1.23). Methane accounts for 10 to 30% of total hydrocarbons determined by continuous analyzer, and about half of the hydrocarbons analyzed by GC (Figures 4.3.1.8 and 24). Non-methane hydrocarbon emission factors computed by difference between THC and methane are shown in Figures 4.3.1.9 for individual traverses, average values in Figure 4.3.1.25. Those computed by difference between the GC determined concentrations are given in Figures 4.3.1.10 and 26.

CO_2 emission factors for barley and wheat straw vary in a manner consistent with the variation in CO emission factors for these fuels in the two configurations. With higher CO, the CO_2 emission factor, indicative of the combustion efficiency, would be expected to decline proportionately. For rice and corn the trend is opposite this on average (Figure 4.3.1.27). This is most likely the result of the errors in the CO_2 analyses, possibly due to aliasing caused by grab sampling.

On average (Figure 4.3.1.29), the SO_2 emissions account for 70 to 90% of total stack sulfur, although there is uncertainty in the total S analyses, and the comparison is largely qualitative. The large discrepancy in the results for the test of 10 July 92 with rice straw is apparent in Figure 4.3.1.13. The emission factors for both SO_2 and total S for this CEWF test are substantially lower than observed in the previous tests with the same straw in the CRNF configuration. The discrepancy in SO_2/total S is thought to be due to an error in calibrating or setting the total S analyzer.

Particulate matter emission factors for total PM, PM10, and PM2.5 are given in Figures 4.3.1.14 - 16. Averages by configuration are shown in Figure 4.3.1.30. Quite distinct is the high particulate matter emission factor for the first CEWF test with corn (traverse 1, 9 October 92). As described above, the result is substantially different from that of the second test on the same date in the same configuration, and appears to be the result of changes in fuel condition after being left 44 h in the wind tunnel. Although not a general result, there is a trend that the first test on each date produces higher particulate matter

emission factors than subsequent tests on the same day. The reason for this may be related to increasing air temperature and improved combustion over the course of the experiments for most dates. Higher PM emission factors might also occur as a result of greater condensation of organic materials on particles at lower stack temperatures prior to collection. The hydrocarbon analyses do not in general support this argument.

Median particle diameters for the different tests are summarized in Figure 4.3.1.31. The barley straw tests yielded larger diameters in both wind tunnel configurations. The values for corn, rice, and wheat are comparable.

4.3.2. Pile fires

Individual test results derived from the measured stack gas velocities are given in Figures 4.3.2.1 - 17. The emission factors derived from the computed velocities (from carbon balances) are shown in the same figures for comparison. Summaries by fuel type are shown in Figures 4.3.2.18 - 33.

The higher emission factors for CO with smoldering are apparent in the results for the final part of the second test with almond tree prunings (Almond/T2f in the figures) and the second traverse with Douglas fir (DougFir/2) and Ponderosa pine (Pine/2). Because the total fuel consumption was small during smoldering in these tests, the total emission factors (Figure 4.3.2.18) are dominated by the flaming stage.

Average NO_x emission factors correspond quite closely in relative magnitude to the fuel nitrogen concentrations. The higher N contents of the walnut and almond prunings (0.6 and 0.5% N respectively) correspond to the higher emission factors for these fuels. The Douglas fir, with a fuel nitrogen concentration of 0.27%, produces nearly the same NO_x as Ponderosa Pine, with 0.3% fuel nitrogen. The more vigorous fires in Ponderosa pine did not produce proportionately greater NO_x emissions. Sulfur emissions also appear to correspond in relative magnitude to fuel concentrations. The sulfur concentration in the walnut fuel was nearly double that in the other wood fuels. The sulfur emissions for walnut are 2 to 3 times higher than for almond, Douglas fir, or Ponderosa pine, all three having similar sulfur contents.

When computed from the measured stack gas velocities, the particle emission factors on average are not greatly different among all four wood fuels. The particle emission factors for Douglas fir, Ponderosa pine, and walnut tree prunings increase by roughly 0.2% absolute when derived from the velocity calculated by closing the carbon balance. The values for almond are not much changed. The mass median aerodynamic diameters (MMAD) were slightly larger for Douglas fir and Ponderosa pine.

4.4. Particulate matter compositions and bulk aerosol absorption

Particulate matter compositions are summarized by fuel type and by individual species type. The data from the DRI analyses are used for these summaries. The data from the CNL analyses were in general in good agreement for major species, but more sparse. The CNL filters were also total samples, the DRI samples were size segregated. A comparison of the average elemental concentrations for Fe, Cl, K, and Si determined by XRF from the DRI filters and PIXE from the CNL filters appears in Figure 4.4.1. The correspondence is good from about 10^4 ng m^{-3} upwards, but the PIXE analyses exceed the XRF results for iron below this. Si concentrations appear to follow the same trend.

Emission factors by fuel type are shown in Figures 4.4.2 through 4.4.9. The results are plotted on a logarithmic scale to make apparent those species present in small amounts. The dominance of K, Cl, and S in the compositions for all fuels is quite evident. The analysis for chloride ion quite frequently gives values exceeding those for elemental chlorine. This is a result of the two different techniques used, but also indicates that most of the chlorine is present in water soluble form. Not shown is bromine, although of the minor species it appears in comparatively high concentrations.

Summaries by individual major elements appear in Figures 4.4.10 through 4.4.21. The greater yield of chlorine and potassium in the particulate matter from the cereal crop residues is quite clearly shown in Figure 4.4.11 and 4.4.12. Barley and wheat both show large potassium emissions. The enrichment of Ca, Si, and Fe in the larger particle size fractions is also evident in the figures. The sulfur emission in particulate matter from barley straw (Figure 4.4.15) is greater than that from any other fuel, with much of it present as sulfate (Figure 4.4.18). The sodium emission from barley straw was also higher than for other fuels (Figure 4.4.20).

Bulk aerosol absorption coefficients, B_{ap} ($m^2\ g^{-1}$) were determined from the CNL total filter samples by the laser integrating plate method (LIPM). The results are given in Table 4.4.1. The values shown for B_{ap} were determined from the ratio of the intensities of transmitted light before (I_0) and after (I_e) filter exposure, the area of filter exposed (A_f), the mass concentration of collected particulate matter (C_{PM}), and the sample volume (V_s), as

$$B_{ap} = \frac{k' \ln\left(\frac{I_o}{I_e}\right) A_f}{V_s C_{PM}} \qquad [51]$$

Without dividing by C_{PM}, the aerosol absorption coefficient b_{ap} (km^{-1}) is obtained, representing the extinction per unit length. As shown in Table 4.4.1, the values of B_{ap} for all samples lie in the range of 0.78 to 5.41 $m^2\ g^{-1}$, with the lowest values for the 1992 crop year rice straw (21, 23 October 92) and the highest for the first traverse (unstoked) in walnut tree prunings (12 November 92). The global mean is 2.7 $m^2\ g^{-1}$.

4.5. VOC and PAH emissions

Average concentrations for volatile organic compounds are listed in Table 4.5.1. Emission factors are listed in Table 4.5.2. Consistently observed were benzene, phenol, toluene, benzaldehyde, styrene, xylene, and naphthalene. Benzofuran was observed in the barley, rice, wheat, and almond experiments. Terpene compounds were identified with both Douglas fir and Ponderosa pine.

Emission factors are compared by fuel type for selected species in Figures 4.5.1 and 4.5.2. The large emission of styrene from the barley straw experiments is apparent in Figure 4.5.1. Also apparent in the figures are the large emissions from the Ponderosa pine experiments.

Average emission factors were also determined separately for the spreading fires in the CEWF and CRNF configurations. The results are shown for selected species in Figures 4.5.3 through 4.5.8. Benzene appears to be emitted in greater amounts from the CEWF fires, as does toluene. Results are not as consistent for other species. Comparisons were

also made between the flaming and smoldering periods of the burns in Douglas fir and Ponderosa pine. Results for benzene, styrene, and naphthalene are given in Figures 4.5.9 - 11. The Ponderosa pine fires suggest larger benzene and styrene emissions during smoldering. The results for Douglas fir do not confirm this trend. Results for both fuels suggest that naphthalene is emitted in greater strength during flaming.

Volatile organic compounds arise principally as a result of incomplete combustion. For heterogenous combustion processes, especially fires of the type observed here, the emission levels of these trace products can be expected to be highly variable. Even under more controlled conditions, the composition of unburned products can vary significantly. The uncertainties associated both with the determination of fuel consumption during the smoldering stage and the determination of VOC concentrations in general make these comparisons rather qualitative.

Total PAH emission factors determined for each test are listed in Table 4.5.3. The total includes only the 19 species analyzed. A large number of other species were likely present, but were not determined. Ramdahl and Becher (1982) identified 30 PAH derivatives, not examined here, from wood burning in a small air-tight wood stove which amounted to an additional 28 mg kg^{-1}. For barley straw burned in a stoker fed furnace, 25 PAH derivatives were identified yielding an additional 11 mg kg^{-1}.

The values shown in Table 4.5.3 for walnut prunings are based on the measured stack gas velocities. Those for almond prunings, Ponderosa Pine, and Douglas fir utilize the stack gas velocities derived from the carbon balance. Cereal fuels all utilize measured velocities.

Also shown in Table 4.5.3 are the totals for the 17 species excluding naphthalene and 2-methylnaphthalene. Despite extensive washing by Soxhlet extraction with methanol, dichloromethane, and hexane, several batches of XAD-2 yielded substantial amounts of naphthalene and 2-methylnaphthalene in field blank analyses. In separate studies we have observed that acidic vapors (perhaps including NO_2) can cause depolymerization of the XAD-2 polymer, yielding an assortment of aromatic byproducts that interfere with analysis of naphthalene and alkyl-naphthalenes. No definite trend exists in comparisons of NOx with the two naphthalenes, however. Nor is there a clear correlation between emissions of 2-methylnaphthalene and naphthalene, although there is a general trend of mutually increasing concentrations.

The correspondence between the PAH-determined naphthalene and the VOC-determined naphthalene is shown in Figures 4.5.12 (full range) and 4.5.13 (low range). A few tests show large discrepancies (Figure 4.5.12) between the VOC and PAH analyses. Below 200 mg kg^{-1}, however, the results are comparable (Figure 4.5.13). These results suggest that for most tests, naphthalene is not present only as an artifact of the sampling. Naphthalene has been observed to constitute a major share of total PAH in other studies with biomass (Nielsen and Jensen, 1991). The very high naphthalene emission for the wheat straw CRNF-1 test is suspicious, however, and may be an artifact, or an error.

Total PAH emissions shown in Table 4.5.3 for all fuel types and fire configurations range from 5 to 683 mg kg^{-1} dry fuel, or 2 to 100 mg kg^{-1} if naphthalene and 2-methylnaphthalene are excluded. For the wheat straw test giving the highest total emission rate (CRNF-2), naphthalene comprises nearly all (98%) of the PAH determined. When naphthalene is excluded, the emission factor is 12 mg kg^{-1} for this test.

Corn stover (with the exception of the first CEWF test) and rice straw yield relatively low emission rates for PAH compared to the other cereal residues. This is believed to be due to the higher loading rates and denser fuel bed structures leading to improved ignition and flame structure compared with barley and wheat straw.

The two wind tunnel configurations used with spreading fires in the cereal fuels also suggest influences of flame structure and ventilation on the total PAH emission rate. For wheat and barley straw, with poorer ignition due to the lower loading and heat release rates, the CEWF configuration yields a higher PAH emission rate than the CRNF configuration. In the CEWF configuration, the flames appeared shorter and blown over. The opposite trend in PAH emission was observed in the case of corn (if CEWF-1 is excluded for reasons mentioned above) and rice. The higher oxygen availability in the CEWF configuration appears to have resulted in more complete combustion, at least for PAH, under these more vigorous burning conditions with higher loading rates.

The results for rice straw in Table 4.5.3 also reveal some differences which might be due to the fuel source. Total emission rates are somewhat lower on average for the 1991 crop year straw compared to the later tests with 1992 straw.

The more vigorous burning conditions also appear to have led to lower PAH emission rates for the wood fuels. Emission levels are reduced in both almond and walnut tests where stoking was conducted. The almond fuel yields somewhat lower emissions overall, possibly as a result of reduced fuel moisture. The high flaming stage (traverse 3) of the Douglas fir test also yielded lower emission rates for PAH than the low flaming stage (traverse 1). Similarly, the flaming stage of the Ponderosa pine tests yielded lower emission levels than the late flame and smolder stages, based on the fuel involved in each stage.

Average emission factors by fuel type and PAH species are listed in Tables 4.5.4, 4.5.5, and 4.5.6. For cereal straws, the emission factors are averaged over all tests with each fuel type, but excluding traverse 2 from the experiment of 10 July 92 for rice straw. The Ponderosa pine test was conducted to yield an estimate of total emission factor, which is shown by the mass averaged values in Table 4.5.6. In this case, the total emission increases 70% (including naphthalene and 2-methylnaphthalene) over the flaming stage alone, or 50% if the naphthalenes are excluded. The increase is due both to the increase in assigned mass (the fuel weight used to compute the emission factor increases by 30% in the mass averaged total compared to the flaming stage only), and to the higher emission levels for the less vigorous burning stages of the fire. The high average emission factors for corn in comparison to rice are due to the inclusion of the single test mentioned above. This test yielded high levels of higher molecular weight PAH, in particular benzo[a]pyrene emitted at 29 mg kg^{-1}. Other tests in corn yielded an average benzo[a]pyrene emission factor of about 0.024 mg kg^{-1}, a factor of about 1,200 smaller. In general, the cereal residues produced more of the higher molecular weight PAH than the woods.

Although the Method 429 is not intended to determine partitioning of PAH among gas and condensed phases, the filter, sorbent, and tubing/impinger components were analyzed separately. Above molecular weight about 200, most of the PAH was found on the primary in-stack filter. Below this, most was found in the sorbent. About 1% was typically found in the backup filter, and less than 1% in the impinger/tubing rinsate. The wood fuels generally yielded lower fractions in the higher molecular weight range, likely because of the higher sampling temperatures with these more intense pile fires. A general trend towards declining mass fraction on the filter with elevated stack gas temperature

was observed, as shown in Figure 4.5.14. The highest filter fraction shown occurred with the CEWF-1 test in corn stover described earlier.

Concentrations of PAH in the particulate matter by species are listed in Tables 4.5.7 - 4.5.9. The total concentrations across fuel types are fairly consistent for the more vigorously burning types. Barley straw and wheat straw show much higher concentrations due primarily to the poorer burning encountered with these fuels. This also resulted in cooler stack gas temperatures (lower heat release rates). The high concentrations for corn stover are due again to the CEWF-1 test giving high total PAH emission. Without this test, the corn stover concentrations are more similar to those for rice straw.

Total PAH concentrations of particulate matter bracket concentrations measured for various woody and herbaceous type Australian fuels and burning conditions (Freeman and Cattell, 1990). The wind tunnel concentrations for the lower molecular weight species on particulate matter are generally lower than those for large-scale bush fires and open burns of native vegetation reported by Freeman and Cattell. This may be the result of the cooler plume temperatures at the point of sampling compared to the wind tunnel. The concentrations of higher molecular weight species are comparable among wood fuels, corn stover (excluding CEWF-1), and rice straw tested in the wind tunnel. The wind tunnel emissions from wheat and barley straw show greater concentrations of higher molecular weight species, in particular benzo[a]pyrene, than do the field values. The influence of burning conditions would appear to be important in this regard.

Atkinson (1988) has shown that concentrations of certain PAH species in ambient air can be correlated. Good correlations were obtained between phenanthrene and fluoranthene, and fluoranthene and pyrene. Wind tunnel results also show fairly good correlations between these species, as shown in Figures 4.5.15 and 4.5.16. Fluoranthene is emitted at about half the level of phenanthrene up to about 1,000 $\mu g\ kg^{-1}$, above this the behavior is erratic. The emission level for pyrene is nearly identical to that of fluoranthene up to 3,000 $\mu g\ kg^{-1}$.

Other species show reasonably good correlations as well. The emission rate for anthracene is consistently about one-fifth that of phenanthrene (Figure 4.5.17). Benzo[e]pyrene is emitted at about 1.5 times the level of benzo[a]pyrene over the full range measured (Figure 4.5.18). Not all species are well correlated to any single species, however.

4.6. Element balances

Results of carbon balances for individual tests are compared for spreading fires in Figure 4.6.1 and for pile fires in Figure 4.6.2. For most spreading fires, the carbon balances are closed to within ±20%. Six tests exceed this value. The lack of closure is thought to be primarily the result of errors in the determination of CO_2 concentrations in the stack gas, to which the balance is quite sensitive. The carbon balances for the pile fires are closed only to within ±40%, although CO_2 concentrations were determined continuously for three of the four experiments. The poor closure for many tests is indicative of the problems in measuring stack gas velocity, as discussed above.

Results from nitrogen balances are compared in Figures 4.6.3 and 4.6.4 for spreading fires and pile fires, respectively. Shown in each figure is the ratio of nitrogen in NO_x to the nitrogen in the fuel. For spreading fires, this ratio ranged from 7 to 17%, and similar levels were seen for Ponderosa pine and Douglas fir. The values for almond and walnut

tree prunings are substantially higher, however, ranging as high as 45%. The differences do not appear to be related to burning intensity, as shown later. Both almond and walnut fuels had nitrogen contents about twice those of the pine and fir fuels, but similar to the concentrations found for the cereal crop fuels.

The amounts of nitrogen in ash, NO_x, and particulate matter are shown relative to fuel nitrogen in Figure 4.6.5 for spreading fires and 4.6.7 for pile fires. Normalized distributions among these three product species are given in Figures 4.6.6 and 4.6.8. Both the corn stover and rice straw from the 1992 crop year show more N in particulate matter than for other tests. Both fuels were run during October 1992, but what influence this by itself might have is unknown. Results for wheat straw show somewhat elevated levels of N in particulate matter as well. Figure 4.6.6 shows that nitrogen in ash ranges from about 20 to 60% of total nitrogen in the three product species. Pile fires (Figures 4.6.7 and 8) show very little nitrogen in anything except NO_x, with the exception of the smoldering burns in forest slash (DougFir/2 and Pine/2), which produced much less NO_x and may have errors introduced from the assumptions concerning the fuel composition at the start of smoldering. The other smoldering burn in almond tree prunings (Almond/T2f), does not show as much nitrogen in ash as the forest fuels.

The fraction of fuel sulfur emitted as SO_2 is shown for each spreading fire test in Figure 4.6.9, and each pile fire in Figure 4.6.12. The low amounts of SO_2 observed with barley and wheat fuels are readily apparent. The CEWF configurations tend to show reduced fractions relative to the CRNF configurations. The amounts of sulfur accounted for in ash, SO_2, and particulate matter are shown for the spreading fires in Figure 4.6.10 and on a normalized basis for the three products only in Figure 4.6.11. Similar results for the pile fires are shown in Figures 4.6.13 - 14. The low SO_2 concentrations observed with barley straw are compensated by the large fractions of sulfur seen in the ash and particulate matter, and the sulfur balances are closed to between 80 and 90%. The tests in rice straw show a decline in measured SO_2 fraction after 9 June 92 (the 3 tests on 30 April 92 and 3 tests on 9 June 92 make up the first 6 tests shown in the figures), although the sulfur balances are not as well closed after this date. The rice straw fuels from the 1987 and 1992 crop years on average retained more sulfur in the ash than the 1991 crop year straw, which accounts for some of difference seen in the fraction of fuel sulfur emitted in SO_2. Other possible reasons for the differences in SO_2 fraction include errors in calibration, possibly as a result of stratification of species in the gas cylinders, although unlikely at the concentrations maintained. Calibration errors of this sort would come from an apparent increase in SO_2 concentration in the cylinder. Also possible is the absorption of SO_2 in water in the sampling line, but no condensation was ever observed in any part of the line. Stack humidities in every test were below saturation, as well. The barley data showing sulfur enrichment in the particulate matter relative to other fuels suggest heterogeneous reactions of sulfur in the stack. Sulfur in particulate matter for other fuels is not sufficient to suggest a substantial loss of SO_2 in this manner. Errors due to stack gas velocity measurements are possible, but results of the carbon balances do not in general support this argument for the spreading fires. Errors in the determination of fuel and ash sulfur concentrations are also possible. Emission of sulfur in other forms was only partially investigated, as the results of the total S analyses are at best qualitative indicators of the relative amount of stack sulfur in SO_2. Why the relative proportion of sulfur as SO_2 for the same rice straw fuel type should show a declining trend due to emission of sulfur in other forms is unclear. The poor closure observed with Ponderosa pine and Douglas fir may indicate the presence of alternate species. Overall, the results suggest that the SO_2 emission factors may be low by a factor of 2 to 3 (not to exceed total available sulfur) where low yields of SO_2 were obtained relative to fuel sulfur.

4.7. Burning conditions

Burning rates were observed to vary by substantial amounts depending on fuel type. Closely related to burning rates were the heat release rates. The values for both are compared by individual tests in Figures 4.7.1 - 4. For spreading fires, the burning rates ranged from below 2 g s^{-1} for wheat straw in a CEWF configuration to over 14 g s^{-1} for rice straw in a CRNF configuration. With both corn and rice, the CRNF configurations on average produced faster burning rates than the CEWF configurations. No clear distinctions were observed between the two configurations with wheat and barley straw, possibly because of the lower fuel loading rates used with these fuels. Burning rates for the flaming stages of the wood fires ranged from 4 to 22 g s^{-1}, the fastest rate obtained with Ponderosa pine. Smoldering rates were 1 to 3 g s^{-1}.

The burning rates for pile fires were largely sensitive to the type of fuel and loading arrangement. No general influences due to either ambient air temperature or fuel moisture content were observed among all wood fuel types combined, although the number of tests was quite limited. Results from all of the tests for these two parameters individually are plotted in Figures 4.7.5 and 6. The rates at zero moisture for pile fires in Figure 4.7.6. are for smoldering burns in which the fuel (char) moisture was simply assumed to be zero. The inclusion of the data for spreading fires in these figures is primarily for reference. What appears to be a general influence (and contrary to experience for individual fuels) of fuel moisture on burning rate for spreading fires is coincidental. Underlying the differences in burning rate for the spreading fires are multiple influences from fuel type, loading rate, fuel moisture, wind speed, air temperature, and relative humidity. Other influences not quantified also probably affect the burning rates, including fuel bed structure and morphological and physical properties of individual fuel elements.

A simple attempt was made to correlate the external variables to the fire burning rates. Multiple linear regression models were derived to predict burning rates from inlet air temperature, relative humidity, fuel moisture content, inlet air mass flow rate (representing wind speed), and fuel loading rate. In the data presented, the results of the pile fires are excluded because of the substantial differences due simply to fuel type. An attempt to correlate all fuels together in this manner, including pile fires, resulted in a rather poor model fit ($r^2 = 0.42$). Because of the higher burning rates during the flaming stages of the pile burns, such regression also yielded a positive effect from increasing fuel moisture content.

The results of the regression analysis for spreading fires are listed in Tables 4.7.1 through 4.7.4. Included in the tables are the model coefficients, significance, and confidence intervals. The first analysis (Table 4.7.1) utilized data from all four cereal crop types, with 31 separate observations, 19 of them with rice straw. Here again, influences due to fuel type were apparent. Although the model fit was improved compared to the case with all fuels combined ($r^2 = 0.83$), increased fuel moisture was still seen to have a positive impact on burning rate. The effect was not significant, however. Only inlet air temperature and fuel loading rate were significant at the 95% level for this analysis. The model prediction is plotted against measured burning rate in Figure 4.7.7.

To eliminate effects due to fuel type, burning rate was regressed against the same parameters for rice straw alone, the fuel for which the largest number of tests were conducted. Only results from the present study were included. The regression statistics are listed in Table 4.7.2. The model fit was reasonably good ($r^2 = 0.87$), and fuel moisture was observed to have negative impact on burning rate, although the effect was

not significant at the 95% level. Inlet air temperature and mass flow rate were significant, with a positive impact from air temperature and a negative impact from flow rate (wind speed). Relative humidity was not observed to be significant in this analysis.

A similar analysis was performed for the more directly measured spreading rate. The results are listed in Table 4.7.3, and closely resemble the results for burning rate, as expected, with differences in the magnitudes of the coefficients, of course (a spreading rate of 1 m min^{-1} in the rice straw tests was equivalent to a burning rate of 12 g s^{-1}, approximately). The model predictions are plotted against measured spreading rate in Figure 4.7.8.

Inlet air temperature was highly significant as a factor influencing burning and spreading rates for rice straw. Results of a simple linear regression of spreading rate against air temperature are listed in Table 4.7.4. The fit is still reasonably good, with $r^2 = 0.74$. The model predicts an increase of about 0.05 m min^{-1} in spreading rate for each 1 K increase in inlet air temperature (similar to the multiple regression result of Table 4.7.3). The model predictions are plotted against measured spreading rates in Figure 4.7.9.

As a way of relating the observed emission levels to the ambient and fuel conditions, emission factors for individual species from individual fuel types were compared against burning rate. The results appear in Figures 4.7.10 - 15. The CO_2 emission factor, shown in Figure 4.7.10, is, of course, influenced principally by fuel carbon content. The values shown also reflect the assumptions made concerning the fuel carbon concentrations during stoking and smoldering. The relation of CO_2 and other species to the fuel carbon conversion is discussed later. The emission factors for CO, hydrocarbons, and particulate matter showed a common increasing trend as burning rate decreased below about 5 g s^{-1}, although there is much scatter and the conclusion is weak. The very low values for hydrocarbons from rice straw in Figure 4.7.12 were those determined by GC. The highest CO emission factors were observed during the smoldering periods with almond and fir. The general increase in CO emission below 5 g s^{-1} burning rate is consistent with the greater smoldering observed in general for weakly spreading fires. Effects of burning rate on NO_x and SO_2 are also weakly suggested, with some general decline at lower rates. Effects due to fuel nitrogen and sulfur concentrations appear more pronounced.

Emission factors for pollutants from a number of different agricultural fuels were determined by Darley in two studies using the UC Riverside burning tower (Darley, 1977; Darley, 1979). Results from Darley's studies for barley, corn, rice, wheat, almond, and walnut residues are reproduced for each test at each moisture in Tables 4.7.5 through 4.7.10. All values are corrected to dry fuel basis. Darley did not test walnut prunings during the second study, and only values from the 1977 report are listed. For cereal crop residues Darley tested both heading and backing type fires. The results listed in the tables include only the data for backing fires to compare with the results here. Total fuel consumption in each test was 1 to 4 kg. Darley conducted backing fires by placing the fuel on an incline, so as to induce an opposed up-slope wind. Two different slopes were used in the first study, 15 and 25%. Only the 25% slope was used in the second study. Emission factors from pile fires were determined for two conditions, "cold" and "roll-on." Results listed under the cold conditions were obtained by allowing the pile to burn nearly to completion, with just a bed of glowing embers remaining. The roll-on fires were conducted by "rolling" a pile of fuel onto the glowing embers from the first cold test. The roll-on test was to simulate a field practice in which new fuel is added to a pile as it burns down. Darley computed a MMAD based on particle size distributions obtained on a 5 stage cascade impactor. The direct measurement of SO_2 in grab samples by GC

apparently proved infeasible, and Darley computed an SO_2 emission factor on the basis of the difference between the sulfur contents of the fuel and ash, assuming complete conversion to SO_2. Darley recognized that this overestimated SO_2 emissions, but had no further data by which to adjust his difference values.

Results for barley straw in Table 4.7.5 may be compared against those from the wind tunnel experiments listed in Table 4.1.1. On average, the tests conducted by Darley were at higher fuel moisture than the wind tunnel experiments. Results of Darley's second study (1979) are in general closer to the wind tunnel results, although conducted at nearly twice the moisture content. The SO_2 emission factor computed by Darley of about 0.3% based on the difference between fuel and ash sulfur is 78 times higher than that from the direct wind tunnel measurements. As mentioned earlier, the wind tunnel determined SO_2 emissions for barley straw were quite low, with a high yield of sulfur in the particulate matter. Darley's value for MMAD is an order of magnitude lower than the wind tunnel result.

Results for corn stover (Tables 4.7.6 and 4.1.2) are similar except Darley reports somewhat higher CO and NO_x. The SO_2 computed by difference is in this case fairly close to the direct wind tunnel determination.

For rice straw (Tables 4.7.7 and 4.1.3), Darley reports higher CO in the two tests conducted during the first study than determined by wind tunnel experiments. No CO results were obtained during Darley's second study due to a malfunctioning analyzer. The particulate matter and hydrocarbon emission factors obtained for rice in the second study are substantially below the values of the first study. MMAD from the first study are quite similar to wind tunnel results.

For wheat straw (Tables 4.7.8 and 4.1.4), the burning tower and wind tunnel results are similar except for MMAD and SO_2. Both tables show a fair amount of variation in the emission factors depending on conditions maintained. MMAD from Darley are about one-third wind tunnel results, SO_2 is again roughly an order of magnitude higher.

Emission factors for particulate matter, CO, and hydrocarbons from almond prunings were consistently lower at lower moisture content in Darley's first study (Table 4.7.9). The emission factors were increased for the roll-on fires relative to the cold fires. Results from the wind tunnel (Table 4.1.5, complete fire, similar to Darley's "cold" condition), based on the stack gas velocity computed by closing the carbon balance, appear to be intermediate to the values given by Darley, even though the fuel moisture for the wind tunnel tests was below that of any of Darley's tests. NO_x is lower by roughly half in the burning tower experiment, and SO_2 higher by roughly a factor of 3. Wind tunnel results for walnut prunings (Table 4.1.8) are within the range reported by Darley (Table 4.7.10), except for particulate matter, which are lower when the velocity determined by carbon balance is used. Unfortunately, Darley did not report NO_x or SO_2 data for walnut prunings. The wind tunnel results support Darley's conclusion that further drying below 35% moisture does not reduce the emission levels. The wind tunnel data are not sufficient to test Darley's conclusions concerning moisture above 35%.

Darley (1979) does report some VOC emission factors. For backing fires, only two compounds are quantified--benzene and toluene. Darley lists emission factors for 13 compounds from the fires in almond tree prunings. Where matching compounds are identified, the results of Darley are in many cases of the same order as those from the wind tunnel. For barley, benzene was found by Darley at 92 mg kg^{-1}, whereas the average wind tunnel value was 149 mg kg^{-1} (Table 4.5.2). Darley's value for toluene at

18 mg kg^{-1} is about 20% that from the wind tunnel, but the uncertainty in both estimates is quite high. The emission factor for toluene from rice straw listed by Darley is about 5% of the value listed for benzene. Wind tunnel results show them to be nearly equal. Wind tunnel emission factors for benzene, toluene, and xylene (30, 19, and 3 mg kg^{-1}) from almond tree prunings are quite similar to those reported by Darley (50, 11, and 3 mg kg^{-1}), but styrene and furfural emissions are about 10 times higher.

Field data on particulate matter emission factors for rice straw burned in various configurations is available in Goss and Miller (1973). Six configurations were evaluated: heading fires in dried straw spread behind the combine harvester, straw windrowed behind the harvester, and straw in a larger windrow formed by raking two smaller windrows together. Dry fuel loading rates varied from 450 g m^{-2} in spread straw to 3,400 g m^{-2} in the raked windrows. Straw moistures varied from 5 to 13% wet basis, except for one heading fire in raked straw at 23%. For all fires, the particulate matter emission factors varied from 0.09% to 3.1%, the latter for a backing fire in raked straw at 9% moisture. PM emission factors from backing fires in spread straw ranged from 0.15% at 6% moisture content to 0.48% at 7% moisture content. The total moisture content variation was 6 to 13% wet basis. The PM emission factor at 13% fuel moisture was 0.43%. Ash carbon concentration ranged from 10 to 20%. Ambient temperatures at the time of the fires were 13 to 29°C, with relative humidities between 24 and 43%. Results from individual trials for spreading rates were not reported, but a calculation described indicates spreading rates between 0.8 and 1.5 m min^{-1} were observed in the field. The wind tunnel results appear to be reasonably consistent with the field data, at least for these parameters.

Wind tunnel results for Douglas fir and Ponderosa pine slash may be compared against the results of field experiments reported by Ward, et al. (1989). Ward investigated emissions of CO, CO_2 (used to determine emission factors by carbon balance and for comparison with fuel consumption determined by direct inventory), CH_4, non-methane hydrocarbons (NMHC), total particulate matter (PM), and PM2.5. NO_x and SO_2 were not analyzed, and so no comparison with wind tunnel results can be made. A number of different fuels and burning conditions were monitored. Results for four of these are summarized in Tables 4.7.11 through 4.7.14. The first two experiments (Tables 4.7.11 and 12) were broadcast burns in Douglas fir and long-needle pine (mixed species). The other two experiments (Tables 4.7.13 and 14) were pile burns with mixed conifer slash. In one case piles were created by pushing up the slash with a bull-dozer, in the other by piling with a crane. Ward segregated the results by flaming and smoldering fire stages, then mass averaged the results to obtain emission factors for the entire fire.

A comparison of the wind tunnel results (complete fires) in Tables 4.1.6 and 7 with the field data of Tables 4.7.11 - 14 shows them to correspond quite closely to the results from the flaming stage of the field burns. The emission factor data listed for smoldering in the field burns are consistent for most pollutants with those obtained during smoldering in the wind tunnel. The exception to this is particulate matter. The smoldering results weigh more heavily on the total fire emission rate in the field burns because the fuel mass allocated to smoldering is much greater. Ward attributed 36% of fuel mass to smoldering in the crane piled burns, and 42% to smoldering in the dozer piled burns. These are about double the amount of fuel consumption attributed to smoldering in the wind tunnel burns. The difference is due to the fineness of the fuels used in the wind tunnel tests. The similarity of the results for flaming and smoldering imply that wind tunnel results can be scaled to the field by applying appropriate mass fractions to the two phases, with the exception of particulate matter.

The field burns give PM2.5 values consistently about half the total particulate matter emissions. The wind tunnel burns yield about 90% of total particulate matter as PM2.5. The wind tunnel PM emission factors are closer in magnitude to the field PM2.5 values. The emission of larger particles in the field burns is not unexpected, as these fires burn with greater total intensity. The average heat release rate from the field experiments, including pile fires with one exclusion, was 66 kW m^{-2}, and compares to the heat release rates from the wind tunnel. Total heat release rates were substantially greater in the field burns, however, with vertical gas velocities approaching 13 m s^{-1} measured at the samplers during the flaming stages. With higher gas velocities, larger particles from the pile would be entrained in the fire plume. The fine particle fractions from the flaming stages of the field burns match relatively well those from the wind tunnel. The very much larger PM emission factors for smoldering compared to flaming are not duplicated in the wind tunnel results, however, most likely as a result of the very low smoldering rates in the wind tunnel. Total carbon concentrations in PM2.5 ranged between 56 and 72% for the entire fire, which compares well with the average concentration of 69% for PM2.5 from wood fuels in the wind tunnel experiments. The field data for the entire fire show higher organic carbon fractions than the wind tunnel data, with only 2 to 10% elemental carbon compared to approximately 30% elemental carbon in the wind tunnel results. Once again, the wind tunnel results more closely resemble the flaming stages of the field burns. Ward, et al., show up to 32% of carbon as elemental carbon in particulate matter from the flaming stages. Potassium, chlorine, and sulfur are the major inorganic species listed by Ward for the PM2.5 fraction. Calcium also appears in quantity, especially in the results from the dozer built piles, which suggests a soil origin for at least part of the emission. Zinc appears in the field data at about half the concentrations seen in the wind tunnel.

Ward, et al. (1989) also attempted to correlate primary pollutant emission factors against a parameter defined as "combustion efficiency." The combustion efficiency was computed as the ratio of the observed CO_2 emission factor to the maximum possible CO_2 emission factor based on complete conversion of the fuel carbon. Some correlation between the carbonaceous species CO, hydrocarbons, and particulate matter with CO_2 emission can be readily anticipated. Fuel carbon not retained in the ash, and not found as CO_2, would appear principally in these three species. The independent sensitivities of these to the combustion efficiency, or fuel carbon conversion to CO_2, follow directly from the carbon balance, as below.

Fuel carbon is partitioned principally into CO_2, CO, hydrocarbons, particulate matter, and ash, as:

$$C_{fC} = \sum_{i=CO_2,CO,THC} f_i \frac{W_C}{W_i} + f_{PM} C_{pC} + y'_a C_{aC} \qquad [52]$$

If the combustion is complete, that is, if all fuel carbon is converted to CO_2, the CO_2 emission factor is simply

$$f_{CO_2,complete} = \frac{W_{CO_2}}{W_C} C_{fC} \qquad [53]$$

which differs from the maximum emission factor found from the stack carbon flow of equation [14] by the amount of carbon in the ash. By equation [53], Ward, et al. (1989) calculated $f_{CO_2,complete}$ = 183 for all wood fuels from an assumption that half of the dry

fuel consists of carbon. Wind tunnel results presented later utilize actual fuel carbon concentrations because of the high ash contents of certain fuels. The relative fuel carbon conversion to CO_2 or combustion efficiency can be defined as

$$\frac{f_{CO_2}}{f_{CO_2,complete}} = 1 - \frac{1}{C_{fC}}\left(\sum_{i=CO,THC} f_i \frac{W_C}{W_i} + f_{PM} C_{pC} + y'_a C_{aC} \right) \qquad [54]$$

The effect of a unit change in CO emission factor on the relative carbon conversion can be found by taking the partial derivative with respect to f_{CO}:

$$\frac{\partial}{\partial f_{CO}} \frac{f_{CO_2}}{f_{CO_2,complete}} = -\frac{1}{C_{fC}} \frac{W_C}{W_{CO}} \qquad [55]$$

which for C_{fC} = 50% yields a decrease in relative carbon conversion of approximately 0.009 (or roughly 1%) for each 1% increase in f_{CO}. The sensitivities to the other factors can be determined similarly. Equation [55] simply says that for each mole of carbon reacted to form CO, one mole is unavailable as CO_2. The results of Ward et al., (1989) showed f_{CO} increased by 200 g/kg or 20% absolute when combustion efficiency declined from 95 to 75%. This is consistent with the sensitivity given by equation [55].

An increase in CO is usually accompanied by an increase in total hydrocarbons and may be accompanied by increases in particulate carbon and carbon in ash. For this reason, the sensitivity of the relative carbon conversion fraction to a change in CO will normally be greater than that determined by equation [55], or, alternatively, a decrease in combustion efficiency will not necessarily manifest as large an increase in CO emission factor due to carbon in other products.

The application of the combustion efficiency to the analysis of the wind tunnel data is hindered by the sometimes excessive or poor closure of the carbon balance. In a number of instances, the measured CO_2 emission factor gives a value of $f_{CO_2} / f_{CO_2,complete} > 1$. To compare the results in this manner, the values of f_{CO_2} giving full closure of the carbon balance were used instead (i.e., equation [54]). The two values are compared in Figure 4.7.16. An alternative expression of relative carbon conversion to CO_2 can be made from the stack species (gas phase and particulate matter) alone, in which the ratio of carbon in CO_2 as a fraction of total determined stack carbon is computed. This CO_2 conversion fraction is plotted against the relative carbon conversion, or combustion efficiency (fuel carbon as CO_2) in Figure 4.7.17. Differences due to actual CO_2 determinations and carbon in ash are apparent.

In Figure 4.7.18, the CO emission factor has been plotted (symbols) against the ratio $f_{CO_2} / f_{CO_2,complete}$ computed via equation [54]. Also plotted (lines) are the sensitivities for each fuel type computed from equation [55]. Barley, corn, and wheat give nearly the same slope, as do almond and walnut, and fir and pine. Rice has a considerably lower carbon concentration due to high ash content, and appears separately. All but one of the values lie beneath the sensitivity lines of equation [55], as expected. With low combustion efficiency, carbon not only appears in elevated emissions of CO, but also in hydrocarbons, particulate matter, and ash. The trends for total hydrocarbons and total particulate matter are shown in Figures 4.7.19 and 4.7.20, respectively. Results for NO_x and SO_2 (Figures 4.7.21 and 4.7.22) show no clear trends overall, although for

rice straw and wheat straw, the emission factors appear to increase with increasing conversion fraction. Influences due to nitrogen and sulfur concentrations in the fuel are pronounced.

The PAH and VOC emission rates are influenced by the burning rate and combustion efficiency. The emission of these species is due to incomplete combustion of the fuel. As seen above, the less vigorous burning conditions yielded higher emission levels of PAH. Like the fraction of PAH on the filter, the PAH emission factor was also observed to increase at lower stack temperatures, as in Figure 4.7.23. As the stack temperature depends directly upon the heat release rate (as well as the air flow rate), the correspondence of PAH with stack temperature is more directly related to the burning rate as shown in Figure 4.7.24. The emission level increases below about 5 g s^{-1}. As shown in Figure 4.7.25, the lower burning rates are associated with lower combustion efficiencies in general. An increase in PAH would be expected to accompany a decline in combustion efficiency. This is in fact the case, as shown in Figure 4.7.26, where a general trend towards increased PAH emission occurs as combustion efficiency declines. The high PAH emission (100 mg kg^{-1}) for the CEWF-1 corn stover test at high combustion efficiency (93%) is somewhat of an anomaly, in that although the fire produced higher total hydrocarbon and particulate matter emissions than the other corn stover fires, it produced lower amounts of CO, and overall generated a higher combustion efficiency. The trend is somewhat clearer if PAH emission is plotted against the fraction of carbon in the stack present in the form of CO_2 (Figure 4.7.27), the remaining being in CO, particulate matter, and hydrocarbons. The trend towards increasing PAH emission with declining combustion efficiency is consistent with the trend for total VOC emission (Figure 4.7.28).

There is also a fairly good correspondence between PAH emission and total particulate matter emission, as shown in Figure 4.7.29. Such correspondence is to be expected on the basis of the reduced combustion efficiency under high PM emission conditions, and on the basis of the role of PAH in soot formation. In addition, radiative cooling of the particles in the flame could lead to increased PAH on the particles, but no direct attempt to identify the cause of the correspondence between PAH and particle emission has be made. The effect appears to be enhanced at higher particle concentrations. The apparent correlation between PAH and particulate matter is better than that between PAH and CO, and slightly better than that between PAH and total hydrocarbons.

5. Summary and Conclusions

Emission factors expressing the mass of pollutant emitted per unit mass of dry fuel consumed were determined in wind tunnel simulations of open burning for four cereal crop residues and four wood fuels. The cereal crop residues, including barley straw, wheat straw, rice straw, and corn stover, were burned in what is commonly referred to as backing fires, that is, fires spreading naturally against the wind. The four wood fuels, including almond and walnut tree prunings, Douglas fir slash, and Ponderosa pine slash, were burned in stationary piles of 35 to 45 kg each. Sampling was conducted to quantify emissions of major gas and condensed phase pollutants including CO, NO, NO_x, SO_2, total hydrocarbons, CH_4, non-methane hydrocarbons, total sulfur, CO_2, and particulate matter. Particle size distributions were obtained with a seven stage cascade impactor, and were used to quantify particulate matter emission levels in the two size classes $\leq$ 10 μm and $\leq$ 2.5 μm aerodynamic diameter. Emission factors were determined for volatile organic compounds (VOC), polycyclic aromatic hydrocarbons (PAH), and individual elements contained in particulate matter. Qualitative evaluations were made of the

distribution of elements in particulate matter by size fraction. Bulk aerosol absorption coefficients were determined from light transmission measurements through filter samples.

Emission factors for major pollutants from all eight fuel types were summarized in Tables 4.1.1 through 4.1.8. For spreading fires, averages were set out by individual wind tunnel configuration (CEWF or CRNF). Global averages were also given. The emission factors listed for all compounds analyzed continuously were obtained by integrating the species mass flows over the course of each experiment. Time averaged values were computed for comparison. Particulate matter emission factors represent total integrated samples. The factors analyzed by GC from grab samples could only be computed as time averaged values. Non-methane hydrocarbons were found by difference utilizing both time averaged and mass integrated values, the latter for total hydrocarbons alone. For wood fuels burned in piles, total emission factors for the fire were listed, using integrated mass flows for continuously analyzed species. The results were given for emission factors computed from the measured stack gas velocity, as well as those computed from the stack gas velocity estimated by closing the carbon balance. Results for Douglas fir and Ponderosa pine slash make use of mass averages from the flaming and smoldering stages of the fires. Due to perceived errors in the stack gas velocities measured during the flaming stages of pile burns for almond prunings, Ponderosa pine, and Douglas fir, the emission factors computed from the stack gas velocities derived via carbon balance are considered superior.

Although two major types of fuels were tested, the magnitudes of the emission factors are not, in general, distinguished by fuel class. In many respects they are quite similar. Emission factors for CO vary from a low of 3.2% with rice straw and almond prunings, to a high of 9.9% with barley straw. The average for wheat straw was 6.7%, the second highest measured. The higher CO emissions from barley straw and wheat straw are clearly associated with the poor fire spread and greater levels of smoldering with these fires, perhaps as a result of the lower loading rates for these fuels. High CO emission levels were also observed for smoldering with slash fuels, and appear to be associated with smoldering in general. Comparisons with data reported from field trials suggests that results of wind tunnel or small scale pile burns can be scaled to full size with adequate knowledge of the mass faction burned in each of the flaming and smoldering stages. An exception to this is the particulate matter emission, for which the wind tunnel results are low in comparison to field data. A limited number of smoldering tests were completed in the wind tunnel, but only under low smolder conditions. Wind tunnel results are inconclusive with respect to scaling total fire particulate matter emissions. The particulate matter emission factors are consistent with the reported fine particle fractions emitted from field burns during the flaming stage. Small scale burns fail to reproduce the high gas velocities and higher entrainment rates of field scale burns, and so larger particles are not observed to the same extent.

Barley straw fires also produced the highest emission factors for total hydrocarbons (THC), non-methane hydrocarbons (NMHC), and particulate matter (PM). THC ranged from a low of 0.44% for rice straw, to 1.4% for barley straw. The range for NMHC emission factors was 0.34 and 1.2% for the same fuels, respectively. PM emissions varied from 0.32% for walnut tree prunings, to 0.78% for barley straw. The average value of 0.35% for rice straw was not much different from walnut tree prunings. Rice straw and walnut tree prunings also produced the smallest mass median aerodynamic particle diameters (MMAD), being 0.11 and 0.12 μm for each fuel, respectively. Barley straw fires produced the largest particle sizes, with 0.29 μm MMAD. In the context of the PM10 standards, however, they appear indistinguishable. NO_x and SO_2 emissions are influenced by fuel concentrations and to a more limited extent by burning conditions.

Total NO_x (as NO_2) ranged from 0.18% for corn stover, to 0.36% for almond tree prunings. Almond tree prunings also yielded the highest levels of NO (0.17%), but the lowest levels came from Douglas fir (0.06%). SO_2 emissions ranged from 0.004% for barley straw, to a high of 0.06% for rice straw. SO_2 emission levels were also quite low for almond tree prunings, at 0.006%. Barley straw was unique among the cereal crop fuels in that a very large fraction of fuel sulfur appeared in the particulate matter, rather than as SO_2. Sulfur was also found in quantity in the particulate matter from wood fuels.

VOC emission factors were summarized in Table 4.5.2. VOC emissions from the two slash fuels were higher than from prunings and cereal crop residues. A larger number of compounds were identified from slash fuels, as well. Terpene compounds associated with the slash fuels were not found for other fuels above threshold levels by the automatic search routine employed with the mass spectral library.

Carbon, potassium, and chlorine dominate the cereal crop particulate matter compositions. Sulfur was quite high in the particulate matter from barley straw, ammonium ion was present in relatively high concentration with corn stover. Elemental carbon made up a third to a half of the total carbon in particulate matter for these fuels. Much of the sulfur was present as sulfate, and virtually all of the chlorine and potassium were present in ionic forms. The wood fuel particulate matter was also dominated by carbon, potassium, and chlorine. Carbon concentrations were on average 50 to 100% higher for the wood fuels than the cereal fuels. Elemental carbon made up a quarter to a third of total carbon, giving a higher organic carbon fraction for the wood fuels. Nitrate ion was emitted from wood fuels at about twice the strength of cereal fuels. Bromine emission factors for the cereal fuels were 7 times higher compared to the woods fuels. Potassium and chlorine were enriched at particle sizes below 2 μm. Silicon, iron and calcium were enriched at the larger particle sizes. High levels of zinc were observed with wood fuels, but zinc balances suggest that about two-thirds of the zinc emitted was due to contamination. XRF and PIXE determinations of elemental mass concentrations for major elements were in excellent agreement at concentrations above 10 $\mu g\ m^{-3}$. Below this concentration, PIXE exceeded XRF determinations for iron and silicon.

Of the two wind tunnel configurations employed with spreading fires, the CRNF configuration yielded in each case the lowest emission factor for particulate matter, and in general was associated with the lowest levels of CO and THC emissions, and highest levels of NO_x and SO_2. For rice straw, the result for particulate matter is contrary to the result obtained in an earlier study (Jenkins, et al., 1993a, b) which found PM emission factors reduced in the CEWF configuration. However, PAH emissions suggest that for the more lightly loaded fuels (barley,wheat), flame blow over and extinction are important in the CEWF configuration, whereas at higher loading rates (rice, corn), higher wind speeds in the CEWF configuration are instrumental in reducing the PAH emission. Loading rate appears to be a major factor influencing the results observed here. The high PM emission factor for the CEWF corn stover results is strongly influenced by the test conducted with fuel that had been left on the wind tunnel conveyor for two days following the previous test. The poor spreading characteristics of the barley and wheat straw fires under the higher wind speeds of the CEWF configuration are evident in the emission factors for this configuration. Although the CO emission from barley straw in the CRNF configuration was only slightly lower than the CEWF configuration, hydrocarbons and particulate matter emissions are substantially reduced. NO_x and SO_2 emission factors are elevated for the CRNF configuration with all fuels. Loading rate was shown to have a significant (95% level) influence on burning rate.

Differences for rice straw in particulate matter emission factors observed here compared to the earlier study may be related to the different sources of the straw. Both studies utilized M202 variety rice straw handled in essentially the same manner, but harvested during different years and from different fields. In direct comparisons of two different sources of straw, the fire in one was observed to spread faster on average than in the other under the same test conditions. When the same straw used in the earlier study was burned again in the CEWF configuration, the particulate matter emission factors returned to their earlier levels. The differences are believed to be due to differences in the concentrations of alkali metals and chlorine, especially the latter. Halogens are known fire retardants (e.g., chlorine is thought to be important in terminating free radical chain reactions). Chlorine as well as potassium are readily leached from straw by water, especially if the straw is left in the field and subject to condensation (dew) and precipitation. The lower levels of chlorine observed in the type of straw yielding higher fire spreading rates is consistent with the perceived role of chlorine as a fire retardant. The extent of weathering of straw prior to field burning may have important consequences for the total pollutant emission from the fire.

Emission factors were not found to depend linearly on spreading rate. Increased emission factors were associated with low spreading rates for all cereal fuels, however. Inlet air temperature was also observed to have a significant impact on spreading rate, and may mask influences due to wind tunnel configuration. Multiple linear regressions against fire spreading rate in rice straw, including air temperature as an independent variable, suggest a 0.05 m min^{-1} increase for each 1 K increase in air temperature. With burning rate as the dependent variable, an analysis of the results for the four cereal fuels combined showed a significant 0.7 g s^{-1} increase for each 1 K increase in air temperature. Wind speed, in the form of inlet air mass flow rate, was also a significant influence on spreading rate for rice straw, reducing spreading rate when increased. Wind speed was not a significant parameter when all spreading fires were analyzed together, apparently because of the differences in loading rate, which were significant. Air relative humidity was found to be only marginally significant in affecting fire burning rates for these experiments. When burning rates decreased below about 5 g s^{-1} (4 g m^{-1} s^{-1} if normalized to fire line width in the case of spreading fires), there was a weak trend towards increased emission factors for CO, THC, and PM. The trend is due mostly to the tests with barley and wheat straw, and the smoldering tests with almond tree prunings and Douglas fir and Ponderosa pine slash. PAH shows a similar trend. Both VOC and PAH increase with decreasing combustion efficiency. NO_x and SO_2 emissions exhibit a weakly decreasing trend as burning rate declines below 5 g s^{-1}. The effect is more pronounced for SO_2, although other factors including reactions of sulfur in the stack may bias the sulfur results. Fuel nitrogen is an apparently important source of NO_x, as the emission strengths vary according to the nitrogen content of the various fuels.

Carbon, nitrogen, sulfur, water, and power balances were completed to evaluate possible errors or inconsistencies in the data sets. As already mentioned, carbon balances revealed possible errors in stack gas velocity measurements made during the flaming stages of the wood fuel burns. Maximum errors in measured stack gas velocities under these conditions appear to be of the order of 1 m s^{-1}, or 30 to 50%. Measured velocity was most often found to be lower than the velocity derived via carbon balance. Maximum possible errors in stack gas velocity for spreading fires appear to be of about the same magnitude, but actual errors are thought to be smaller and within ±20%. Including other possible errors in calibration, analysis, and assumptions concerning instantaneous fuel compositions for pile burns, the magnitudes of the emission factors, except for VOCs and PAHs, are probably determined to within a factor of 2. Data from field and other laboratory experiments suggest the uncertainty is not this large, but the error in these

other data is perhaps not less. The only major discrepancies identified between wind tunnel and field data were in the particulate matter emission factors for smoldering in slash burns. The wind tunnel values were substantially lower. The burning conditions are at any rate shown to have a substantial influence on most species.

Possible interactions between the fuel and ambient conditions emerge from the wind tunnel simulations, but require further investigation for a clearer understanding of fire behavior and pollutant emission. Any future experiments should utilize conditioned air to control temperature and humidity. The direct comparisons of rice straw from different sources suggested possible influences due to fuel morphology and other fuel related properties. Conclusions regarding such influences are weakened by the lack of control over ambient conditions, which appear to have significant effects on the parameters investigated. More sophisticated plume velocity measurement techniques should be employed to reduce the associated uncertainty in the emission factors. Although SO_2 emission factors are improved over earlier estimates, the fate of fuel sulfur is still not completely resolved, nor have the fates of many other elements been described.

6. Acknowledgments

This project was supported by a grant from the California Air Resources Board. The authors acknowledge and appreciate the cooperation and assistance of Jack Paskind, Manjit Ahuja, Robert Grant, Andrew Wortman, Jack Rogers, Jack LaBrue, Mac McCormack, Robert Okamoto, and other members of the CARB staff in helping to carry out this work. The authors also appreciate the assistance of Nelson Smith, Burt Vannucci, Wayne Andrade, Leo Palaima, Charles Barden, Lowell Jahn, Brigette Blankenship, Mary Yandel, Diana Kitchen, Kay Resler, Jackie Simmons, Leigh Ann Empie, and Stefan Grass of the Biological and Agricultural Engineering Department, Univeristy of California, Davis. Other assistance was provided by Dale Uyeminami of the Institute for Toxicology and Environmental Health, University of California, Davis; by Sue Littlefield and the staff of the DANR Analytical Laboratory, University of California, Davis; Jeff Reed and Paul Wakabayashi, Crocker Nuclear Laboratory, University of California, Davis; Steve Brimmer, Microanalytical Laboratory, College of Chemistry, University of California, Berkeley; Monem Beitelmal, Mechanical, Aeronautical, and Materials Engineering Department, University of California, Davis; and Fred Rogers and John Watson of the Desert Research Institute, University of Nevada System, Reno. The advice of Forman Williams, University of California, San Diego, is greatly appreciated.

7. References

ASHRAE. 1989. Fundamentals. American Society of Heating, Refrigerating, and Air Conditioning Engineers, Inc., Atlanta, GA 30329.

Atkinson, R. 1988. A survey of ambient concentrations of selected polycyclic aromatic hydrocarbons (PAH) at various locations in California. Final report, CARB Contract No. A5-185-32, Statewide Air Pollution Research Center, University of California, Riverside.

Cahill, T., R. Eldred, D. Shadoan, P. Feeney, B. Kusko and Y. Matsuda. 1984. Complete elemental analysis of aerosols: PIXE, FAST, LIPM, and Mass. Nuclear Instr. and Methods B3:291-295.

Cahill, T.A., P.J. Feeney and T.A. Eldred. 1987. Size-time composition profiling of aerosols using the DRUM sampler. Nuclear Instruments and Methods in Physics Research. B22:344-348.

California Air Resources Board. 1987. Stationary source test methods. Sacramento, California.

Campbell, D.E. 1992. Effects of rice field burning on the visibility and climate in the Sacramento Valley: a test case for biomass combustion source characterization. Unpublished M.S. thesis, University of California, Davis.

Chang, D.P.Y., M.K. Richards and G.L. Huffman. 1988. Spray Combustion Studies of Surrogate Hazardous Waste Incineration. Final Report from Cooperative Agreement No. CR- 813333-01, HWERL, USEPA, Cincinnati, OH.

Chow, J.C. 1987. Quality assurance project plan for the determination of particle size distributions and chemical composition of particulate matter from selected sources in California, Part II: Laboratory operations. DRI document 8096.1F1. Prepared for the California Air Resources Board, Sacramento, California.

Darley, E.F. 1977. Emission factors from burning agricultural wastes collected in California. Final Report, CARB Project 4-011, California Air Resources Board, Sacramento, California.

Darley, E.F. 1979. Hydrocarbon characterization of agricultural waste burning. Final Report, CARB Project A7-068-30, California Air Resources Board, Sacramento, California.

Darley, E.F., H.H. Biswell, G. Miller and J. Goss. 1973. Air pollution from forest and agricultural burning. J. Fire and Flammability 4:74-81.

Fleeter, R.D., F.E. Fendell, L.M. Cohen, N. Gat and A.B. Witte. 1984. Laboratory facility for wind aided firespread along a fuel matrix. Combustion and Flame 57:289-311.

Freeman, D.J. and F.C.R. Cattell. 1990. Wood burning as a source of atmospheric polycyclic aromatic hydrocarbons. Environ. Sci. Technol. 24(10):1581-1585.

Goss, J.R. and G.E. Miller. 1973. Study of abatement methods and meterorological conditions for optimum dispersion of particulates from field burning of rice straw. Final Report, CARB Project 1-101-1, California Air Resources Board, Sacramento, California.

Hinds, W.C. 1982. Aerosol technology. John Wiley & Sons, New York, NY.

James, R.H., et al. 1986. A Simplified Sampling and Analysis System for the Determination of Volatile Organic Compounds in Combustion Effluents. Presented at the 79th Annual Meeting of the Air Pollution Control Association, Minneapolis, MN, June 22-27.

Jenkins, B.M. and J.M. Ebeling. 1985. Correlation of physical and chemical properties of terrestrial biomass with conversion. Energy from biomass and wastes IX, Institute of Gas Technology, Chicago, IL, pp. 371-400.

Jenkins, B.M., D.P.Y. Chang, O.G. Raabe. 1990. Development of test procedures to determine emissions from open burning of agricultural and forestry wastes. Phase I final report, CARB Project A5-126-32, California Air Resources Board, Sacramento, California.

Jenkins, B.M., I.M. Kennedy, D.P.Y. Chang, O.G. Raabe, S.Q. Turn, R.B. Williams, S.G. Hall, and S. Teague. 1993a. Sensitivity of flame structure and particulate matter emissions to the operating configurations of a combustion wind tunnel, Final Report, CARB Project A932-161, California Air Resources Board, Sacramento, California.

Jenkins, B.M., I.M. Kennedy, S.Q. Turn, R.B. Williams, S.G. Hall, and S. Teague, D.P.Y. Chang, O.G. Raabe. 1993b. Wind tunnel modeling of atmospheric emissions from agricultural burning: influence of operating configuration on flame structure and particle emission factor for a spreading-type fire. Environmental Science and Technology 27(9):1763-1775.

Jenkins, B.M., S.Q. Turn and R.B. Williams. 1992. Agriculture, Ecosystems and Environment 38:313-330.

Jenkins, B.M., S.Q. Turn, R.B. Williams, D.P.Y. Chang, O.G. Raabe, J. Paskind and S. Teague. 1991. Chapter 37 in Levine, J.S. (ed.), Global biomass burning: atmospheric, climatic, and biospheric implications. MIT Press, Cambridge, Massachusetts.

Jenkins, B.M., R.R. Bakker and J.B. Wei. 1995. On the properties of washed straw. Biomass and Bioenergy (in press).

Knutson, J. and G.E. Miller. 1982. Agricultural residues (biomass) in California...factors affecting utilization. Leaflet NO. 21303, Cooperative Extension, University of California, Berkeley.

Nielsen, P.A. and L. Jensen. 1991. Emission of PAH and mutagenic activity from furnaces fueled with cereal straws or wood chips. Chemosphere 23(6):723-735.

Pritchett, L., F. Rogers, J. Watson, J. Chow, W. Dippel, R. Purcell and R. Egami. 1992. Agricultural burn emissions dilution sampler (ABEDS) operator's manual. Desert Research Institute, University of Nevada System, Reno, Nevada.

Raabe, O.G. 1968. A general method for fitting size distributions to multicomponent aerosol data using weighted least-squares. Environmental Science and Technology 12(10):1162-1167.

Ramdahl, T. and G. Becher. 1982. Characterization of polynuclear aromatic hydrocarbon derivatives in emissions from wood and cereal straw combustion. Analytica Chimica Acta 144:83-91.

Rothermel, R.C. and H.E. Anderson. 1966. Fire spread characteristics determined in the laboratory. USDA Forest Service, Intermountain Forest and Range Experiment Station, Ogden, UT.

US EPA. 1985. Compilation of air pollutant emission factors, Vol. 1, AP-42, Research Triangle Park, North Carolina.

Ward, D.E., C.C. Hardy, D.V. Sandberg and T.E. Reinhardt. 1989. Mitigation of prescribed fire atmospheric pollution through increased utilization of hardwoods, piled residues, and long-needled conifers. Part III, Final Report, IAG DE-AI179-85BP18509 (PNW-85-423), USDA Forest Service, Pacific Northwest Research Station, Seattle, Washington.